RSC Advances

REVIEW

View Article Online
View Journal | View Issue

Cite this: *RSC Adv.*, 2022, **12**, 4714

A review on advancements in carbon quantum dots and their application in photovoltaics

Pawan Kumar,[ae] Shweta Dua,[be] Ravinder Kaur,[ce] Mahesh Kumar[de] and Geeta Bhatt*[ce]

Carbon quantum dots are a new frontier in the field of fluorescent nanomaterials, and they exhibit fascinating properties such as biocompatibility, low toxicity, eco-friendliness, good water solubility and photostability. In addition, the synthesis of these nanoparticles is facile, rapid, and satisfies green chemistry principles. CQDs have easily tunable optical properties and have found applications in bioimaging, nanomedicine, drug delivery, solar cells, light-emitting diodes, photocatalysis, electrocatalysis and other related areas. This article systematically reviews carbon quantum dot structure, their synthesis techniques, recent advancements, the effects of doping and surface engineering on their optical properties, and related photoluminescence models in detail. The challenges associated with these nanomaterials and their prospects are discussed, and special emphasis has been placed on the application of carbon quantum dots in enhancing the performance of photovoltaics and white light-emitting diodes.

Received 18th November 2021
Accepted 4th January 2022

DOI: 10.1039/d1ra08452f

rsc.li/rsc-advances

1. Introduction

In recent years, carbon-based nanomaterials like fullerenes, carbon nanotubes, graphene, graphene derivatives, nanodiamonds, and carbon-based quantum dots have attracted widespread attention in various disciplines due to their unique structural dimensions, and excellent physical and chemical properties.[1,2] It has been experienced by researchers that nanodiamonds are difficult to prepare and separate, whereas other nanomaterials like CNTs, fullerenes and graphene exhibit poor water solubility and difficulty in providing strong fluorescence in the visible region. These unwanted features have limited their applications in various fields.[2] Non-carbon nanomaterials like semiconductor quantum dots (SQDs) are well known for their good fluorescence, but their toxic nature (due to the presence of heavy metals) is not suitable for biological applications like bioimaging, biosensors, and drug delivery. On the

[a]*Department of Electronic Science, South Campus University of Delhi, New Delhi-110021, India*
[b]*Bhaskarcaharya College of Applied Sciences, University of Delhi, New Delhi-110075, India*
[c]*Deen Dayal Upadhyaya College, University of Delhi, New Delhi-110075, India. E-mail: geeta.bhatt@bcas.du.ac.in*
[d]*CSIR-National Physical Laboratory (NPL), New Delhi-110012, India*
[e]*Non-Collegiate Women's Education Board, University of Delhi, New Delhi-110007, India*

Pawan Kumar has been in academics and research for the past 9 years. He is pursuing his PhD in the application of carbon quantum dots in photovoltaics. He is also interested in the area of microbial fuel cells. He is currently an Assistant Professor at Bhaskaracharya College of Applied Sciences, University of Delhi. He is a recipient of the Ghasi Ram Mittal Memorial Award for academic excellence as well as a recipient of the Transformation Teachers Award from Sharda University, Noida.

Shweta Dua has been in academics and research for the past 10 years. She is pursuing her PhD in the application of carbon quantum dots for sensing. At present, she is also an Assistant Professor at Bhaskaracharya College of Applied Sciences, University of Delhi. She has authored various chapters for the Institute of Life Long Learning (ILLL), Delhi.

other hand, carbon quantum dots (CQDs), novel zero-dimensional fluorescent carbon-based nanomaterials, do not exhibit toxicity and therefore have an edge over other carbon-based nanomaterials.[3] CQDs were accidentally discovered in 2004 by Xu *et al.* while segregating single-wall carbon nanotubes from carbon soot using gel electrophoresis.[4] However, CQDs were not named as such at that time and were known as fluorescent carbon nanoparticles instead. Soon after this discovery, Sun *et al.* (in 2006) synthesized non-toxic carbon nanoparticles of different sizes (<10 nm) *via* laser ablation and their group referred to these nanoparticles as carbon quantum dots (CQDs).[5] Since then, CQDs have appeared as a very valuable asset of nanotechnology and are considered rising stars among the various carbon-based nanomaterials. Due to their strong luminescence, CQDs are also called carbon nano-lights.[6]

CQDs are very well known for their (i) small size (<10 nm), (ii) relatively strong fluorescence, (iii) fast and facile synthesis, (iv) good water solubility, (v) biocompatibility, (vi) chemical inertness (vii) photostability, and (viii) easily tunable optical properties. This allows the use of CQDs even in applications that are limited for other carbon-based nanomaterials such as biomedicine and bioimaging, thus widening their scope. CQDs possess a powerful ability to bind with organic and inorganic molecules due to the existence of various functional groups on their surfaces (–OH, –COOH, $–NH_2$, *etc.*) through a series of chemical treatments. The spectacular electronic properties of CQDs (electron-donor or electron-acceptor, depending on the chemical structure) cause chemiluminescence and electrochemical luminescence. This graces CQDs with potential for suitable application in the fields of optoelectronics, catalysis, photovoltaics, *etc.* They have been intensively researched since the last decade and are considered next-generation carbon nanomaterials because of their interesting properties and manifold applications in solar cells, light-emitting diodes, electrocatalysis, biomedicine, bioimaging, *etc.*[7]

The present research on CQDs is mainly focused on two aspects: (i) developing a more facile, economic and eco-friendly synthetic method and (ii) enlarging the application field of CQDs.

This paper systematically reviews in detail the carbon quantum dot structure, synthesis approaches and recent advancements in synthesized carbon quantum dots, the effects of doping and surface engineering on its optical properties, followed by the emission models. The challenges associated with carbon quantum dots, their future prospects and their application in solar cells are also covered in this review.

2. Structure of CQDs

CQDs have a core–shell structure formed through the nucleation process, which involves the gradual growth of the core and a "self-passivated" shell comprising functional groups.[8]

Detailed investigation revealed that the core (intrinsic states) can be either graphitic crystalline (sp^2) or amorphous (mixed sp^2/sp^3) based on the degree of the presence of sp^2 carbon in the core. Most researchers have reported graphitic crystalline (sp^2) cores.[9–11] The cores are small in size (2–3 nm) with a typical

Ravinder Kaur is currently a Professor with the Department of Electronics at Deen Dayal Upadhyaya College, University of Delhi, New Delhi. She holds a doctoral degree in Electronics (Material Science) from the University of Delhi, South Campus, New Delhi, India. She has an extensive teaching experience of close to three decades. Her core competency and specialized knowledge is in photovoltaics, microcontrollers, embedded systems and electronic communication.

Mahesh Kumar is a Senior Scientist at the National Physical Laboratory, and an Assistant Professor at AcSIR, New Delhi, an NMI of India. He has worked in surface physics and nanostructures and is currently working on ultrafast optoelectronics and terahertz photonics. He has vast experience in surface science, with more than 50 publications and two books. In 2013, he established a new facility with an ultrafast transient absorption spectroscopy system and a femtosecond laser, and since then the lab has been producing high-quality research.

Geeta Bhatt has been in academics and research for the past 25 years. She obtained her PhD from Mumbai University in 2005. Her early research was on the characterisation of low-energy-implanted semiconductor thin films. She has also worked in the area of electronic waste. Her present research interests include nanotechnology, and the applications of organic semiconductors and optical sensors. She currently serves as the Director of the Non-Collegiate Women's Education Board (NCWEB) at the University of Delhi. She is also the recipient of the Meritorious Teacher's award from the Delhi Government.

lattice spacing of ~0.2 nm.[12] The type of core depends on the synthesis technique, precursors used, and other synthetic conditions (like temperature, duration, pH, *etc.*).[13,14] In general, reaction temperatures over 300 °C lead to outstanding graphitization (sp^2), whereas lower temperatures lead to an amorphous core unless sp^2/sp^3 hybridized carbon is present in the precursor.[14] The present understanding of the core is simply an outcome of the evidence based on different characterization techniques like Transmission Electron Microscopy (TEM) or High Resolution (HR)TEM, X-ray diffraction (XRD), and Raman spectroscopy.

TEM or SEM provides morphological information and is often used to measure the size of the CQDs.[15] The crystal structure can be observed using TEM if the electron diffraction pattern is observed.[16] The crystal structure of CQDs can also be studied by XRD where the broad peak at 23° specifies highly amorphous carbon. However, the presence of two broad peaks at 25° and 44°, indicates a low-graphitic carbon structure corresponding to (002) and (100) diffraction.[17]

The degree of disordered graphite is determined by Raman spectra, where peaks found near 1360 cm^{-1} and 1560 cm^{-1} represent the D and G bands. The intensity ratio of the two bands (I_D/I_G), indicates the atomic ratio of sp^3 *vs.* sp^2 carbon hybridization.[18,19]

The shell of CQDs is typically amorphous, consisting of functional groups (resulting in surface states) such as oxygen, amino-based groups or polymer chains, *etc.*, which depend on the starting materials or dopant species. The functional groups and general structure of CQDs are determined through X-ray photoelectron spectroscopy (XPS), Fourier transform infrared (FTIR) spectroscopy, nuclear magnetic resonance (NMR), elemental analysis (EA), and matrix-assisted laser desorption ionization time-of-flight (MALDI-TOF).[20]

XPS is used for the quantitative analysis of the elemental composition and carbon bonding configurations of the CQDs, which were qualitatively verified by FTIR and NMR.[21] The surface area of the carbon structure is measured by nitrogen sorption analysis.[20] UV/Vis absorption spectroscopy also gives qualitative information about the abundant C=C and C=O conjugate structures present in CQDs.[22]

CQDs can be easily functionalized with different functional groups over their surface (like hydroxyl, carboxyl, carbonyl, amino, epoxy, *etc.*) and allow the binding of both organic and inorganic moieties (Fig. 1).[23] Based on the functionalities, the surfaces of CQDs exhibit either hydrophilic or hydrophobic properties that eventually decide the thermodynamic stabilities of CQDs in different solvents (especially in water) *i.e.*, the surface chemistry of the shell controls the stability of the CQDs aqueous solution.[24]

Sun *et al.* in 2006, observed that the bare CQDs did not exhibit emission upon photo excitation but strong photoluminescence (PL) was recorded for the surface-modified CQDs.[5]

The magnitude of the surface zeta potential indicates the degree of electrostatic repulsion among CQDs. The smaller the magnitude of the zeta potential, the lower is the electrostatic repulsion, which suggests less stability of the CQDs aqueous solution and the tendency of CQDs to aggregate. The shell of the CQD defines its unique optical properties and its ability to act as an electron-donor/acceptor.[25] Surface alteration by different functionalities, passivating agents, and solvent brings substantial variation in the optical properties of CQDs.[23] Depending on the surface moieties, the surface-related electronic acceptor levels can be modulated, which may affect the PL properties of CQDs. All in all, the structure of CQDs defines their intrinsic properties.[20]

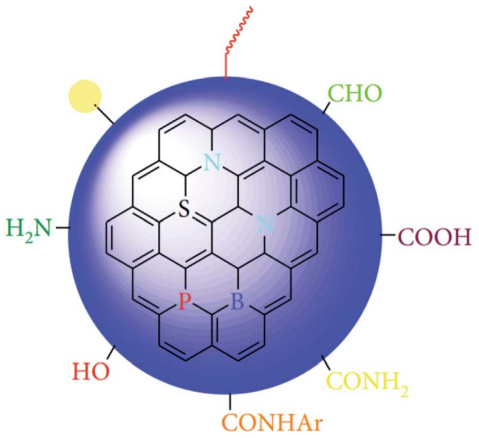

Fig. 1 General structure of CQDs (This figure has been adapted/reproduced from ref. 23 with permission from Hindawi, Copyright 2019).

3. Synthesis approach

There are various methods for the synthesis of CQDs, which are broadly categorized into two approaches, namely the "bottom-up" and the "top-down" approaches, schematically represented in Fig. 2. Although the synthesis of the CQDs is facile, there are certain major challenges associated with their synthesis such as the aggregation of nanoparticles during carbonization, controlling the size and uniformity, and tuning of surface properties.[7]

In the bottom-up approach, nanostructures are built up from organic molecules (carbohydrates, organic acids and amines) or polymer precursors by hydrothermal/solvothermal, microwave, or pyrolysis methods. On the other hand, in the top-down approach, nanoparticles are obtained by cleaving or cutting the large carbon cluster structure into small carbon nanoparticles until the desired particle size is reached. This is achieved either *via* chemical or physical techniques like laser ablation, arc discharge, chemical ablation, or the electrochemical method.[27,28]

In general, the top-down approaches facilitate the synthesis of crystalline CQDs with relatively intact structures but this typically requires several steps for the decomposition of carbon materials in harsh conditions and involves strong oxidants, concentrated acids, and elevated temperatures. Also, the size distribution and morphology of CQDs produced with this approach cannot be precisely controlled.[29]

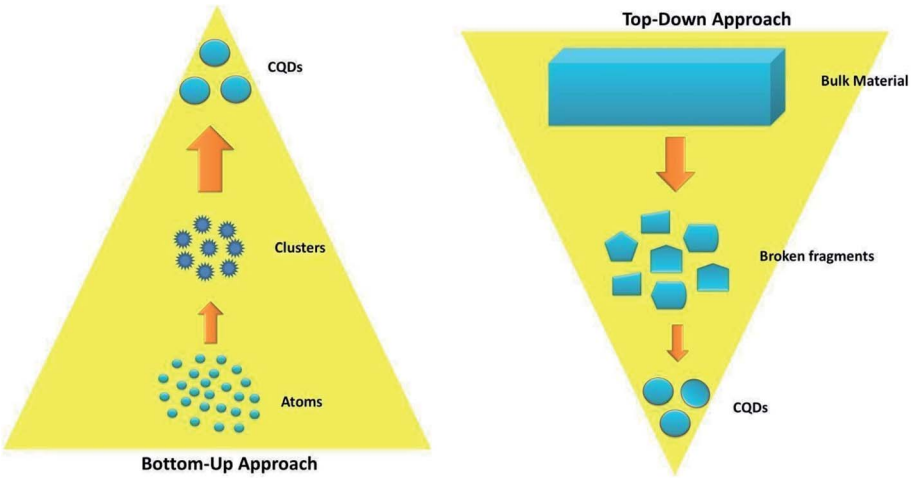

Fig. 2 Schematic illustration of the synthesis approaches of CQDs.

On the other hand, the bottom-up approach tends to produce amorphous CQDs (amorphous carbon cores) with abundant doping sites and functional groups.[28] However, crystalline CQDs have also been reported by some researchers.[11]

In the bottom-up approach, the structure and size of CQDs are dependent on various factors like the molecular structures of the precursors, solvent, reaction conditions (reaction time, temperature, pressure, *etc.*). The reaction conditions are crucial because they impact the reactants and the highly random nucleation and growth process of CQDs. Though very difficult, some research groups have been successful in synthesising size and composition-controlled CQDs by careful optimization of reaction parameters.[28]

Although both approaches have been used for the synthesis of CQDs, the bottom-up approach is cost-effective and environmentally friendly and is thus most commonly used.[30]

In both approaches, post-treatment can be done to modify the surface functional groups and improve the performance of CQDs. Also, the CQDs can be modified during the synthesis. Surface passivation of CQDs removes the emissive traps from the surface and thus enhances the quantum yield (QY). Similarly, doping with heteroatoms such as N_2 and P or metals such as Au or Mg can be done to improve their electrical conductivity and solubility.[27]

3.1 Bottom-up approach for the synthesis of CQDs

As mentioned previously, the bottom-up approach is based on the synthesis of the nanostructures from organic molecular precursors. This approach is broadly divided into three types: (i) hydrothermal/solvothermal method, (ii) microwave irradiation method and (iii) pyrolysis method.

3.1.1 Hydrothermal/solvothermal method. Hydrothermal synthesis is a one-step, cost-effective, non-toxic, and eco-friendly synthetic technique to synthesize the CQDs *via* chemical reactions. In this process, the chemical species with solvent are transferred to a Teflon-lined stainless steel chamber called an autoclave and the solution is heated above ambient temperature and pressure.[27]

The optical and electronic properties of these CQDs can be tuned by varying the organic precursors and altering the temperature but it offers poor control over the size of the CQDs.[7]

In 2010, Zhang *et al.* for the first time synthesized CQDs by using L-ascorbic acid (carbon source) in the presence of ethanol through a one-pot hydrothermal method. This one-step process does not require any chemical (strong-acid) treatment or additional surface engineering. The average diameter of CQDs was ~2 nm, QY of 6.79% and the CQDs aqueous solution was stable at room temperature for over 6 months. In addition, the fluorescence of these CQDs remained insensitive over a broad pH range and even in solvents having strong ionic strengths (*e.g.* 2 M NaCl).[32]

In 2016, Takashi *et al.* synthesized a series of nitrogen-doped carbon quantum dots (N-CQDs) from an aqueous solution of citric acid and urea at various heating rates, reaction times, reaction temperatures, and precursor concentrations. They concluded that temperature is a more important factor for obtaining highly fluorescent N-CQDs than reaction time and reported the highest QY of 39.7%. These N-CQDs were then embedded in polyvinyl alcohol (PVA) nanofibers and it was observed that the luminescence intensity of the N-CQD–PVA composite nanofibers was two times that of the N-CQDs in solution.[33]

In 2019, Zhao, *et al.* developed ultra-high yield CQDs from renewable biomass hydrothermal carbons in the presence of low-concentration $NaOH/O_2$ solution. The average diameter of the CQDs was 2.9 nm with QY up to 16.6%. These CQDs were used for the effective and selective detection of Cu^{2+} with a linear range of 0–30 μmol L^{-1} and detection limit of 85 nmol L^{-1}. This enables the application of CQDs as fluorescent Cu^{2+} nanoprobes.[34]

In 2020, Yang, *et al.* synthesized amorphous CQDs from expired passion fruit shells through hydrothermal synthesis. The CQDs were spheres with diameters <5 nm and QY of 1.8%. Their research provided novel ideas and trends for the resource utilization of expired fruits.[35] The synthesis of CQDs from citric

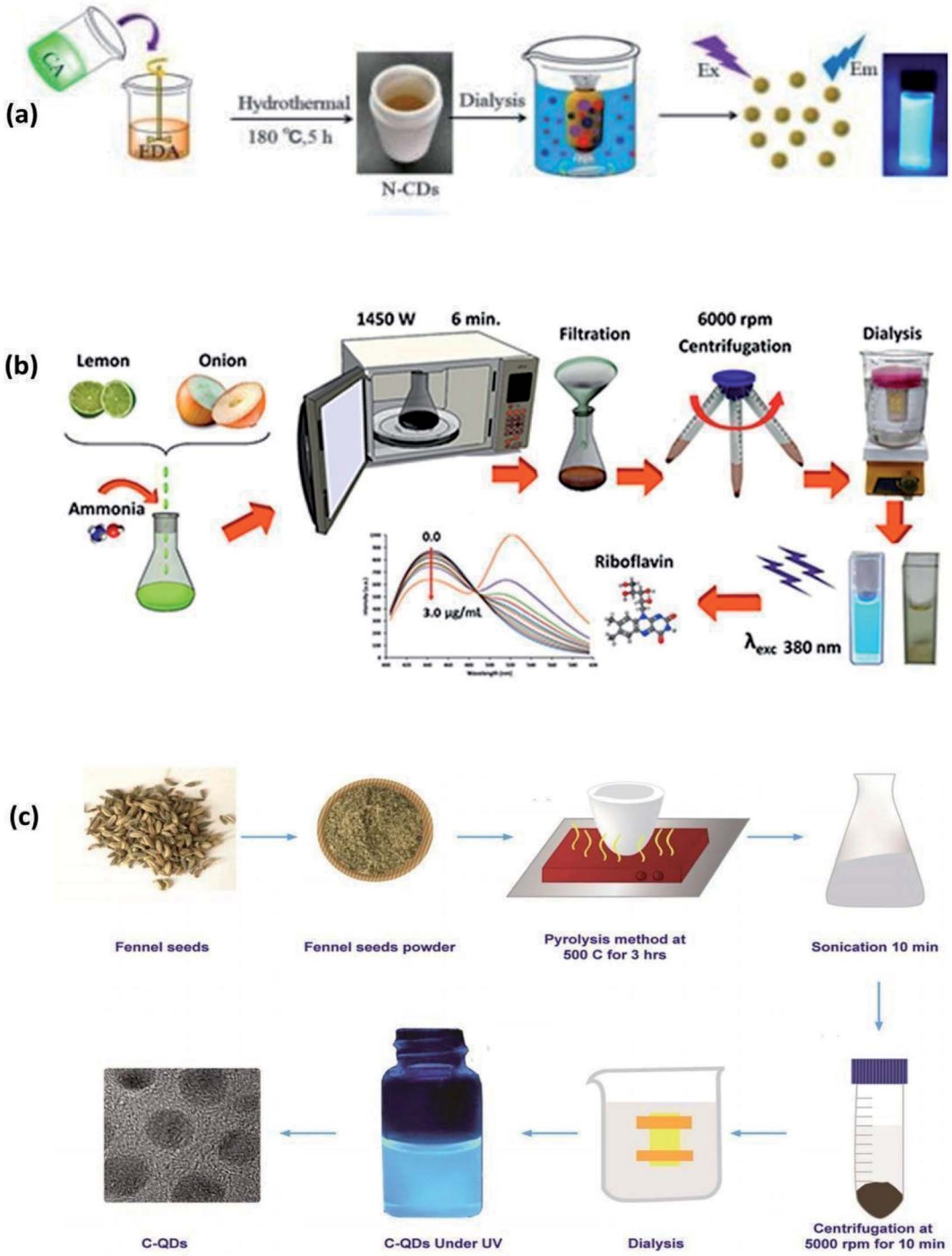

Fig. 3 (a) Synthesis of CQDs from citric acid and EDA through a hydrothermal method (this figure has been adapted/reproduced from ref. 31 with permission from World Scientific, Copyright 2018). (b) Synthesis of CQDs from lemon juice, onion juice and ammonia through the microwave method (this figure has been adapted/reproduced from ref. 39 with permission from Elsevier, Copyright 2019). (c) Synthesis of CQDs from fennel seeds *via* the pyrolysis method (this figure has been adapted/reproduced from ref. 11 with permission from Nature, Copyright 2019).

acid and EDA through hydrothermal methods is shown in Fig. 3(a).

3.1.2 Microwave irradiation method. In comparison to hydrothermal synthesis, the microwave irradiation method is faster, requires a lower temperature and can be halted at any time to avoid overheating the sample.[36] In recent years, this synthetic technique has received significant attention due to its rapid, cost-effective, easily scalable, energy-efficient,[37] and eco-friendly nature,[7,23] but it is difficult to precisely control the size of CQDs with this method.[7]

In this method, the aqueous solution consisting of carbon precursors is heated in the microwave oven till the CQDs are

synthesized. The microwave radiation can heat the polar molecules, which have an electric dipole moment. An oscillating external electric field rotates the polar molecules and this process is called dipole rotation, dipole polarization, or dielectric rotation. These rotating molecules push, pull or collide with the neighbouring molecules and energy gets transferred to all parts of the material in the form of heat. This is because the temperature of molecules is related to their kinetic energy (angular velocity). This phenomenon of heating is called dielectric heating.[36,38] Synthesis of CQDs from lemon juice, onion juice and ammonia through microwave methods is shown in Fig. 3(b).

In 2009, Zhu *et al.* developed a microwave irradiation method to synthesize CQDs. They heated an aqueous solution of saccharide (glucose, fructose, *etc.* as a carbon source) and PEG200 (a coating agent) for 2–10 min at a power level of 500 W in a microwave oven. The solution gradually changed from colorless to yellow and then to a dark brown solution upon heating. The resultant product was further diluted with distilled water to finally obtain the fluorescent CQDs. The particles had a diameter between 2.75–3.65 nm with narrow distribution based on heating duration, and the highest reported QY was 6.3%. The results showed that particle size and the fluorescent QY of CQDs depend on the reaction time.[29]

In 2012, Wang *et al.* synthesized fluorescent (blue) and water-soluble CQDs from eggshell membranes (a common protein-rich waste in daily life), which can be obtained easily and cheaply. The CQDs were spherical with a diameter of ~5 nm and QY of 14%. They designed a sensitive CQD–Cu^{2+} system for the detection of glutathione, which exhibited a linear range of 0.5–80 μmol L^{-1} and detection limit of 0.48 μmol L^{-1}.[37]

In 2017, Roshni *et al.* synthesized highly fluorescent, aqueous soluble and significantly photostable nitrogen-doped CQDs from sesame seeds. The CQDs were spherical with an average diameter of 5 nm and QY of 8.02%. The prepared CQDs were effectively used for the detection of Fe(III) and the limit of detection (LOD) was found to be 2.56 μM of Fe(III).[40]

In 2018, Vaneesa *et al.* prepared a white-light-emitting CQD solution consisting of nitrogen-doped blue fluorescent CQDs and 2,3-diaminophenazine (DAP), a yellow fluorescent dye. These were synthesized simultaneously upon microwave-heating the mixtures of *o*-phenylenediamine (*o*PD) and citric acid (CA) for 10–15 min. During synthesis, the *o*PD has two roles: it serves as a doping agent to improve the blue fluorescence intensity of the CQDs while simultaneously reacting with itself to form the yellow fluorescent dye DAP. The prepared CQDs solution exhibits two fluorescence emission peaks; one at 430 nm and the other at 560 nm, originating from the CQDs and DAP, respectively. They found that the intensity ratio of both fluorescence peaks is pH-dependent. Thus, the emission colour of the CQD solution can be tuned precisely and reproducibly from blue to white to yellow by careful control of the pH. The size of the synthesized CQDs was 1.1 ± 0.3 nm and the QY was 5.4% for the pH value of 5.4.[41]

In 2020, Aysel *et al.* synthesized fluorescent CQDs from roasted chickpeas (as carbon source) in a single step through microwave heating without using any chemicals. The obtained CQDs were amorphous with an average diameter < 10 nm, and the highest QY of 1.8%. They demonstrated that these CQDs were sensitive and selective for the determination of Fe^{3+} ions.[42]

In 2020 one research group synthesized CQDs from citric acid and urea for different heating durations. The majority of the CQDs exhibited blue emission under UV radiation (365 nm) and the emission was excitation independent. It was observed that the heat duration affected the stability and bandgap of the synthesized CQDs. The stability was highest for the CQDs synthesized in 165 s (minimum heat duration required for CQD synthesis in our study) but at the cost of lower PL.[36]

3.1.3 Pyrolysis method. In this process, the organic compounds are decomposed at an elevated temperature (usually above 430 °C) and under pressure in the absence of oxygen. Sometimes, a strong acid or alkali is also used, which serves as a catalyst. This process simultaneously involves changes in the physical phase and chemical composition and is an irreversible process. The synthesis of CQDs from fennel seeds *via* the pyrolysis method is shown in Fig. 3(c).

Liu *et al.* in 2009 reported a novel route for the synthesis of CQDs through pyrolysis. The CQDs were derived from surfactant-modified silica spheres (carrier) and resol (carbon precursor). Although the synthesis of CQDs requires multiple steps, it does not require elaborate equipment. The prepared CQDs (blue emission) were amorphous with diameters of 1.5–2.5 nm and QY of 14.7% (when passivated with PEG). Furthermore, the CQDs were stable for a wide range of pH values (pH 5–9) with only a slight decrease in the photoluminescence QY to 11.0% and 12.1% for pH 5 and 9, respectively.[43]

Multistep procedures are considerably time consuming and complicated; some comparatively simple but less effective preparative methods had also been developed by that time.[44]

To overcome these problems, In 2010, Pan *et al.* reported a fairly effective one-step synthetic method for highly fluorescent CQDs through the pyrolysis of ethylenediamine-tetraacetic acid (EDTA) salts at low temperatures. The CQDs produced highly blue fluorescence, with a PL quantum yield (QY) as high as 40.6%, much higher than those reported up until that time (QYs < 15%). The average diameter of the CQDs was ~6 nm. They also observed that the PL properties strongly depend on pH, solvent, spin, and excitation wavelength.[45]

In 2015, Martindale *et al.* (2015) synthesized CQDs by the pyrolysis of citric acid at 180 °C. The prepared CQDs exhibited an average diameter of ~6 nm and QY of 2.3% (excitation at 360 nm).[46]

In 2016, Wang *et al.* synthesized nitrogen-doped carbon dots (N-CQDs) by the direct pyrolysis of citric acid and ammonia at 200 °C for 3 h with a heating rate of 10 °C min^{-1} in the air. The CQDs had a diameter of 10.8 nm and exhibited a high QY of ~36%. They observed that the excitonic absorption of CQDs depends on the concentration of N-dopant in CQDs, which can be readily modified by the mass ratio of the reactants.[47]

In 2017, Rong *et al.* also synthesized N-CQDs by a one-pot solid-phase pyrolysis method using guanidinium chloride and citric acid as the catalyst, nitrogen and carbon source. The synthesis was free of acid, alkali, organic solvent, or further modification and passivation. These N-CQDs had an average

size of 2.2 nm and QY of 19.2%, and have been intensively used in metal-ion detections (like Fe^{3+}) and bioimaging.[48]

3.2 Top-down approach

3.2.1 Chemical ablation. Chemical ablation is an oxidative acid treatment for the synthesis of CQDs. In this process, strong oxidizing acids (like H_2SO_4, HNO_3, hydrogen peroxide) convert small organic molecules to carbonaceous materials (carbonization), which can be additionally cut into tiny sheets by controlled oxidation. This method is most accessible and allows various sources to be used but requires harsh conditions, drastic processes, multiple steps and also offers poor control over the sizes of CQDs.[7]

In 2007, Liu *et al.* used the combustion soot of candles for the synthesis of CQDs by utilizing an oxidative acid treatment (using HNO_3 or H_2O_2/AcOH). The resultant black homogeneous solution was then purified through a series of processes such as centrifugation, dialysis and polyacrylamide gel electrophoresis (PAGE) to get pure fluorescent CQDs of different particle sizes. This oxidative acid treatment (i) breaks down the carbon aggregates into CQDs, (ii) solubilizes the CQDs, and (iii) influences the PL properties of CQDs. The size of the CQDs was ~2 nm and the maximum obtained QY was 1.9% (excitation at 366 nm).[44]

In 2009, Peng and Travas-Sejdic synthesized CQDs using carbohydrates as the starting material. They dehydrated the carbohydrates with conc. H_2SO_4, producing carbonaceous materials that were then broken into individual CQDs with HNO_3. These CQDs were finally passivated with amine-terminated compounds (4,7,10-trioxa-1,13-tridecanediamine). This surface passivation significantly enhanced the PL intensity such that the QY dramatically increased from 1% to 13%. The CQDs were crystalline with a diameter of ~5 nm and lattice spacing of 0.32 nm. The zeta potential of the CQDs changed from a negative value (−37.3 mV) to a positive value (3.46 mV) after passivation due to the conversion of the carboxylic functional groups to amide groups. They concluded that the emission wavelength of CQDs could be tuned by changing the precursor and the duration of the HNO_3 treatment.[50] In 2014, Mingbo *et al.* reported the synthesis of N-CQDs using petroleum coke and ammonia as shown in Fig. 4(a). The petroleum coke was oxidized in the mixture of H_2SO_4 and HNO_3, followed by functionalization through hydrothermal ammonia treatment. They observed that the QY and fluorescence lifetime of CQDs were enhanced significantly from 8.7 to 15.8% and 3.86 to 6.11 ns, respectively, after the hydrothermal treatment in ammonia (incorporation of N). The CQDs (untreated with ammonia) and N-CQDs were both soluble in water, had uniform particle distribution, strong luminescence, and high sensitivity to pH (in the range of 2.0–12.0). Nitrogen doping and uniform size distribution helped in improving the radiative recombination and hence the fluorescence properties of CQDs.[51]

Post-synthesis surface passivation was done in most of the research to enhance the QY of the CQDs but it adds one more synthesis step. To overcome this, In 2019 Chao, *et al.* synthesized CQDs of different microstructures by the selective oxidation of graphitized activated carbon using HNO_3/$HClO_4$ as the oxidant. The fluorescence of the CQD solution was tuned from yellow to green by regulating the degree of graphitization of the carbon precursor through heat treatment at elevated temperature (up to 2500 °C) without any post-synthesis surface passivation. The QY of CQDs increased from 2.3% to 8% at the higher temperature. The fluorescence properties of the CQDs were further improved upon their chemical reduction by sodium borohydride (reducing agent). The prepared CQDs had no cytotoxicity and thus were used for $HepG_2$ cell bioimaging.[52]

3.2.2 Electrochemical carbonization. The electrochemical approach is a non-selective chemical cutting process of a carbon material such as graphite, carbon nanotubes, or carbon fiber electrodes for the synthesis of ultrapure CQDs. In this method, an electrochemical cell is used, which typically consists of three electrodes (working, counter and reference) and electrolyte solution. The working electrode is made of carbon (graphite, carbon-nanotube, *etc.*) and the counter electrode was platinum (Pt). The potential was applied on the electrode(s), which caused the judicious cutting of carbon material into ultra-small particles (tiny particles of graphite) yielding CQDs. This synthesis of CQDs results in the change in the colour of the electrolytic solution from yellow to dark brown. The alkaline solution is necessary for the synthesis of CQDs.[53]

Among all the various methods, the electrochemical method is advantageous because of its simplicity,[2] low cost and easy manipulation.[53] It allows the fine-tuning of the size and nanostructure[7] by controlling the applied voltage/current, can proceed under aqueous or nonaqueous solutions,[27] and can be used at normal temperature and pressure.[2] The only limitation with this technique is that it allows only very few small molecular precursors for CQDs synthesis.[7]

In 2007, Zhou *et al.* first reported the synthesis of CQDs from multiwalled carbon nanotubes (MWNTs) in the presence of tetrabutylammonium perchlorate (TBAP) as an electrolyte. They used the MWNTs-coated carbon paper as the working electrode and Pt wire as the counter electrode. The applied potential was cycled between −2.0 and 2.0 V at a scan rate of 0.5 V s^{-1}. As the cycles increased, the electrolytic solution was found to change from colourless to yellow and finally to a dark brown colour, and emitted a blue colour upon UV irradiation. This solution was further purified and filtered to give the CQDs. The obtained CQDs exhibited a uniform spherical shape, narrow size distribution (2.8 ± 0.5 nm in diameter), and QY of 6.4% (excited at 340 nm).[55]

In 2009, Zheng *et al.* used graphite as a working electrode and Pt mesh as the counter electrode (along with a reference electrode) in the presence of phosphate buffer solution (PBS) at neutral pH. The potential applied at the working electrode was cycled between −3.0 V and 3.0 V at 0.1 V s^{-1}. As the number of scan cycles increased, the colour of the electrolyte solution changed from colourless to yellow and finally to dark-brown. This resultant solution was directly ultra-filtered through a 10 kDa molecular weight cutoff membrane and as a result, spherically-shaped nanoparticles (CQDs) with an average size of ~2 nm were obtained.[56]

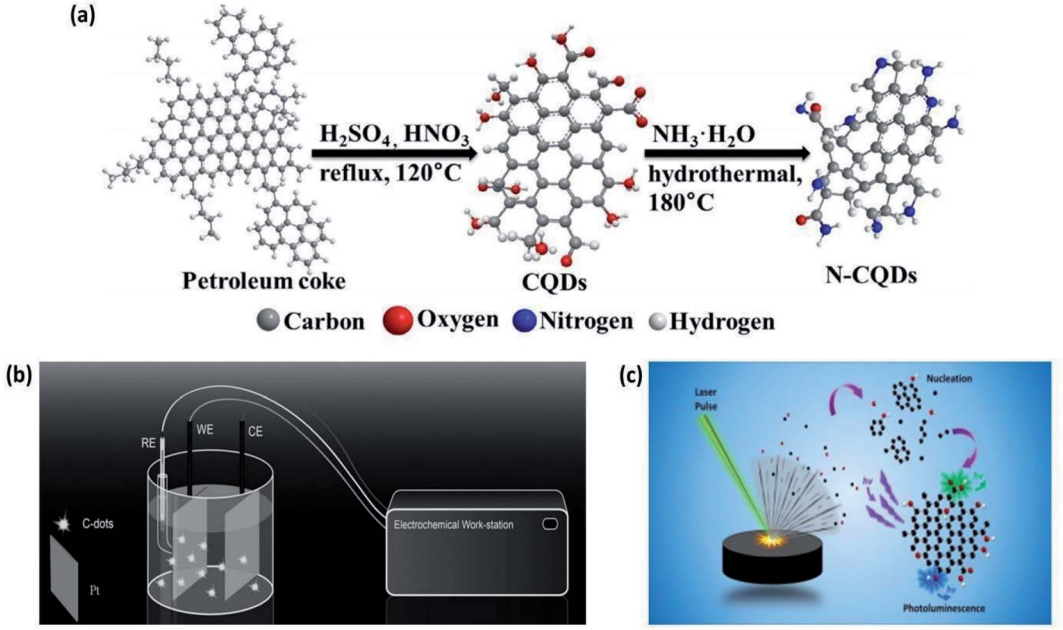

Fig. 4 (a) Preparation of CQDs and N-CQDs from petroleum coke through the chemical ablation method (this figure has been adapted/reproduced from ref. 51 with permission from Elsevier, Copyright 2014). (b) Electrochemical synthesis of CQDs from simple organics. In simple conditions, one Pt sheet was used as the anode, the other one as the cathode and the simple organics as the carbon source. Under a suitable DC control, the organics were broken into CQDs (this figure has been adapted/reproduced from ref. 53 with permission from Wiley-VCH, Copyright 2014). (c) Synthesis of CQDs through the laser ablation method (this figure has been adapted/reproduced from ref. 92 with permission from Elsevier, Copyright 2018).

This conventional electrochemical method needs complicated post-synthesis purification of CQDs. Thus, to overcome this complicated time-consuming step, in 2014, Deng *et al.* synthesized CQDs by a novel one-pot electrochemical carbonization technique. They used two Pt electrodes (as anode and cathode) and one calomel electrode (reference) with NaOH/EtOH as the electrolyte (alkaline medium with OH^- species) as shown in Fig. 4(b). The synthesis potential was varied from 3.0–9.0 V (electrochemical carbonization time was between 3–4 h) and this successfully resulted in high-quality CQDs from different small molecular alcohols. They speculated that the CQDs were synthesized from ethanol electrochemical oxidation and dehydration at a suitable potential. The size of the as-prepared CQDs was adjusted simply by varying the applied potential and they observed the diameters of 2.1, 2.9, 3.5, and 4.3 nm, for 3.0, 4.0, 6.0, and 7.5 V, respectively (which increased with the applied potential). These CQDs also exhibited a high QY of 15.9%, which is typically not attained with the conventional electrochemical method. In addition, they successfully demonstrated the luminescence microscopy of the CQDs in human cancer cells. The results specified that the prepared CQDs have acceptable toxicity and hence, are suitable in imaging applications.[53]

In 2019, Priyanka *et al.* synthesized carbon nanospheres (CNSs) with an average diameter of 7 nm through an electrochemical method by using only two graphite electrodes (working and counter electrode) immersed in ultrapure water (an electrolyte medium). The synthesis of the CNSs took place due to multiple cyclic voltammetry (CV) scans (35 cycles) in the potential range of ±2.0 V. They fabricated sensors using CNSs for the successful detection of the antibiotic ciprofloxacin.[57]

In 2020, Xiao *et al.* prepared a platinum (Pt), CQDs-coloaded graphene composite through the electrochemical method followed by hydrothermal treatment. They used the graphite powder as the cathode and Pt wire as the anode immersed in propylene carbonate (PC) with tetrabutylammonium tetrafluoroborate (TBA BF_4; 0.1 M), and a voltage of 30 V was applied for 12 hours. As a result, graphene was obtained by the electrochemical exfoliation of graphite, while carbon quantum dots (CQDs) and Pt nanoparticles (NPs) were simultaneously generated *in situ* in the electrolyte. CQDs (with an average size of 4.1 nm) evolved from the propylene carbonate solvent and Pt nanoparticles were derived from the reduction of the Pt intermediate species generated from the anodic dissolution of the Pt counter electrode during the electrolysis process. They observed that with the increase in the working voltage, the color of the electrolyte solution turned from colorless into dark brown, and the concentrations of CQDs and Pt NPs in the solution increased.[58]

Typically, the CQDs synthesized through this process do not possess good QY and thus are not used in imaging and sensing applications.[25]

3.2.3 Laser synthesis. Laser synthesis has been one of the widely used techniques for synthesizing CQDs of varied sizes. In this method, the laser is used to irradiate complex organic macromolecules (target carbon source) immersed/suspended in liquid, and detaches nanosized carbon particles (CQDs) from the larger molecular structures. The laser can be operated either in continuous wave mode or in pulsed mode.[23]

Laser synthesis methods for CQDs can be classified into two categories: (i) laser ablation of carbonaceous solid targets immersed in a liquid, and (ii) laser fragmentation of suspensions containing powdered carbon material.[59] A demonstration of the synthesis of CQDs *via* laser is shown in Fig. 4(c).

Since laser synthesis constitutes a single-step, green, and straightforward procedure that neither requires the use of external chemical agents nor creates the by-products that may lead to further cross chemical effects, this technique has stood out above the various synthesis techniques of the bottom-up approach and guarantees the synthesis of high-purity CQDs.[59] In addition, this method is rapid and allows tuneable surface states but at the cost of low QY and with poor control over the size of CQDs.[7]

In 2006, Sun and co-workers used this technique for the first time for the synthesis of CQDs. They used a Nd:YAG laser (λ = 1064 nm and pulse frequency = 10 Hz) to irradiate a carbon target (a processed blend of graphite powder and cement) in the presence of water vapor using Ar as a carrier gas (at 75 kPa and 900 °C). The resultant nanoparticles were refluxed in HNO_3 (for 12 hours) and the surface was passivated by coupling organic molecules such as amine-terminated polyethylene glycol (PEG1500N) and poly(propionyl ethyleneimine-*co*-ethyleneimine) (PPEI-EI). The passivated CQDs exhibited bright luminescence with QY varying from 4% to >10%. This variation in QY might depend on the effectiveness of the reaction for surface passivation.[5]

In 2009, Du *et al.* reported an effective method for synthesizing and simultaneously modifying the surface of fluorescent CQDs. They used a Nd:YAG pulsed laser (wavelength of 1.064 μm and power density of 6.0×10^6 W cm^{-2}) to irradiate graphite powders dispersed in three kinds of solvents, namely diamine hydrate, diethanolamine, and polyethylene glycol (PEG200N), respectively. To accelerate the motion of carbon particles, ultrasound was also employed during laser irradiation. As a result, a homogeneous black suspension was obtained, which upon centrifugation resulted in a colourful supernatant. The supernatant from the suspension of graphite in PEG200N, diamine hydrate and diethanolamine resulted in CQDs with QY of 5%, 3.7% and 7.8%, respectively. Interestingly, the size distributions of CQDs in all three solvents were identical. The results proposed the surface states to be the cause of the origin of the luminescence.[61]

Khan *et al.* in 2009, Liu *et al.* in 2010, and Singh *et al.* in 2010 made various attempts at controlling the size and novel nanostructures of CQDs by adjusting the liquid medium.

In 2011, Shenglian *et al.* tailored the size of CQDs by modifying the laser parameters. They synthesized CQDs with average sizes of about 3, 8, and 13 nm with QY of 12.2%, 6.2% and 1.2%, respectively, by irradiating graphite flakes in polymer solution with a laser. It was observed that the size of CQDs could be controlled by tuning the laser pulse width. They concluded that (i) the laser pulse width could affect the nucleation and growth process of CQDs, thus producing the different size distribution, and (ii) the long-pulse-width laser would be a better option for controlling the size and morphology of the nanostructures in the diverse material frameworks in comparison with a short-pulse-width laser.[62]

In 2018, Carlos *et al.* synthesized CQDs from carbon glassy particles suspended in polyethylene glycol 200. The average size of the CQDs was ~3 nm and the highest QY observed was 4.5% when synthesized by flow jet. They applied the synthesized CQDs in bio-imaging for cancer epithelial human cells and observed that the CQDs preserved the information of cells even if the cell died.[59]

3.2.4 Arc discharge. This is the first method by which the CQDs were synthesized. In 2004, Xu *et al.* synthesized SWCNTs by the arc discharge method and when these SWCNTs were separated and purified through preparative electrophoresis, carbon nanoparticles with fluorescence (CQDs) were also accidentally obtained.[4] Since their discovery in 2004, CQDs have attracted the attention of various researchers.

In 2006, Bottini *et al.* synthesized CQDs from pristine and SWCNTs using an arc discharge method that resulted in CQDs displaying bright emission (PL) in the violet-blue and blue-green regions, respectively.

Moreover, the pristine carbon nanotube-derived CQDs were hydrophobic and had a narrow distribution of the maximal lateral dimension. On the other hand, SWNTs-based fluorescent CQDs were superficially oxidized and/or additionally coated with a thin layer of carbon. These CQDs had the capacity to aggregate when dispersed in water, showed a wider distribution of maximal lateral dimension and exhibited molecular-weight-dependent PL.[64]

The morphological characteristics of the CQDs synthesized by different methods using various precursors are summarized in Table 1 below.

Efforts were made to analyse the effects of the synthesis methods on the crystal structure through a statistical distribution (Fig. 5) for the research articles summarized in Table 2. The papers reviewed in this article have been taken as representative samples based on various CQDs techniques, precursors used and the CQD structure from the broad repertoire. Interestingly, the statistics show that the hydrothermal technique is the most frequently used method for the synthesis of CQDs. This must be due to the simple operating conditions, low energy consumption, and low-cost apparatus as concluded in various reports.[33,34,114] On the other hand, the electrochemical method is the least frequently used technique because of the small number of available precursors for this technique and the tedious purification process.[7,53] Also, the statistics show that the chemical oxidation method offers a high possibility of providing crystalline CQDs, followed by hydrothermal methods. It is important to note that many research groups do not specify the crystal structure in their study. As a consequence, it would be incorrect to draw any correlation between the crystal structure and the synthesis method. It has been mentioned in various studies that a large number of parameters like synthesis time, temperature, method, pH, precursors, *etc.*, affect the synthesis of CQDs,[13,14] but it becomes very important to statistically analyse these parameters so that optimised control conditions can be well described for reproducing CQDs with the same properties.

Table 1 Morphological comparative descriptions of CQDs synthesized by different methods using different precursors[a]

Year	Synthesis technique	Precursor(s)	Synthetic procedure (brief)	Av. size of CQDs (nm)	Crystallinity	Ref.
2006	Laser ablation	Graphite powder and cement	Q-Switched Nd:YAG laser ($\lambda = 1064$ nm, pulse frequency = 10 Hz) was incident on the carbon target which was kept in the presence of water vapour (through a water bubbler) using Ar as a carrier gas at 900 °C and 75 kPa. Finally, the CQDs were treated with PEG1500N	~5 nm	Not mentioned	5
2009	Pyrolysis followed by chemical treatment	Satellite-like polymer/F127/ silica composites	The subsequent high-temperature treatment of precursor and removal of silica carriers generated nanosized CQDs. Acid treatment and simple surface passivation finally resulted in water-soluble, multicolor photoluminescent CQDs	Distributed in the range of 1.5–2.5 nm	Amorphous	43
2009	Chemical oxidation	Carbohydrates (glucose)	The carbohydrates were dehydrated using concentrated sulfuric acid, producing carbonaceous materials that were then broken down into individual carbogenic nanoparticles by treatment with nitric acid. Finally, these nanoparticles were passivated using amine-terminated compounds (4,7,10-trioxa-1,13-tridecanediamine (TTDDA))	~5 nm	Crystalline	50
2010	Laser irradiation	Carbon nanoparticles	Nano-carbon material was dispersed in 50 ml of solvent (such as ethanol, acetone, or water) through ultrasonication and 4 ml of this prepared mixture was dropped into a glass cell. A Nd:YAG pulsed laser (pulse frequency = 30 Hz, pulse width = 8 ns, beam diameter = 8 mm with a second harmonic wavelength of 532 nm) was used to irradiate the mixture without focusing	Not mentioned	Amorphous	102
2010	Pyrolysis	Ethylenediamine-tetraacetic acid (EDTA)	EDTA-2Na was calcined in a tube furnace at 400 °C for 2 h at a heating rate of 10 °C min^{-1} in a N_2 atmosphere. The product was purified and the resultant homogeneous supernatant contained strongly fluorescent carbon nanoparticles	~7.5 nm	Amorphous	45
2011	Laser ablation	Graphite flakes	A Nd:YAG pulsed laser ($\lambda = 1064$ nm and power density of 5×10^6 W cm^{-2}) was irradiated (4 hours) on graphite flakes (average size 2 μm) dispersed in the poly(ethylene glycol) (PEG1500N) solution. Also, ultrasound was employed during the laser irradiation to expedite the movement of graphite powders	Sample A: 03.2 nm Sample B: 08.1 nm Sample C: 13.4 nm	Crystalline	62
2012	Microwave irradiation	Eggshell membrane (ESM) ashes	ESM was carefully peeled off from a fresh eggshell and washed thoroughly with a mass of deionized water to remove impurities. The cleaned ESM was dried and combusted in a muffle furnace at 400 °C for 2 h to form ESM ashes. ESM ashes were mixed in 5 ml of NaOH solution and heated in a domestic microwave oven for 5 minutes	~5 nm	Not mentioned	37
2012	Chemical oxidation	g-Butyrolactone	g-Butyrolactone was heated to 100 °C in air then dehydrated using concentrated sulphuric acid and subsequently neutralized with aqueous Na_2CO_3 solution and dialyzed against deionized water	9 ± 6 nm	Crystalline	120
2014	Chemical oxidation	Petroleum coke	Petroleum coke was oxidized with a mixture of concentrated H_2SO_4 and HNO_3 in a flask under ultrasonic conditions for 2 h, then heated under constant stirring in an oil bath at 120 °C for 12 h in reflux. They were finally filtered through a membrane and further dialyzed with 3500 Da MWCO for 72 h to get CQDs. The as-made CQDs were treated (functionalized) hydrothermally in ammonia to make N-CQDs	CQD: 5.0 nm N-CQD: 2.7 nm	Both were amorphous	51
2014	Electrochemical carbonization	Low-molecular-weight alcohols	Two Pt sheets (4×4 cm^2) placed at a distance of 3 cm were used as the working and counter electrodes. A calomel electrode mounted on a freely adjustable Luggin capillary acted as the reference electrode and NaOH/EtOH as electrolyte. The applied potential was varied	CQD(3.0 V): 2.1 nm CQD(4.5 V): 2.9 nm CQD(6.0 V): 3.5 nm CQD(7.5 V): 4.3 nm	Amorphous	53

Table 1 (*Contd.*)

Year	Synthesis technique	Precursor(s)	Synthetic procedure (brief)	Av. size of CQDs (nm)	Crystallinity	Ref.
			from 3–9 volts for 3–4 hours which resulted in the synthesis of CQDs of different sizes			
2015	Hydrothermal	Urea and *p*-phenylenediamine	Urea and *p*-phenylenediamine were dissolved in 50 ml of water, the solution was transferred into a poly(*para*-phenol)-lined stainless steel autoclave and heated at 160 °C for 10 h, followed by natural cooling and purification through column chromatography	~3 nm	Crystalline to amorphous (amorphousness increased with the degree of oxidation)	26
2015	Hydrothermal	Citric acid (CA) and ethylene diamine (EDA) or *N*-ethylethane-1,2-diamine (Et-EDA) or *N*-(2-aminoethyl) acetamide (Ac-EDA)	CA and EDA were dissolved in ultrapure water and the solution was transferred to a Teflon-lined autoclave and heated at 140 °C for 10 h. The reactors were then allowed to cool naturally to room temperature. The resultant CQD solution was evaporated to get CQD powder which was purified through chromatography. This resulted in the CQDs in different batches (each batch has a unique property)	Distributed in the range of 2–6 nm	Some batches were crystalline and some amorphous	108
2015	Hydrothermal	Citric acid (CA), ethylenediamine (EDA) and ammonia water (AW)	CA, EDA and various amounts of AW were mixed in 10 ml deionized water (DI-water), and then heated in a Teflon-lined autoclave at 160 °C for 3 h followed by quick cooling to room temperature. This results in well-dispersed CQDs solution	~3.7 ± 0.7 nm	Crystalline	126
2016	Pyrolysis	Citric acid (CA) and ammonia	CA and ammonia are dissolved in 10 ml distilled water and transferred into a porcelain boat and then heated in air at 200 °C for 3 h with a heating rate of 10 °C min^{-1} followed by ultrasonication and centrifugation	10.8 nm (distributed in the range of 7–15 nm)	Amorphous	47
2016	Hydrothermal	Citric acid (CA) and diaminonaphthalene (DAN)	CA and DAN were dissolved in an ethanol solution, followed by solvothermal treatment at 200 °C for different reaction times and different concentrations of precursors in the presence/absence of concentrated sulfuric acid. The reactants were allowed to cool naturally to room temperature followed by centrifugation. This results in CQDs of different dimensions	CQD(B): 1.95 nm (blue) CQD(G): 2.41 nm (green) CQD(Y): 3.78 nm (yellow) CQD(O): 4.90 nm (orange) CQD(R): 6.68 nm (red)	High degree of crystallinity	90
2016	Hydrothermal	Citric acid and amine precursors: ethylenediamine or hexamethylenetetramine or triethanolamine	Citric acid and one of an amine precursor were dissolved in 10 ml of water and placed in a Teflon-lined stainless steel autoclave and heated at 200 °C for 5 h. It is then allowed to cool to room temperature followed by filtration	E-CQDs, H-CQDs not measured due to agglomeration T-CQDs: <10 nm	Not mentioned	104
2016	Microwave irradiation	Citric acid, urea and formic acid	Precursors with different concentrations were dissolved in water and the solution is heated for 5 min in a microwave oven followed by centrifugation. This results in CQDs of different dimensions	CQD1: 0.5–2.0 nm (green) CQD2: 0.7–2.5 nm (red)	Not mentioned	116
2016	CVD	C_2H_2	The quartz tube was heated to 1000 °C in an Ar atmosphere. Then a mixture of C_2H_2/Ar was introduced into the reactor at a rate of 70/700 ml min^{-1} for 2 h. After the reaction, the quartz tube was cooled to room temperature under the protection of flowing Ar followed by sonication and filtration	3.5 nm (distributed in the range of 2–7 nm)	Crystalline	137
2016	Hydrothermal	Citric acid and *p*-phenylenediamine	Precursors were dissolved in 10 ml of deionised water and the resultant solution was heated at 200 °C for 5 h, with a heating ramp of 5 °C min^{-1}. This resulted in a brown-black solution that underwent centrifugation and CQDs were obtained, dispersed in water	Not measured due to agglomeration	Not mentioned	141
2016	Hydrothermal	Citric acid and urea		<2 nm		33

Table 1 (*Contd.*)

Year	Synthesis technique	Precursor(s)	Synthetic procedure (brief)	Av. size of CQDs (nm)	Crystallinity	Ref.
			CA and urea were dissolved in pure water at 25 °C for 10 min. The precursor solutions were transferred into a 50 ml stainless steel autoclave and heated at 130–180 °C while being stirred. The total concentration of CA and urea in the precursor solutions was varied and various N-CQDs were prepared		Partially crystalline	
2017	Hydrothermal	*o*-Phenylenediamine (0.36 g) or 4,5-difluoro-1,2-benzenediamine	*o*-Phenylenediamine or 4,5-difluoro-1,2-benzenediamine and tartaric acid was dissolved in ethanol. Resultant solutions were transferred to a Teflon-lined stainless-steel autoclave and heated to 180 °C for 8 h and naturally cooled to room temperature. Undoped CQDs and F-CQDs were purified *via* silica column chromatography	F-CQD: 5.52 nm Undoped-CQD: 5.18 nm	Amorphous	75
2017	Alkali-assisted ultrasonic chemical method	Glucose	Glucose was dissolved in 50 ml deionized water followed by the addition of an equal volume of NaOH solution (1 M). The solution was ultrasonicated (300 W, 40 kHz) for 4 h at room temperature. The resultant solution was treated with HCL, ethanol and $MgSO_4$	1–3 nm	Crystalline	138
2017	Pyrolysis	Citric acid and ethylenediamine	An aqueous solution containing citric acid and ethanediamine was sealed in an autoclave and pyrolyzed at 180 °C for 24 h	2–6 nm	Low crystallinity (amorphous)	137
2018	Microwave irradiation	*o*-Phenylene-diamine (*o*PD) and citric acid (CA)	*o*PD and CA were dissolved in 100 ml ultrapure water along with NaOH and the resultant solution was heated for 5 min at 125 °C by a microwave reactor (power of 300 W). The resultant product consists of a mixture of blue-emitting CQDs and the yellow-emitting organic (2,3-diaminophenazine) DAP	1.1 ± 0.3 nm or ∼1.1 nm	Not mentioned	41
2018	Hydrothermal	3,4,9,10-Perylenetetracarboxylic dianhydride (PTDA) and triethylamine	PTDA and triethylamine were dispersed in 4 ml of ultrapure water and the resultant solution was transferred to a Teflon-lined stainless-steel autoclave and heated to 220 °C for 48 h, followed by the chromatographic separation of CQDs of different sizes	3.01 ± 0.32 nm 4.32 ± 0.38 nm 4.82 ± 0.48 nm 5.50 ± 0.44 nm	Crystalline	109
2019	Laser cum thermal process	Poly(vinyl alcohol) (PVA) film doped with dense gold nanoparticles	The femtosecond laser pulses (repetition rate of 76 MHz, duration of 130 fs) were irradiated (through 60× objective lens (NA = 0.85) of an inverted microscope) on the AuNP/PVA film. As a result, the electrons in AuNPs are excited to the high-energy states and the thermalization of hot electrons causes the temperature rise of AuNPs and the surrounding environment. Once the environment temperature becomes higher than 160 °C, the intramolecular dehydration of PVA molecules occurs, leading to the formation of CQDs	Not mentioned	Not mentioned	98
2019	Pyrolysis	Fennel seeds (Swati seeds, India)	Ground greenish fennel powder was heated (in crucible cup) using a heat plate at a constant temperature of 500 °C for 3 hours. Subsequently, the crucible was allowed to cool down to room temperature and a dark-gray product was obtained. It was mixed with deionized water and processed to get CQDs	3.90 ± 0.91 nm	Crystalline	11
2019	Hydrothermal	Hydrothermal carbon biomass (hemicelluloses, lignin, chitosan, and cellulose)	Hydrothermal carbon was added to a Teflon-lined stainless-steel autoclave with 25 ml of NaOH (0.1 M). The chamber was sealed, and then O_2 was blown into the autoclave to remove air and keep the pressure at 1 MPa. The autoclave was heated at 160 °C (or 100 °C, 120 °C, 140 °C, and 180 °C) for 1 h with stirring (1000 rpm) followed by natural cooling, treatment with HCL and filtration	CQD(100 °C): 2.3 nm CQD(120 °C): 1.3 nm CQD(140 °C): 1.9 nm CQD(160 °C): 2.9 nm CQD(180 °C): 2.4 nm	Amorphous	34

Table 1 (*Contd.*)

Year	Synthesis technique	Precursor(s)	Synthetic procedure (brief)	Av. size of CQDs (nm)	Crystallinity	Ref.
2019	Electrochemical carbonization	Graphite rod	Two graphite rods were used as the working and counter electrode and ultrapure water as an electrolyte medium. Cyclic voltammetry scans at the potential range of ±2.0 V for 35 cycles. The resulting solution was centrifuged to remove aggregate particles and to get the desired CQDs	6 nm	Not mentioned	57
2019	Hydrothermal	Citric acid and DAN	Citric acid and DAN were dissolved in 100 ml of ethanol, sonicated and heated in a Teflon stainless steel autoclave for 9 hours at 200 °C. The resultant brown solution then cooled naturally to room temperature, and underwent separation by column chromatography	5 nm (distributed in the range of 3–6 nm)	Crystalline (with amorphous surface)	127
2019	Microwave irradiation	Ammonium citrate	Ammonium citrate solution was heated at 180 °C for 2 h in an oven followed by dissolving in 10 ml of deionized water. The resulting solution was centrifuged and dialysed to get the desired CQDs	~4 nm	Not mentioned	139
2019	Hydrothermal	Non-centrifugal cane sugar (Jaggery) and urea	Jaggery syrup was dissolved in 25 ml methanol and heated at 140 °C for 2.5 h in the Teflon-coated stainless steel pressure chamber of the autoclave. After the completion of the reaction, the autoclave was allowed to cool down naturally at room temperature and the resulting product (dark brown solution) was rinsed with dichloromethane (DCM) to remove unreacted particles and centrifuged to give CQDs	9.5 ± 1.9 nm	CQD: crystalline	135
			Jaggery syrup and urea were dissolved in 25 ml methanol and heated at 140 °C for 2.5 h in the Teflon-coated stainless steel pressure chamber of the autoclave. After the completion of the reaction, the autoclave was allowed to cool down naturally at room temperature and the resulting product (deeply black coloured solution) underwent centrifugation yielding N-CQDs		N-CQD: mediocre crystalline	
2020	Hydrothermal	Expired passion fruit shells (EPFS)	EPFS powder added in 40 ml ultra-pure water was put into a polytetrafluoroethylene lined reactor and heated for 3 h at 180 °C. The resultant brown solution was filtered followed by centrifugation and dialysis to obtain the CQDs	<5 nm	Amorphous (with weak crystalline phase)	35
2020	Hydrothermal	Chitosan powders	Chitosan powder was dissolved in 70 ml of pure water and the resultant solution was transferred into a 100 ml Teflon-lined autoclave at 180 °C for 0.5, 1, 2, 4, 8 and 16 h	2 nm (distributed in the range of 1.5–3 nm)	Amorphous	136
2020	Hydrothermal	DHB and hydrazine monohydrate	DHB (solid) and hydrazine monohydrate (liquid) were dissolved in a mixture of ethanol and NH_4OH (100 : 50 ml). The mixture was then heated for 7 h at 200 °C in a Teflon-lined stainless-steel hydrothermal chamber under continuous stirring. The resulting solution is cooled to room temperature and subjected to column chromatography to yield hollow N-CQDs. On the other hand, CQDs were synthesized by hydrothermal treatment of citric acid and NaOH, followed by centrifugation	N-CQD: 7–17 nm Average size 11 nm CQD: ~10 nm	N-CQD: amorphous CQD: crystalline	129
2020	Hydrothermal	Citrus lemon juice	Filtered fresh lemon juice (20 ml) and ethylenediamine (2 ml) co-reagent were mixed in a 100 ml hydrothermal autoclave and kept in a furnace at 200 °C for 3 h. The as-obtained black paste was cooled down to room temperature and then dissolved in 15 ml of water followed by multi-step centrifugation. Finally, the brown-yellow supernatant was passed through column chromatography to give the desired N-CQDs	3 nm (distributed in the range of 1–6 nm)	Amorphous	112
2020		Waste cotton linter		10.14 nm	Amorphous	113

Table 1 (*Contd.*)

Year	Synthesis technique	Precursor(s)	Synthetic procedure (brief)	Av. size of CQDs (nm)	Crystallinity	Ref.
	Microwave irradiation		Acidic cotton linter waste was mixed with 20 ml water in a quartz tube and the tube was placed in a Teflon reactor, which was then heated in a microwave for 5 min at a maximum power level of 400 W. The resultant product was filtered and centrifuged to give the desired CQDs			
2020	Microwave irradiation	Roasted chickpeas	Roasted chickpeas fine powder (2 g) was added in 40 ml of ultra-pure water and ultrasonicated for 15 min. This mixture was then heated in a microwave oven at 350 watts for 2 min. The resultant solution was cooled to room temperature and followed by centrifugation at 3000 rpm for 15 min. Then filtration followed by re-centrifugation results in CQDs	8.7 nm (distributed in the range of 4.5–10.3 nm)	Amorphous	42
2021	Hydrothermal	Cambuci juice (Campomanesia phaea)	Fruit paste (15 g) was added in 15 g of distilled water in the autoclave. Then, the pH was corrected with two bases: sodium hydroxide and ammonium hydroxide. Then the mixture was heated for 6 hours at 190 °C followed by purification through centrifugation and filtration to give the CQDs	3.7	Amorphous	114
2021	Hydrothermal	Microcrystalline cellulose, hydroxymethylfurfural, and furfural	The hydrothermal reactor was loaded with a 45 ml solution containing 10% (w/v) of precursor and the rest was deionized (DI) water. The reactor is closed and heated at 220 °C for a residence time of 30 min. After that, the heater was turned off and the reactor was rapidly cooled to room temperature (∼30 °C) by placing it in an ice-water bath. The obtained solution was purified through filtration and centrifugation to give the CQDs. Different CQDS were obtained for the three different precursors	6.36 ± 0.54 nm (microcrystalline cellulose) 5.35 ± 0.56 nm (hydroxymethylfurfural) 3.94 ± 0.60 nm (furfural) (Diameter range: 2–9 nm)	Not mentioned	115
2021	Microwave	Ethylenediaminetetraacetic acid (EDTA) and 4,7,10-trioxa-1,13-tridecanediamine (TTDDA)	Predetermined amounts of EDTA and TTDDA were completely dissolved in 10 ml of deionized water and the resultant precursor solution was heated in the microwave oven for 5 min. The obtained dark-brown solid residues were cooled to room temperature naturally, then 100 ml of deionized water was added to form a crude dark-brown CQD solution, followed by centrifugation and filtration	<20 nm	Amorphous	117
2021	Microwave	Citric acid	Citric acid (100 g) was dissolved in 100 ml of deionized water and this solution was heated in a microwave oven at high potency for 8 min. The obtained residue was purified by repeated dialysis in ultrapure water for 2 days and finally, the solution was dried using a hot-air oven to produce solid structures of CQDs	3.81 nm diameter range: 1.5–4.5 nm	Crystalline	118

[a] Important: "not mentioned" in the above table includes the paper and the ESI of that paper (wherever present).

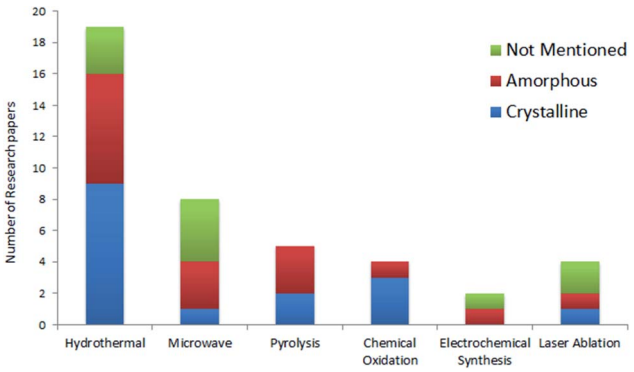

Fig. 5 Types of CQDs reported by various research groups for different synthesis methods.

4. Optical properties of CQDs

It was the optical properties of CQDs that drew the immediate attention of researchers towards them after their discovery. Whether synthesized through the bottom-up or top-down approach, CQDs show excellent optical properties, namely absorbance and photoluminescence (PL), which are useful in many applications. This section briefly covers the optical properties of CQDs.[23]

4.1 Absorption

In the UV region of each curve, a single peak was observed at 255 nm with a shoulder at 282 nm, corresponding to the π–π* transitions of C=C and C=N bonds, respectively, in the aromatic rings, which do not typically generate PL.[20,26]

An absorption peak at around 335 nm corresponds to the n–π* transition of the C=O bond,[25] while the visible absorption band is attributed to the amino groups on the surface of N-CQDs.[47]

Typically, CQDs exhibit strong absorption in the ultraviolet (UV) region (250–350 nm) and a weak absorption tail in the visible spectrum. The entire absorption spectrum is distributed into three bands, namely, (i) the core band, (ii) edge or molecular band, and (iii) surface band, as shown in Fig. 5.[66]

The absorption peak appears at around ~240 nm due to the π–π* transition of C=C bonds (core-sp^2 carbon network), whereas the peaks at around ~340 nm correspond to the n–π* transitions of C=O and C=N bonds (N- and O-containing structures present as functionalities) at the edge of carbon structures as shown in Fig. 6.[25] The extended long tail in the visible region of the spectrum arises from the lower energy surface states (surface functional groups).[65] Sometimes the absorption band is also seen in the visible region and that is related to the functional groups such as the amino group.[47]

Sometimes the shoulder is also observed at ~280 nm due to the π–π* transition of C=N bonds in aromatic rings. The peaks/shoulder of the UV region arising from π–π* transitions typically do not contribute to emission.[20,26] Broad spectral features in the absorption spectrum of CQDs are due to the surface defects ingrained in CQDs.[66]

The optical properties of CQDs can be modified by (i) passivating agents, (ii) functional groups and (iii) doping/co-doping with heteroatoms.[67] Surface passivation involves the formation of a thin insulating (protective) layer of coating materials such as oligomers (poly ethylene glycol (PEG)), thionyl chloride, thiols and spiropyrans, *etc.*, on the surface of carbon quantum dots. This protective layer shields CQDs from the adhesion of impurities, and provides stability, long usage of CQDs,[63] and eliminates the dissipation of photoinduced carriers from surface sites, which improves their fluorescence intensity.[68] In contrast to the bare counterparts, surface-passivated CQDs become highly optically active, displaying significant PL from the visible to near-infrared spectral regions.[68] Surface passivation enhances the quantum yields of carbon quantum dots to the maximum of 55–60%.[67] Peng *et al.* observed that the absorbance of CQDs increased to longer wavelengths in the range of 350–550 nm after surface passivation with 4,7,10-trioxa-1,13-tridecanediamine (TTDDA).[69] Surface functionalization can be accomplished by coordination, π–π interactions and covalent bonding. Since the CQDs are oxygenous in nature, they are feasible for covalent bonding with functionalizing agents.[67]

Surface functionalization introduces functional groups like carbonyl, carboxyl, hydroxyl, amines, *etc.*, on the surface of CQDs, which can greatly contribute to the absorption and emission in the UV-visible region. CQDs rich in surface oxygen groups are usually p-doped due to the larger electronegativity of oxygen atoms relative to carbon atoms. Replacing oxygen functional groups on the CQDs surface with nitrogen-containing groups can readily transform CQDs into an n-type semiconductor.[70]

Compared to bare CQDs, the functionalized ones exhibit excellent photo-reversibility, high stability, good biocompatibility and low toxicity. Surface passivation/functionalization stabilises the defects and thus facilitates more effective radiative recombination of surface-confined electrons and holes.[67] A schematic illustration of surface modification is shown in Fig. 7. Yongqiang Dong *et al.* used branched polyethylenimine during the synthesis of CQDs, which served as both passivation and functionalization agents and thus no additional modification steps were required during the post-synthetic treatments.[71]

Doping/co-doping with heteroatoms (like nitrogen (N), boron (B), fluorine (F), phosphorous (P) and sulphur (S)) is also an effective way to alter the absorption spectrum of CQDs. The dopant alters the π–π* energy level (associated with core-sp^2 carbon network) and thus modifies the electronic structure, bandgap and hence the optical properties of CQDs.[72]

Darragh Carolan *et al.* noticed that the bandgap of the CQDs increase gradually from 2.2 to 2.7 eV with the increase in the N-dopant concentration.[60] On the contrary, various studies have shown that nitrogen-doping results in CQDs size reduction (notable redshift of the optimal excitation wavelength and the strongest emission peak), which may depend on the distribution of varying sizes of N-CQDs and the features of multi-surface emission points.[54]

JingJing Yu *et al.* calculated 2.15 eV as the bandgap of undoped CQDs, which decreased to 2.14, 1.94, and 1.54 eV with

Table 2 Comparative emission characteristics of CQDs synthesized by various research groups

Synthesis by group	Synthesis technique	% QY[a] (highest)	Emission characteristics	Emission caused by type (band, surface states, *etc.*)	Doping/surface passivation	Prepared CQDs employed in application	Ref.
Ya-Ping Sun	Laser ablation	>10%	Blue emission @ 400 nm excitation Excitation-dependent emission: emission intensity decreases and the emission peak red shifts as the incident wavelength increases	Surface states and quantum confinement	Surface passivation	No	5
Ruili Liu	Pyrolysis followed by chemical treatment	14.70%	Blue emission @ 365 nm excitation Excitation-dependent emission: the emission intensity varies and the emission peak red shifts as the excitation wavelength increases from 320–500 nm	Surface states and quantum confinement	Surface passivation	Bioimaging	43
Hui Peng	Chemical oxidation	13%	Blue emission @ 360 nm excitation Excitation-dependent emission: the emission intensity varies and the peak red shifts as the excitation wavelength increases beyond 360 nm	Surface states and quantum confinement	Surface passivation	No	50
Xiangyou Li	Laser ablation	—	Blue emission @ 360 nm excitation Excitation-dependent emission: the emission intensity varies and the peak red shifts (from 400–520 nm) as the excitation wavelength is increased from 300–480 nm	Surface states and quantum confinement	Surface passivation	No	102
Dengyu Pan	Pyrolysis	40.6%	Blue emission @ 365 nm excitation Excitation-dependent emission: the emission intensity decreases and peak red shifts (from 425–510 nm) as the excitation wavelength is increased from 320–500 nm Emission is also sensitive to pH, solvent and spin	Large HOMO–LUMO gap of small sp^2 clusters	N-Doping	No	45
Shengliang Hu	Laser ablation	Sample A: 12.2% Sample B: 06.2% Sample C: 01.2%	Blue emission @ 365 nm excitation (all 3 samples) Excitation dependent emission in all the samples: the emission intensity and peak varies with the excitation wavelength	Quantum confinement	No	No	62
Qi Wang	Microwave irradiation	14%	Blue emission @ 365 nm excitation Emission intensity increases with pH	Not mentioned	Not mentioned	A fluorescent probe for sensitive turn-on sensing of glutathione	37
Mingbo Wu	Chemical oxidation + hydrothermal (for N-CQD)	CQD: 8.7% N-CQD: 15.8%	Excitation-dependent emission in both CQDs CQD: yellow emission @ 340 nm excitation. The emission intensity varies and peaks red-shift from 480 to 600 nm as the excitation wavelength increases from 320 to 580 nm N-CQD: blue emission @ 340 nm excitation. The emission peak remains at 475 nm when excitation wavelength increases from 320 nm to 400 nm. As the excitation wavelength further increases to 520 nm, the maximum emission wavelength shows a red-shift from 480 to 540 nm	Quantum confinement and surface states	N-Doping and surface passivation (N-CQD)	No	51

Table 2 (*Contd.*)

Synthesis by group	Synthesis technique	% QY[a] (highest)	Emission characteristics	Emission caused by type (band, surface states, *etc.*)	Doping/surface passivation	Prepared CQDs employed in application	Ref.
Jianhui Deng	Electrochemical carbonization	CQD(6.0 V): 15.9% CQD(3.0 V): 4.0% CQD(4.5 V): 9.1% CQD(6.0 V): 15.9% CQD(7.5 V): 5.0%	Blue emission @ 365 nm excitation (by all 4-sets of CQDs synthesized under different potentials) The intensity of emission is very low for CQD (3.0 V), it increases for CQD (4.5 V), and reaches a maximum for CQD (6.0 V) and then decreases for CQD (7.5 V) Excitation dependent emission: the emission intensity varies and emission peak red shifts as the excitation wavelength increases from 300 nm–500 nm The PL intensity of the CQDs were independent of pH under acidic conditions, but decreased under basic conditions	Quantum confinement and surface states	Undoped, surface passivation not required	Bio-imaging of Hela cells	53
Hui Ding	Hydrothermal	~35%	Blue, green, yellow and red emission @ 365 nm excitation (by selected 4-sets of CQDs having different degrees of oxidation) Excitation-dependent emission: each of the 4 samples have a specific emission centre that does not change with the excitation wavelength but the intensity varies	Surface states	N-Doping	*In vivo* bioimaging of mice	26
Yubin Song	Hydrothermal	77.07% (Et-EDA CQD) 46.36% (Ac-EDA CQD)	Blue emission @ 360 nm excitation (for Et-EDA CQDs) Excitation-dependent emission: the emission intensity and peak shifts (from blue to green) as the excitation wavelength is increased from 300–500 nm	Molecular states or molecular fluorescence and core states	N-Doping	Bio-application	108
Xugen Han	Hydrothermal	84.80%	Blue emission @ 365 nm excitation Excitation-independent emission: almost no shift in emission peak (peak appears at around 430 nm) but the emission intensity decreases as the excitation wavelength is increased from 300–390 nm Emission intensity is constant for pH values 4–8 but it decreases for too basic or acidic medium	Surface states	N-Doping and surface passivation	Silicon-nanowire solar cells	130
Hao Wang	Pyrolysis	~36%	Blue emission @ 365 nm excitation Excitation-dependent emission: the emission intensity varies and peak red shifts (from 425–510 nm) as the excitation wavelength is increased from 300–500 nm	Surface states	N-Doping	QDSC	47

Table 2 (*Contd.*)

Synthesis by group	Synthesis technique	% QY[a] (highest)	Emission characteristics	Emission caused by type (band, surface states, *etc.*)	Doping/surface passivation	Prepared CQDs employed in application	Ref.
Fanglong Yuan	Hydrothermal	~75% (blue CQD)	Blue, green, yellow, orange and red emission @365 nm excitation (5 different colors of CQDs were prepared by modification in the synthesis process with the highest QY for blue CQDs) Excitation independent emission: the emission peak intensity varies but the position remains the same, irrespective of the excitation wavelength for all the CQDs	Quantum confinement (bandgap emission)	N-Doping, surface passivation	LED	90
Julian Schneider	Hydrothermal	53% (ethylenediamine-CQDs)	Blue emission @ 320 nm excitation (by all 3 types of CQDs) Excitation dependent emission: the emission peak intensity and peak position changes as the excitation wavelength varies from 300–480 nm	t-CQDs: quantum confinement (core bandgap emission) and surface states e-CQDs h-CQDs: molecular fluorescence and surface states	N-Doping	No	104
Gancheng Zuo	Hydrothermal	F-CQD: 31% Undoped CQD: 28%	Excitation-dependent emission in both CQDs F-CQD: yellow emission @ 360 nm excitation Emission varies from 550–600 nm as the excitation varies from 360−580 nm Undoped-CQD: green emission @ 360 nm excitation Emission varies from 480–550 nm as the excitation wavelength varies from 360–500 nm	Surface states	F-CQD: F-doping, N-doping	Red cell imaging and sensitive intracellular Ag + detection	75
Hinterberger Vanessaa	Microwave irradiation	5.4%	Blue emission @ 400 nm excitation The emission spectra is also pH sensitive	Molecular fluorescence	Surface passivation	White LED	41
Zexi Liu	Hydrothermal	79.1% (blue)	Blue to infrared @ 365 nm excitation (by different sets of CQD) Out of 25 sets of CQD solutions, some sets exhibited excitation-independent emission and some exhibited excitation-dependent emission	Quantum confinement and surface states	N-Doping	No	109
Akansha Dager	Pyrolysis	9.5%	Blue emission @ 365 nm excitation Excitation-independent emission: no shift in the PL peak position as the excitation wavelength varies from 240–340 nm only the peak intensity decreases Changing the pH from acidic to basic resulted in a gradual increase in the PL intensity of CQD	Surface states	Undoped, surface passivation not required	No	11

Table 2 (*Contd.*)

Synthesis by group	Synthesis technique	% QY[a] (highest)	Emission characteristics	Emission caused by type (band, surface states, *etc.*)	Doping/surface passivation	Prepared CQDs employed in application	Ref.
Yushuang Zhao	Hydrothermal	16.6%	Blue-green emission @ 365 nm excitation Excitation-dependent emission: the emission intensity varies and peak gradually red shift (from 443–489 nm) as the excitation wavelength increases from 320–400 nm. The peak also red shifted (342–379 nm) as the excitation wavelength increased from 400–540 nm. These CQDs exhibited the upconversion emission (anti-Stokes type emission) as the excitation wavelength varied from 760–940 nm	Surface states and carbon core states	Undoped, non-passivated	Fluorescent Cu^{2+} nanoprobe	34
Takashi Ogi	Hydrothermal	39.7%	Blue emission @ 365 nm excitation Emission intensity varies with the heating time/temperature and initial precursor concentration Emission is affected the most by the temperature, and the emission intensity first increases and then decreases with the temperature	Not specified	N-Doping, surface passivation not done	Polyvinyl alcohol (PVA) nanofibers	33
Rabia Riaz	Hydrothermal	70%	Green emission @ 360 nm and 400 nm Excitation-independent emission: almost no shift in the emission peak (peak appears at around 520 nm) but the emission intensity decreases as the excitation wavelength increases from 360–400 nm	Quantum confinement (bandgap emission) and surface states	N-Doping	DSSC	131
Hang Yang	Hydrothermal	1.8%	Yellow-green emission @ 360 nm excitation Excitation-dependent emission: the emission intensity varies and the peak shifts as the excitation wavelength varies from 300–450 nm	Surface states	—	No	35
Qiming Yang	Hydrothermal	Not mentioned	Blue emission @ 365 nm excitation Excitation-dependent emission: the emission intensity varies and peak shifts as the excitation wavelength increases from 310–550 nm Also, as the excitation wavelength changes from 700 to 1000 nm, the PL emission peaks are located in the range from 450 to 540 nm (up-conversion transition or a multi-photon absorption process)	Surface states	N-Doping	DSSC	140
Mumtaz Ali	Hydrothermal	61% (red)	Red emission @ 360 nm excitation Excitation-independent emission is attributed to the single-transition mode PL of the NR-CQDs, which resulted from the conjugated structure	Quantum confinement and surface states	N-Doping	Crystalline silicon solar cells	133
Lili Tong	Hydrothermal	90.49% (green)	Green emission @ 400–520 nm excitation Excitation-independent emission: no shift in the emission peak (peak appears at around 530 nm) but the emission intensity increases and then decreases as the excitation wavelength increases from 400–520 nm	Dehalogenation crosslinking and structural reorganization of reactants	N-Doping, surface passivation	Lysosome imaging	152

Table 2 (*Contd.*)

Synthesis by group	Synthesis technique	% QY[a] (highest)	Emission characteristics	Emission caused by type (band, surface states, *etc.*)	Doping/surface passivation	Prepared CQDs employed in application	Ref.
Aysel Başoğlu	Microwave irradiation	1.8%	Blue emission @ 265 nm excitation Excitation-dependent emission: the emission intensity varies and peak shifts as the excitation wavelength increases from 300–400 nm	Not specified	Undoped, surface passivation not required	Determination of Fe^{3+} ions	42
Haitao Lin	Microwave irradiation	85%	Blue emission @ 355 nm excitation Excitation-dependent emission: the emission intensity varies and peak red shifts as the excitation wavelength increases from 300–400 nm	Surface states	Surface functionalization while synthesis	Dopamine fluorescence probe and cellular imaging	153
Lei Tian	Chemical oxidation	0.43%	Blue emission @ 310 nm excitation	Surface states	Surface functionalization	No	154

[a] QY is irrespective of the excitation wavelength.

Fig. 6 Different bands of the absorption spectrum of CQDs (this figure has been adapted/reproduced from ref. 66 with permission from the American Chemical Society, Copyright 2017).

Fig. 7 Schematic illustration of the surface modification of CQDs (this figure has been adapted/reproduced from ref. 94 with permission from the Royal Society of Chemistry, Copyright 2019).

the doping of pyridine N, amino N, and C=O groups, respectively. Dipayen Sen *et al.* observed that the doping of boron (B) in CQDs introduced new electronic states and pulled down the conduction band minimum (CBM), resulting in the intense reduction of the CQDs bandgap (by ~48–57%).[49]

In 2014, Zhou *et al.* proposed that phosphorus can form substitutional defects in CQDs, thus behaving as an n-type donor. Based on this, they synthesized phosphorus-doped CQDs (P-CQDs) *via* a hydrothermal process for different reaction time periods (1, 3, 5, and 9 h at 200 °C) using phosphorus tribromide (P source) and hydroquinone. The P-dopant in CQDs showed strong blue emission (25.1% QY) in comparison to the un-doped/pristine CQDs (3.4% QY), as shown in Fig. 8.[73]

In 2015, Bourlinos *et al.* observed that B-doped CQDs have a substantially enhanced nonlinear optical response in contrast to the un-doped CQDs.[74] In 2017, Zuo *et al.* prepared F-doped CQDs *via* a hydrothermal method (180 °C for 8 h) from citric acid (as the C source), and 4,5-difluorobenzene-1,2-diamine (as the F source). F atoms were chosen because they possess high

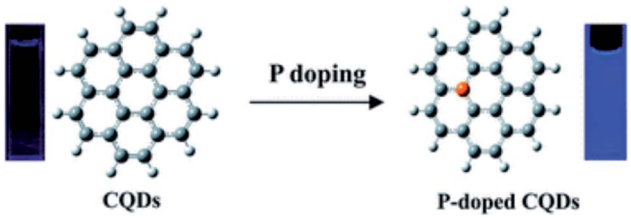

Fig. 8 Changes in the fluorescence properties of CQDs after p-doping (this figure has been adapted/reproduced from ref. 73 with permission from the Royal Society of Chemistry, Copyright 2014).

stability in the aromatic ring. They also prepared un-doped CQDs for comparison and observed that (i) the F-CQDs exhibited two maximum emissions: one at 550 nm (yellow fluorescence) when excited by wavelengths of 360 to 500 nm, and another at 600 nm (red fluorescence) when excited by wavelengths of 540 nm to 580 nm. This was quite different from the excitation-dependent feature of un-doped CQDs, where (ii) a striking red shift (more than 50 nm) in emission wavelength was measured due to the F-doping, and (iii) F- CQDs displayed enhanced QYs of 31% and 14%, corresponding to the emission wavelengths of 550 nm and 600 nm, respectively. The un-doped CQDs exhibited QYs of only 28% and 11% at emission wavelengths of 500 nm and 550 nm, respectively.[75] The emission behaviours of the as-synthesized CQDs are shown in Fig. 9.

This doping method has been proved to be an effective way to enhance the electron transfer and thus the performance of the CQDs as photocatalysts. Wu *et al.* synthesized Cu–N co-doped CQDs through a one-step pyrolytic synthesis and they observed that the electron accepting/donating abilities of CQDs could both be enhanced, together with the increased electric conductivity. These merits ultimately facilitated the entire electron-transfer process in CQDs and further improved the photocatalytic oxidation of 1,4-dihydro-2,6-dimethylpyridine-3,5-dicarboxylate (1,4-DHP).[76]

In 2018, Meiling *et al.* reported the highest QY of 90% for the N-doped CQDs after optimizing (i) the precursors, (ii) the reaction duration, (iii) excitation wavelength and (iv) the pH-dependence of the photophysical properties of N-CQDs.[77]

4.2 Photoluminescence

Photoluminescence (PL) is the emission of light from a material upon the absorption of light (photon). There are two types of PL, namely, fluorescence and phosphorescence. Fluorescence is prompt photoluminescence that occurs very shortly after the photoexcitation of a substance. In this type of PL, the radiative transition does not require a change in the spin multiplicity. On the other hand, phosphorescence is long-lived photo-luminescence that continues long after the photo-excitation has ceased. In this type of PL, the radiative transition involves a change in the spin multiplicity. It is fluorescence that is often seen in the CQDs and thus, the term PL is used synonymously with fluorescence unless explicitly specified.

Typically, the main emission band of CQDs is located at ~450 nm (blue) when excited in the n–π* absorption band (~350 nm) and this emission is quite intense,[65] while the excitation in the far UV (~250 nm) band (π–π* absorption transition) typically returns very low, or shows no photoluminescence.[20,26] The distinguishing emission property of CQDs is that its photoluminescence spectrum is mostly excitation-wavelength dependent, where the emission undergoes (i) a bathochromic shift as the excitation (beyond 400 nm) red shifts, and (ii) a decrease in intensity because of low optical absorption in the visible range.[65]

According to previous reports, most of the CQDs emit blue to yellow irrespective of the top-down or bottom-up methods used. Moreover, the strongest luminescence is often blue or green.[78,79] Wang *et al.* reported that functional oxidized carbon groups contribute to green emission in CQDs.[80,81] In 2018, Sun *et al.* prepared three kinds of CQDs using citric acid and urea for different precursor mass ratios (citric acid : urea) and methods. The optical characteristics of all the prepared CQDs are shown in Fig. 10. They reported that the oxidized functional groups (containing C=O) are responsible for the green luminescence (the carboxyl groups play the key role in it) and the blue

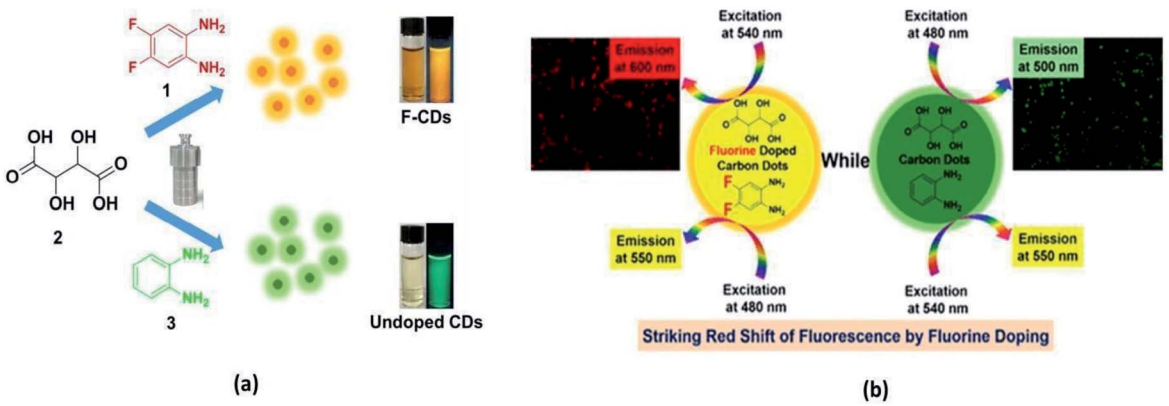

Fig. 9 (a) Synthesis of F-CQDs (yellow) and un-doped CQDs (green) by a hydrothermal process. (b) Comparison of excitation/emission in both F-CQDs and un-doped CQDs (this figure has been adapted/reproduced from ref. 75 with permission from the American Chemical Society, Copyright 2017).

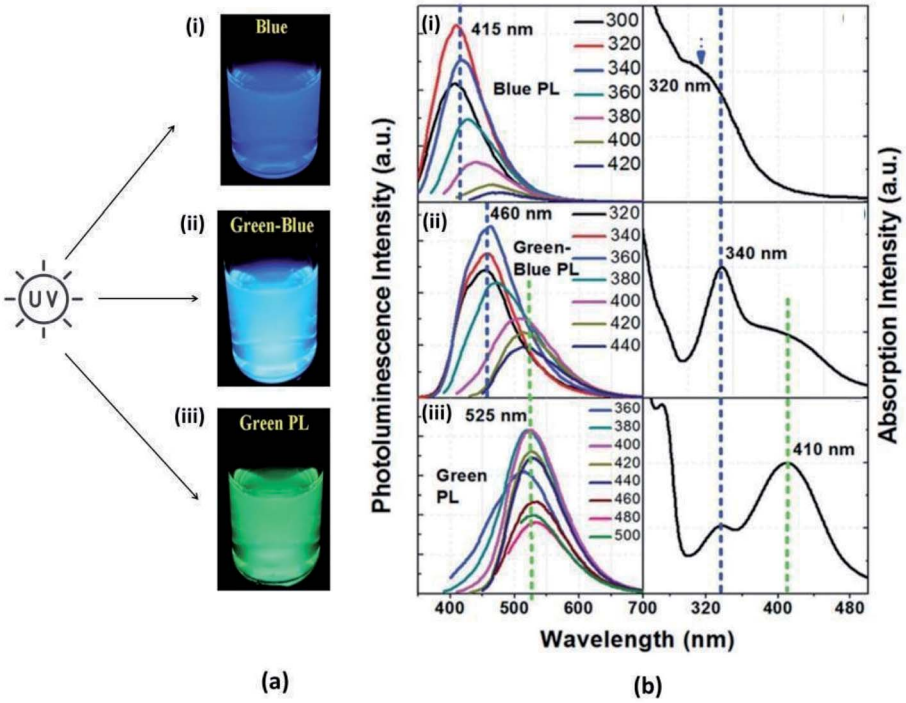

Fig. 10 (a) Fluorescence images of CQDs synthesized by (i) a hydrothermal method (1 : 1), (ii) microwave method (1 : 1), (iii) microwave method (1 : 2) under UV radiation (excitation 365 nm); (b) the absorption and emission spectra of CQDs in (i), (ii) and (iii) (this figure has been adapted/reproduced from ref. 82 with permission from the Royal Society of Chemistry, Copyright 2018).

emission must be caused by the hydroxyl surface functional groups.[82]

Interestingly, the PL properties of the CQDs can be tuned by modifying the surface states, varying the synthesis route, doping with a heteroatom, choosing different precursors, and various other ways.[7]

As per the review by Mintz *et al.*, QY largely depends on the synthesis conditions, with the highest values being recorded in bottom-up technique approaches (up to 99%), whilst the QY in top-down routes is typically not larger than 15% (but a value of 50% was reported for Zn-doped CQDs prepared by laser ablation). The lifetime of the fluorescence was in the nanosecond range (4–15 ns), and no significant differences were recorded with the different synthetic approaches (with very few exceptions).[83]

4.2.1 Fluorescence. PL is one of the most alluring features of CQDs, both from the fundamental and application points of view. Unfortunately, it is simultaneously the most controversial topic from an understanding point of view because the luminescence mechanisms of CQDs are not precisely clear due to incomplete experimental and theoretical understanding. This considerably impedes the advancement of CQDs with preferred optical properties.[84]

The majority of researchers observed that CQDs exhibit excitation-dependent emission behaviour, whereas independent excitation-emission (contrary behaviour) has also been reported by several researchers. Generally, this disagreement in the PL mechanism of CQDs originates due to the different phenomena observed in the same kind of material. Thus, the researchers are focussing on pursuing the origin of the excitation-dependent photoluminescence. However, this chase is inherently difficult because of the diversity of preparation methods, precursors and other parameters that affect both the structure and the composition of the CQDs.[65]

With the evolution of CQDs, theories related to the origin of PL have also gradually matured. To date, three theories that explain the excitation-dependent PL have been considered the most, namely, (1) size-dependent emission (quantum confinement effect or the core emission), which is related to the conjugated π-domains of the carbon core; (2) the surface states, which are related to the presence of functional groups connected to the carbon backbone; (3) the molecular state, where the emission originates from free or bonded fluorescent molecules.[25,65,68,83]

(1) Size-dependent emission (quantum confinement effect) or the core emission. Several published research articles suggest that quantum confinement (QC) in CQDs is responsible for the excitation-dependent emission and some of them give strong evidence for it.

The QC theory is very natural to consider because metal-based quantum dots are well known to possess emission based on this phenomenon. This phenomenon is related to the size of the nanoparticles[25] and typically, the size distribution of the synthesized CQDs is <10 nm, which is comparable to the quantum size range.[83]

When the size of CQDs is smaller than their exciton radius, they would exhibit particle size-dependent PL behaviour, which

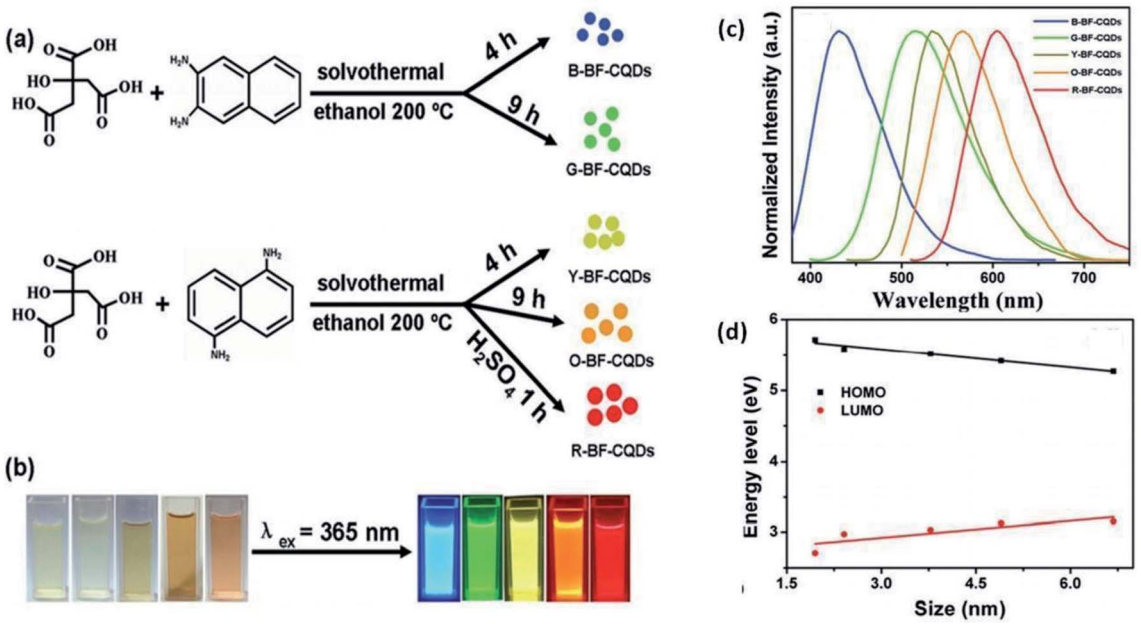

Fig. 11 (a) Synthesis of MCBF-CQDs *via* hydrothermal synthesis from CA and DAN under different synthetic conditions. (b) The synthesized MCBF-CQDs under daylight (left) and UV light (right). (c) Normalized fluorescence of blue, green, yellow, orange and red CQDs. (d) Variation of the HOMO and LUMO energy levels with the size of MCBF-CQDs (this figure has been adapted/reproduced from ref. 90 with permission from Wiley-VCH, Copyright 2017).

essentially originates from the energy band-gap transition of conjugated π-domains in the sp^2-carbon-constructed core.[84]

A series of theoretical calculations have demonstrated the relationship between PL emission and sp^2-domain size. It is worth mentioning that the size of sp^2-domains (core) is the main controlling factor of the quantum confinement effect, though the particle size seemingly shows a similar algebraic relation with the PL emission.[68]

Carbon-core states participate in the PL of CQDs through the radiative recombination of electrons and holes in the core, resulting from the π–π* transitions of sp^2 clusters assisted by the quantum confinement effect.[65,85]

The core emission is usually at shorter wavelengths with low QY but the presence of graphitic nitrogen and hybridized oxygen functional groups with the core[85] allows the red-shifting of emission properties.[65]

Li *et al.* suggested that the excitation-dependent emission is due to the optical selection of differently sized nanoparticles for different excitation wavelengths.[86]

Bo Zhi *et al.* synthesized CQDs from malic acid with the size distribution ranging from 6.2 ± 2.0 to 9.2 ± 1.7 to 15.6 ± 6.0 nm. These CQDs correspond to decreasing optical bandgap energies from 2.97 eV to 2.91 eV to 2.21 eV, respectively. They observed the red-shifts in emission with the increase in the excitation wavelength.[87] Yang *et al.* generated a series of highly crystalline nitrogen-doped CQDs by carefully controlling the synthesis conditions. The authors observed that along with the emission red-shift, the average CQD diameters increased from 1.95 nm (blue CQDs) to 6.68 nm (red CQDs). They deduced that the red shifting emission revealed the bandgap transitions in CQDs derived from the quantum confinement effect.[83,87,88] Kang *et al.* also reported the red-shift in the emission from the UV to the near-IR as the dimensions of CQDs increased from 1.2 to 3.8 nm and correlated with the phenomenon of the quantum-confinement of the nanoparticles.[89]

Yuan *et al.* successfully synthesized bright multicolour (blue to red) bandgap fluorescent CQDs (MCBF-CQDs) through hydrothermal synthesis with a QY of up to 75% for blue fluorescence. This was done by controlling the fusion and carbonization of citric acid (CA) and diaminonaphthalene (DAN) with a unique amino-substituted rigid carbon skeleton structure (nitrogen source). The prepared MCBF-CQDs were highly crystalline, highly surface-passivated and nitrogen-doped. They chose five different conditions and thus attained the CQDs with five different average sizes (different bandgaps and different colours). The CQDs with the average size of 1.95 nm, 2.41 nm, 3.78 nm, 4.90 nm and 6.68 nm resulted in blue, green, yellow, orange and red fluorescence, respectively, when excited by UV light (365 nm) as shown in Fig. 11. The gradual increase in the size of CQDs was consistent with the red-shifted PL wavelength and the first excitonic absorption peak wavelength. This clearly reveals that the emission in these CQDs is due to the bandgap transitions that originate from the quantum confinement effect. They effectively took advantage of the excellent bandgap emission of these MCBF-CQDs and for the first time, fabricated monochrome LEDs from blue to red by directly using MCBF-CQDs as an active emission layer. The L_{max} reached about 136 cd m^{-2} for blue LEDs, which is the best performance ever reported for CQD-based monochrome electroluminescent LEDs. The LEDs all showed substantial stable EL and voltage-independent emission color, which are of great significance for display and lighting technology.[90]

Though some researchers give strong evidence for QC theory, several published papers do not have the data to support this theory, thus it is not the most common theory. In recent years, most researchers have not used quantum confinement as the only factor for the PL mechanism of CQDs but it is often used in conjunction with another concept.[25]

(2) Surface states. The theory of surface states is frequently used and thus received general acceptance for the PL mechanism of CQDs. According to this theory, it is the surface state that controls the emission of the CQDs. Solid-state physicists explained that the surface state controls the electronic properties/structure of semiconductors.[91] Sun, *et al.* applied this concept to CQDs for the first time in 2006.[5] Semiconductor surface states are classified into intrinsic and extrinsic surface states. Intrinsic surface states are electronic states that occur due to the termination of the crystal lattice (clean and well-ordered surface) facing the environment (semiconductor/vacuum interface).

Intrinsic surface states are modelled computationally either as Shockley or Tamm states. Shockley surface states are modelled using a "nearly-free electron" approximation and can be used accurately for narrow-gap semiconductors (bandgaps of approximately 1–2 eV). Tamm states are modelled using the "tight bound" approach, where electronic states are expressed as a linear combination of atomic orbitals (LCAO). These states are quite accurate for broad gap semiconductors (2–4 eV bandgaps).[25]

Extrinsic surface states or surface states are the electronic states that arise from (i) the surface with defects (where the translational symmetry of the surface is broken), (ii) the surface with adsorbed or bonded chemical species (functional groups), and (iii) the interfaces between two materials (semiconductor–oxide or semiconductor–metal interface). Extrinsic surface states are much more difficult to characterize and model than intrinsic surface states.[25]

In CQDs, the surface state is determined by the hybridization of carbon backbones and functional groups connected to CQDs, and their energy gap is correlated to the extent of the π-electron system and surface chemistry.[84] The surface states in CQDs are associated with the (i) functional groups, (ii) defects (accompanied by a large number of non-perfect sp^2 domains) and (iii) heteroatom dopants that can serve as a capture center for excitons and thus result in surface states-related fluorescence. Different functional groups on CQDs have different structural configurations and hence different energy states, consequently resulting in more recombination possibilities for electrons and holes captured by the surface states.[93]

The abundant surface functional groups associated with CQDs can form broadly distributed surface states and thus a large number of transition modes. These states play dominant roles under different excitations and result in the fluctuation of the PL peak positions and intensities. This is excitation-dependent behavior, which is consistent with the phenomenon observed in some special semiconductors.[36,82]

It has been verified that extrinsic surface states are introduced by both surface functional groups (oxygen/nitrogen-based groups, polymer chains, *etc.*)[25,68] and heteroatoms (N, P, S, Cl, B, *etc.*)[68] in the CQDs, which can provide emissive trap states/sites (ETSs) or the density of states (DOS) for photo-excited electrons, and hence control the PL processes.[5,95] Heteroatoms also manipulate the intrinsic surface states of CQDs. The experimental evidence has shown that radiative recombination induced by surface-confined electrons and holes in the CQDs is the cause of the observed bright PL.[96,97] On the contrary, many research articles claim that extrinsic surface states do not explicitly control the PL of CQDs.[25]

Ding *et al.* synthesized CQDs with tuneable PL from urea and phenylenediamine through a one-pot hydrothermal method and used silica column chromatography for the separation. The separated CQDs showed bright and stable luminescence in gradient colors (blue to red) under UV radiation (365 nm) as shown in Fig. 12(b). These samples exhibited a graphitic carbon core structure with similar particle size (average size 2.6 nm with broad size distributions) but the surface state (especially the degree of oxidation) gradually varied among the samples. With the increasing incorporation of oxygen species (as seen from FTIR and XPS) into their surface structures, the bandgap was gradually reduced and consequently, a red shift in the emission peak was observed from 440 nm to 625 nm. Interestingly, they found that the energy states rely on the surface groups (degree of oxidation) and structures but not on the particle size as shown in Fig. 12;

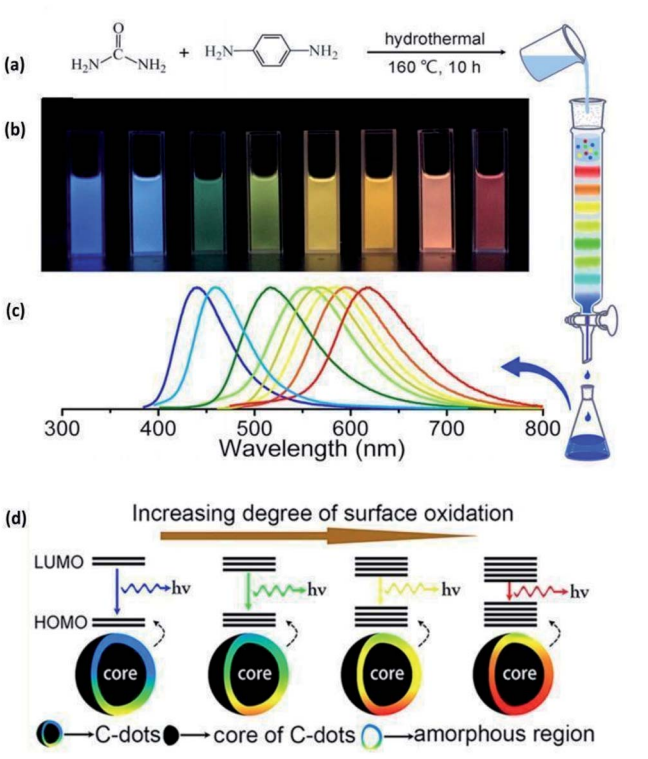

Fig. 12 (a) Synthesis of CQDs from urea and phenylenediamine. (b) Fluorescence of the CQDs under excitation at 365 nm. (c) The emission spectrum of the synthesized CQDs, and (d) the variation in the bandgap of the CQDs (no change in size) with the degree of surface oxidation (this figure has been adapted/reproduced from ref. 26 with permission from the American Chemical Society, Copyright 2015).

thus, surface states were the dominant factor controlling the PL variations.[26]

Zhang *et al.* prepared two types of CQDs (CQDs1 and CQDs2) through different precursors and different methods and found that both of the CQDs displayed blue PL. However, one exhibited excitation-independent PL, while the other showed excitation-dependent PL. XPS showed that the surface oxygen level was higher in the CQDs that exhibited excitation-dependent PL. They also concluded that the surface oxidation controls the PL.[99]

Recently, Yuan *et al.* synthesized four different kinds of CQDs using hydrothermal processes under identical conditions using different nitrogen precursors. They observed that the emission color changed with the variation in nitrogen functionalities. They could see clear differences in the type and amount of nitrogen functionality in each sample. The red emission was attributed to the distortion of *p*-phenylenediamine; green due to pyridinic nitrogen, blue emission due to pyrrolic nitrogen. These relationships were further confirmed by the presence of red and blue emissions in CQDs prepared from proline. Based on the observations, they suggested a representative structure for each type of CQDs and created an energy level diagram to illustrate the effect of surface nitrogen functionalization on the bandgap of CQDs, as shown in Fig. 13.[100]

Sun *et al.* in 2018, hydrothermally synthesized CQDs from citric acid and urea (H-CQDs), which emitted a blue color while those synthesized by microwave radiation (M-CQDs) emitted a green-blue or green light, depending on the mass ratio. XPS revealed that the concentration of C=O was much higher in M-CQDs then H-CQDs and observed the excitation-dependent emission spectrum. They concluded that carboxyl (COOH) and carbonyl (C=O) functional groups are responsible for the green emission while hydroxyl (OH) groups are responsible for the blue emission.[82]

Due to the increasing success of surface state theory to explain the excitation-dependent PL of CQDs, it has become much more common as compared to quantum confinement and molecular state.

Yu *et al.* concluded that both surface states and the carbon core are critical in regulating the PL because the bandgap of the surface states (4.5 eV) is narrower than that of the core (5.0 eV). Oxygen, nitrogen elements, and related chemical bonds will produce impurity levels in the bandgap, which lead to changes in the excitation and emission spectra of CQDs. As shown in Fig. 14, there may be an energy transfer process between the carbon core and the surface state. The CQDs display five emission bands centered at 305, 355, 410, 445, and 500 nm, which are correlated with the electron transition at intrinsic C (4.1 eV), graphitic N (3.5 eV), pyridine N (3.0 eV), amino N (2.8 eV), and C=O (2.5 eV) related levels, respectively.[101]

(3) Molecular state. According to this theory, various "fluorescent molecular fragments" are synthesized, which are free or

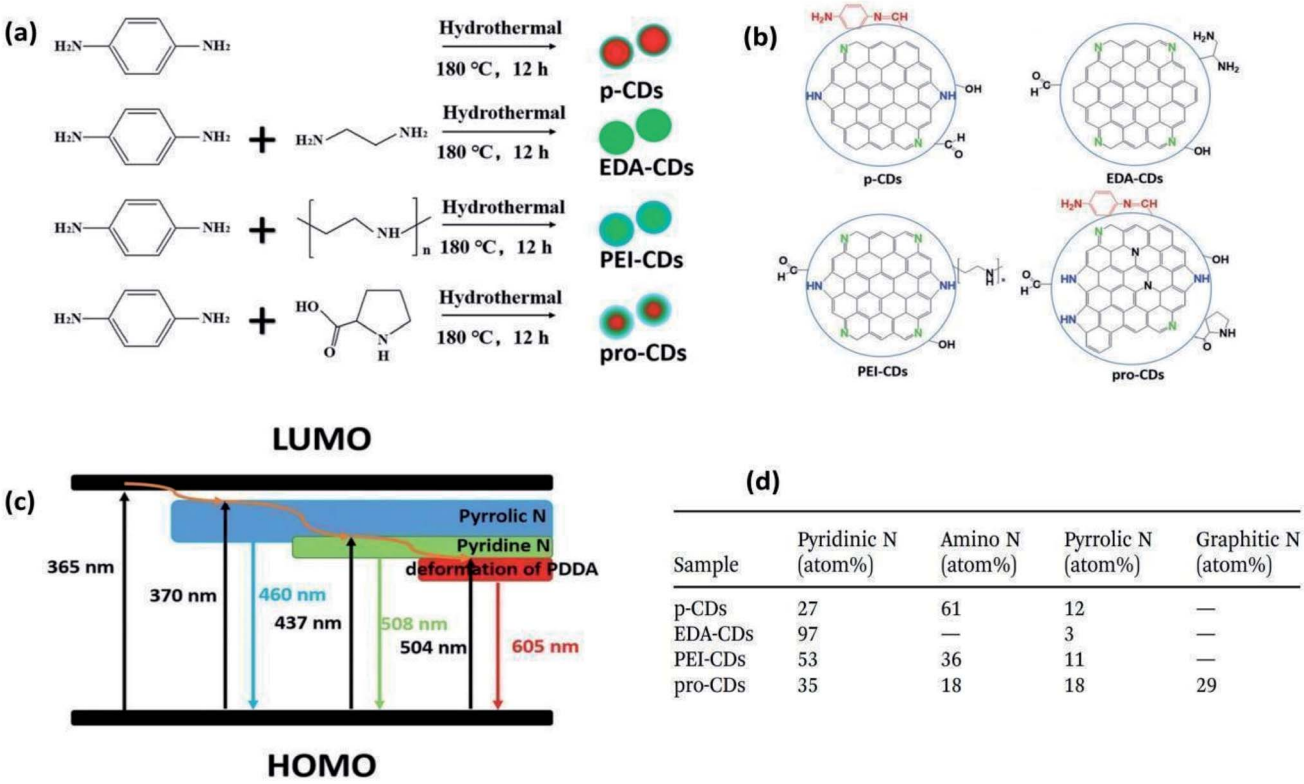

(d)

Sample	Pyridinic N (atom%)	Amino N (atom%)	Pyrrolic N (atom%)	Graphitic N (atom%)
p-CDs	27	61	12	—
EDA-CDs	97	—	3	—
PEI-CDs	53	36	11	—
pro-CDs	35	18	18	29

Fig. 13 (a) Synthesis of CQDs using different precursors, (b) the proposed structures of different CQDs, (c) the proposed energy levels of surface states of CQDs, and (d) nitrogen percentages in different CQDs (this figure has been adapted/reproduced from ref. 100 with permission from the Royal Society of Chemistry, Copyright 2018).

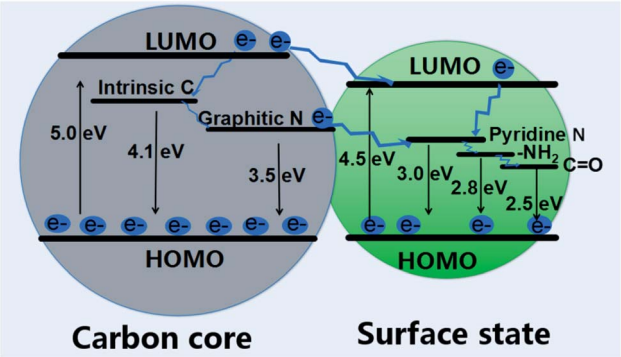

Fig. 14 Energy band structure and possible PL processes for CQDs (this figure has been adapted/reproduced from ref. 101 with permission from MDPI, Copyright 2018).

attached to the surface of CQDs in the preparation process of CQDs by bottom-up methods.[25,83]

Since the bottom-up methods support highly reactive conditions (*e.g.*, a high reaction temperature, high pressure, and/or a long reaction time, *etc.*),[103] one can expect other side reactions as well. In other words, small molecules or even molecular luminophores can be produced during CQDs synthesis, which may attach to the surface of CQD backbones, granting them bright emission characteristics.[83]

Though several papers are available with strong evidence, the scope of this theory is limited to the precursors like citric acid/fluorescent precursors and also this theory cannot completely explain the excitation-dependent emission that CQDs usually possess.[25]

Rogach *et al.* hydrothermally synthesized three different CQDs by reacting citric acid with three different amine precursors (*e.g.*, ethylenediamine, hexamethylenetetramine, and triethanolamine) as shown in Fig. 15. They analysed the carbon and nitrogen species within the CQDs *via* XPS, and compared their optical performance with that of citrazinic acid (a molecular fluorophore belonging to the pyridine family). This study confirmed the presence of the derivatives of citrazinic acid and their contribution to the blue fluorescence of ethylenediamine-CQDs (e-CQDs) and hexamethylenetetramine-CQDs (h-CQDs).[104] The differences in the PL QY of the prepared CQDs are shown in Fig. 15 and 16.

Song *et al.*, in 2015, synthesized high quantum yield CQDs from citric-acid and EDA through a hydrothermal method and discovered a bright blue fluorophore (imidazo[1,2-*a*]pyridine-7-carboxylic acid, 1,2,3,5-tetrahydro-5-oxo-, IPCA) through the separation of CQDs. These CQDs have two PL centres: carbon core states (resulting from the core) with low QY and molecular state (resulting from IPCA) with high QY.[105]

Recently, Righetto *et al.* claimed the observation of free molecules by combining fluorescence correlation spectroscopy and time-resolved electron paramagnetic resonance.[106] However, the reported fluctuations and rotations of carbon layers may account for the estimated molecular hydrodynamic radius in the case of molecules attached to or inserted within the layers.[65] In addition, aggregates of fluorophores were also reported to play a role in the absorption and emission features.[107] According to these findings, CQDs may be

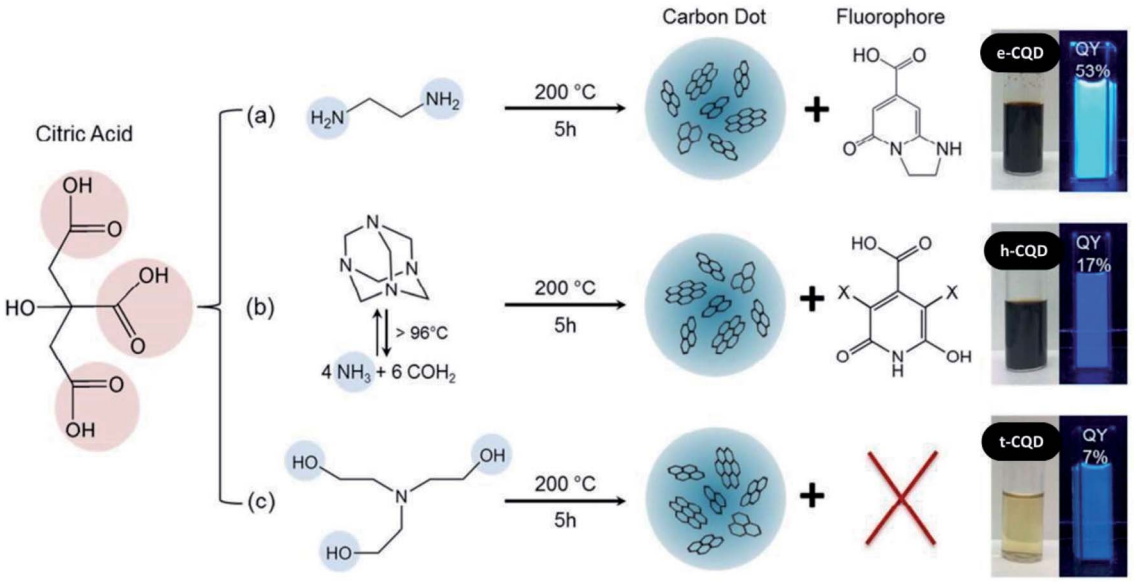

Fig. 15 (a) Reaction of citric acid and ethylenediamine, resulting in e-CQDs and the fluorophore IPCA. (b) Reaction of citric acid with hexamethylenetetramine, producing h-CQDs and citrazinic acid and/or 3,5 derivatives (marked by –X) due to the decomposition of hexamethylenetetramine to ammonia and formaldehyde at temperatures exceeding 96 °C. (c) Reaction of citric acid and triethanolamine, resulting in t-CQDs and no derivatives of citrazinic acid since the tertiary amine prohibits their formation. (a–c) Images of the purified reaction products under ambient light and the corresponding diluted solutions under UV light excitation (this figure has been adapted/reproduced from ref. 104 with permission from the American Chemical Society, Copyright 2016).

rationalized as hybrid particles, built from fluorophores, that eventually aggregated, within or attached to a carbonized core. To further support this picture, it was shown that the temperature and time of synthesis can modify the molecular state/core state equilibrium. It is interesting to note that multiple parallel routes were proposed to explain the formation of CQDs during the hydrothermal synthesis of CA and EDA, including direct carbonization and polymers- or molecules-mediated carbonization, thus supporting the formation of a mix of different emission centers in the same CQD or the formation of a heterogeneous mix of different CQDs characterized by distinct emissions.[65]

4.2.2 Phosphorescence. Phosphorescence is one of the recently discovered properties of CQDs, observed when CQDs

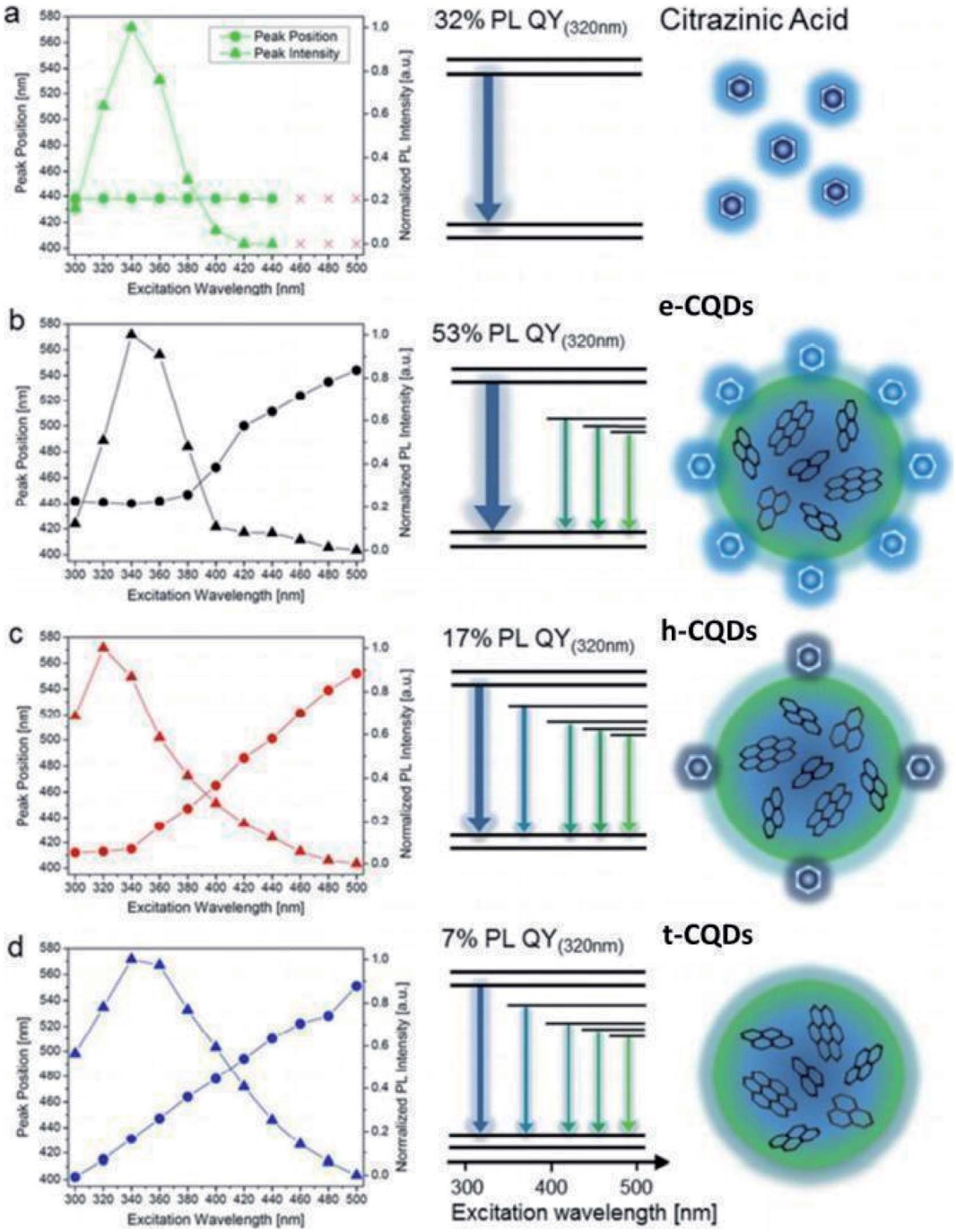

Fig. 16 PL peak position (●) and normalized PL intensity (▲) as a function of the excitation wavelength for citrazinic acid (a) and the three CQD species (b–d). Emission pathways are illustrated in the simplified Jablonski diagrams: the arrow colors represent the shift in the emission wavelengths from blue to green (high to low energies), and arrow thickness indicates the relative intensities of different transitions. Schematic structures for each CQD species are drawn on the right. The attachment of molecular fluorophores is depicted by the hexagons for both e- and h-CQDs (this figure has been adapted/reproduced from ref. 104 with permission from the American Chemical Society, Copyright 2016).

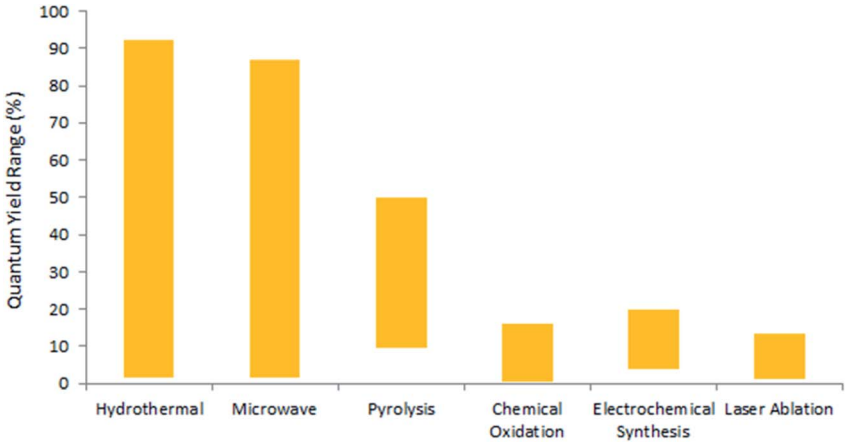

Fig. 17 Minimum and maximum QYs for different synthesis techniques.

are dispersed in a polyvinyl alcohol (PVA) matrix at room temperature and excited with UV light. Several investigations suggested that carbonyl groups attached on the surface of CQDs provide excited triplet states that are responsible for phosphorescence in CQDs. The PVA matrix molecules guard the triplet excited state from rotational or vibrational loss by making these carbonyl groups inflexible with hydrogen bonding.[7]

In 2013, Deng *et al.* reported room-temperature phosphorescence (RTP) from CQDs in a polyvinyl alcohol (PVA) matrix. They obtained a phosphorescence peak at 500 nm with an average lifetime of 380 ms under the excitation of 325 nm (Fig. 12). The phosphorescence emerged from the aromatic carbonyls of CQDs (C=O on the surface), and the PVA matrix effectively shielded their triplet states from being quenched by intramolecular motions and oxygen.[110]

In 2019, Lu *et al.* prepared ultra-long phosphorescent carbon dots (P-CQDs) through microwave synthesis. These P-CQDs exhibited yellow-green (525 nm) phosphorescence for up to 9 s when excited at 354 nm. They observed that (i) the room temperature phosphorescence (RTP) intensity of P-CQDs gradually decreased with increasing pH because protonation dissociated the hydrogen bonds and disturbed the phosphorescent sources and (ii) the phosphorescence of P-CQDs was quenched by introducing the tetracyclines (TCs).[111] The potential applications include chemical and biological sensing and time-resolved imaging.

Comparative emission characteristics of CQDs synthesized by various research groups are given below in Table 2.

Based on the data collected from the research papers reviewed in this article, a statistical distribution of the minimum and the maximum QY for various methods are shown in Fig. 17. It is interesting that the hydrothermal method is capable of providing the maximum QY of ~90% and has been the most commonly used technique for synthesis, as seen in Fig. 5. The microwave technique is a runner up, capable of providing the maximum QY of ~85%. Fig. 17 also shows that CQD synthesis through laser ablation exhibits poor QY with a maximum value of ~12.2%. It is noteworthy that various factors affect the QY of the CQDs, like the precursor, synthesis duration, temperature, *etc.*[13,14]

5. Applications of CQDs in solar cells

The sun provides about 120 000 terawatts of power to the earth's surface, which is approximately 6000 times the present rate of the world's energy consumption. Solar energy is a green and inexhaustible energy resource that, if exploited fully, can bring a paradigm shift and make the planet earth completely free from fossil fuel-based electricity generation.[119] Solar cells are electronic devices (consisting of p–n junctions) that convert light into electricity through the photovoltaic (PV) effect. Research efforts have led to the development of different categories of solar cells like single or multi-junction semiconductor solar cells (Si or GaAs based), thin-film solar cells, quantum dot solar cells, organic/polymer solar cells, perovskite solar cells, dye-sensitized solar cells, *etc.* Flexible, low-weight and transparent solar cells become important in comparison to other PV technologies for certain applications like foldable mobile/media player chargers, transparent door curtains, window shades, *etc.*[120] To attain better performance, these devices usually employ inorganic quantum dots (SQDs) but it happens at the cost of environmental and health issues due to the presence of carcinogenic materials like Cd, Pb, *etc.* in SQDs.[121] In this situation, the low cost and eco-friendly fluorescent CQDs are the best alternative to SQDs. CQDs exhibit large absorption coefficients, broad absorption spectra,[122] and good photo-induced electron transfer/charge separation ability and large two-photon absorption cross-section.[123] These characteristics make CQDs important contestants for photovoltaic applications where they can be used as light absorbers to generate e-hole pairs,[124] electron acceptors/donors, electron sinks (which effectively transfer electrons and prevent the electron–hole pair recombination),[125] or hetero-junction-forming charge dissociation sites, which make them work as charge carrier sources, *etc.*[126,127] Due to these features, CQDs have been used in different functional layers of solar cells: electron-transporting layers (ETL), active absorbing layers, hole-transporting layers

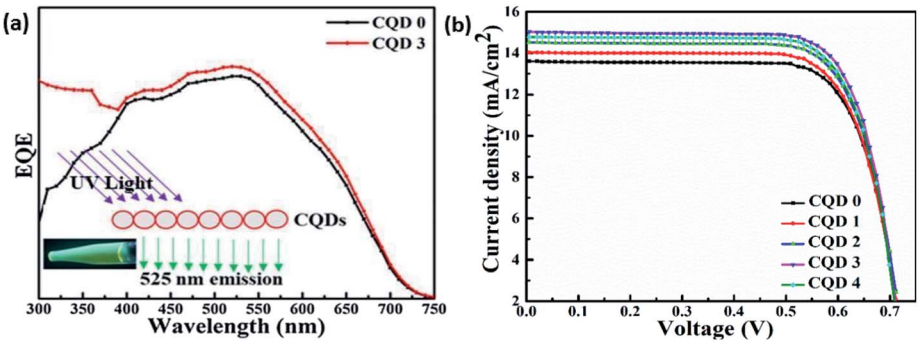

Fig. 18 (a) The external quantum efficiency (EQE) test shows an enhancement mainly in the UV region by the incorporation of CQDs. (b) *I*–*V* curve of DSSC at different numbers of coatings (CQD *X*; *X* is the number of N-CQDs solution coatings) (this figure has been adapted/reproduced from ref. 131 with permission from Elsevier, Copyright 2019).

(HTL), dopants in the active layer, and as an interlayer spacing simply to align and adjust the energy levels of other components.[128] As a result, CQDs-based solar cells are expected to display superior performance. This article reports two recent reviews[119,128] that deal with the role of CQDs in specific types of solar cells. However, the present section is not restricted to any specific type but rather discusses the various possible roles of CQDs in different types of solar cells exploited by the researchers.

5.1 CQDs as energy down-shift (EDS) material

The solar spectrum that reaches the earth's surface ranges from 250–2500 nm. To exploit the extreme potential of solar energy, the solar cell must absorb the maximum spectrum, but in practical scenarios, it is difficult to achieve specifically when considering UV radiation. For instance, UV radiation coming from the sun degrades the sensitizer of the DSSCs and hence affects its long-term stability, especially when Ru-free dyes (indoline dyes D149, *etc.*) are used. Poor long-term stability is the major drawback of the DSSCs.[129] At the same time, Ru-free dyes are highly desired for cost-effective and environmentally friendly photovoltaics systems. Thus, various strategies have been developed to address such concerns. One of the commonly used techniques for such purposes is to use energy down-shift (EDS) materials. EDS materials absorb UV photons and in turn generate low-energy photons. CQDs are among the emerging EDS materials due to their low cost, simple synthesis, good absorbance in the UV region and emission in the visible spectrum, and eco-friendliness. As such, the use of CQDs is one of the very practical approaches to efficiently utilizing the high-energy radiation of the solar spectrum. The application of CQDs in the DSSCs as EDS converts the incident UV into visible light, which is then absorbed by the sensitizer layer. This not only protects the DSSCs from UV radiation but also improves the external quantum efficiency (EQE) in the range of 300–400 nm.[124]

In 2015, Xugen Han *et al.* prepared highly luminescent CQDs (QY up to 84.8%) through a hydrothermal method from citric acid (carbon source) and ethylenediamine (nitrogen source), together with adding moderate ammonia water (AW) to achieve both an appropriate inner structure and excellent N passivation. The high-yield CQDs aqueous solutions were mixed with polyvinyl alcohol (PVA) aqueous solutions (5 wt%) to obtain the CQDs/PVA solution. The resultant solution was spin-coated on the SiNW solar cells and heated at 80 °C for 20 min to form the EDS layers, the thickness of which was adjusted by the spin-coating times. An effective enhancement of J_{SC} and hence the PCE from 10.85% to 10.96% was observed due to the presence of the EDS layer. The underlying mechanism of the enhancement is attributed to the competing result of the deterioration of the surface reflectance and the optical absorption redistribution.[130]

In 2019, Riaz *et al.* synthesized N-doped CQDs by a one-pot hydrothermal method using citric acid and 2,3-diaminonaphthalene (DAN) and applied them as EDS in DSSC. The average size of the synthesized CQDs was 5 nm and QY of 70%. These CQDs absorbed the UV radiation coming from the sunlight and emitted a green wavelength (500–550 nm) that was also absorbed by the active layer of DSSC in addition to the spectrum already absorbed by it. As a result of more photon absorption, more carriers were generated and improved J_{SC} was recorded. The enhanced absorption of photons was verified by the EQE test as shown in Fig. 18(a); consequently, the PCE of the DSSC was enhanced after the incorporation of CQDs as shown in Fig. 18(b). The highest recorded PCE was 8.2% for CQD-3 in comparison to 7.3% for CQD-0. After 3 weeks, the PCEs of CQD-0 and CQD-3 were observed to be 2.1% and 6.3%, respectively, which signifies that the CQDs layer significantly resists the photodegradation of sensitizers. The employment of CQDs not only improved the efficiency by ~10% but also enhanced the stability of the solar cell.[131]

In the same year, 2019, J. E. Pelayo-Ceja *et al.* synthesized CQDs by an electrochemical method and used polymethylmethacrylate (495 PMMA A2 from Microchem) as the matrix for the dispersion of these CQDs because of its high transparency (93%), low fragility, high weather- and UV-resistance and excellent thermal insulation. The resultant PMMA and CQDs solution was spin-cast on the commercially available solar cell. The result indicated that the PCE of solar cells improved by 4.6% upon the incorporation of CQDs. The

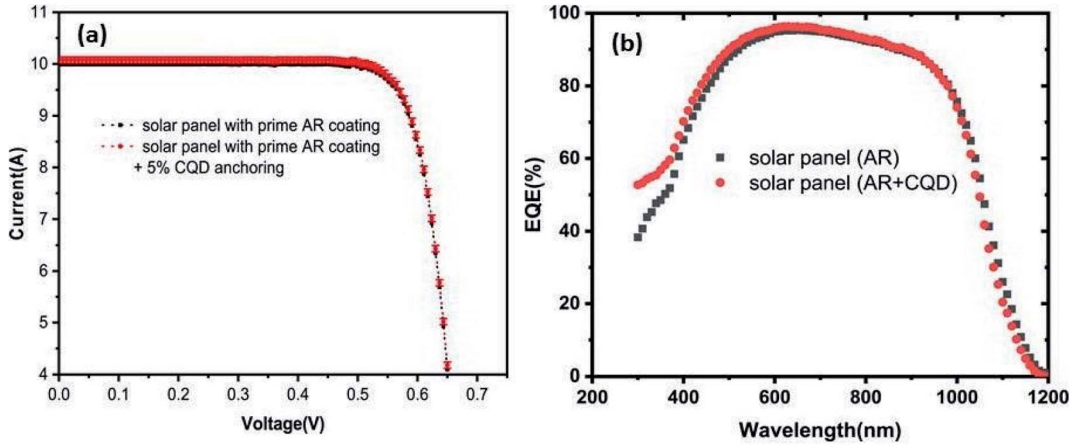

Fig. 19 (a) $I-V$ characteristics of solar cells (with and without CQDs) exhibiting an increase in I_{SC} in the presence of CQDs. (b) Enhanced EQE of solar cells in the presence of CQDs in the UV region (this figure has been adapted/reproduced from ref. 134 with permission from Elsevier, Copyright 2022).

enhancement in the cell efficiency was mainly in the range 300–480 nm due to the improved absorption of incident sunlight by the down-shifting nanostructures (CQDs) present on the incident surface.[132]

In 2020, Mumtaz Ali *et al.* coated (layer by layer self-assembled uniform coating) eco-friendly red-emissive hollow nitrogen-doped CQDs (NR-CQDs) as an efficient energy-down shifting layer on crystalline silicon solar cells (c-Si SC). A unique hollow and conjugated structure of NR-CQDs was designed to achieve a large Stokes shift of around 255 nm (UV excited – red emission) that caused the PCE to increase by 5.8%.[133]

In 2021, Tiezheng Lv *et al.* coated a luminescent and anti-reflective (AR) silica layer on the top glass of a solar panel for solar panel encapsulation by utilizing the covalent bonding between CQDs and porous silica matrix. They found that the PCE of the solar panel was enhanced from 20.76% (only AR coating) to 20.94% (AR-CQD coating) due to the improvement in the short circuit current I_{SC}. Improved I_{SC} is attributed to the higher EQEs by the AR-CQD coating in the UV range (300–400 nm) in contrast to only AR-coated film. However, in the rest of the spectrum, the role of the CQDs was not prominent. EQE was even slightly lower at longer wavelengths in AR-CQD film, probably due to the surface scattering caused by the aggregated CQDs inside porous silica as shown in Fig. 19. The results revealed that the inclusion of CQDs was compatible with the standard AR process of photovoltaic glass with no additional cost and provided a better means for solar panel encapsulation with enhanced performance.[134]

5.2 CQDs as sensitizers or co-sensitizers

Sensitizers are photosensitive materials that absorb incoming light and transfer the excited electrons to the neighbouring molecules. Numerous inorganic and organic/metal-free dyes/natural dyes like N3, N719, N749 (black dye), K19, CYC-B11, C101, K8, D102, SQ, Y123, Z907, Mangosteen, and many more have been utilized as sensitizers in DSSCs.[129] Among the various available dyes, Ru-based sensitizers (dyes) are typically employed in most of the advanced DSSCs because these dyes have carboxylate ligands that anchor the dye to TiO_2 and thus offer extraordinary stability when being adsorbed on the TiO_2 surface.[122,129]

Ru-based sensitizers generally offer superior performance and possess the capability to provide highly efficient DSSCs but their synthesis is often time-consuming, relying on the Ru-metal centre which is rare and expensive, and the range of application of Ru dyes is limited to DSSCs.[129,141] Thus, they are not suitable for cost-effective and environmentally friendly photovoltaic systems and consequently, metal-free organic dyes are developing at a fast pace to address the mentioned challenges. Metal-free organic dyes have low cost, are environmentally friendly and have higher absorption coefficient (one order of magnitude higher than Ru complexes), but the efficiencies based on these devices are lower as compared to those based on Ru dyes and these dyes exhibit poor stability under elevated temperatures.[129] As a consequence, there is a constant search for more suitable and effective sensitizers or co-sensitizers for solar cells. As such, many researchers have employed CQDs as sensitizers or co-sensitizers as novel materials because of their low cost, sustainability and eco-friendliness.[135]

In 2012, Peter Mirtchev *et al.* synthesized the CQDs (sp^2 hybridized core capped with hydroxyl, carboxyl, and sulfonate groups) and applied them as the sensitizer on the photo-anode of nanocrystalline TiO_2 solar cells. These surface functional groups enabled the coordination of CQDs to TiO_2 in the same fashion as done by the carboxylate ligands of the dye and enhanced the PCE of DSSC to 0.13% in comparison to 0.03% (non-sensitized nano-crystalline TiO_2). The enhancement is attributed to the broad absorption spectrum throughout the visible region. Still, the current density, J_{SC}, reported in their study was much lower than the value routinely obtained through Ru sensitizer solar cells. The reason for the lower current density was proposed to be the different emission trap

sites available on the CQDs surface that serve as the recombination centres.[122]

In 2016, Wang *et al.* synthesized the nitrogen-doped CQDs from citric acid and ammonia through a direct pyrolysis method for different mass ratios. The absorption was maximal for the mass ratio of 1 : 4 for ammonia : citric acid with a QY of ~36%. These CQDs were used as the sensitizer in the fabrication of TiO_2-based solar cells with a PCE of 0.79% under 1 sun illumination (AM 1.5). It was the highest recorded PCE for CQDs-based DSSCs at that time. Their group concluded that the enhanced performance of the solar cell was due to the enriched absorption of CQDs/TiO_2 in the visible spectrum and more electron transfer from CQDs to the conduction band of TiO_2.[136]

In 2017, Quanxin Zhang *et al.* grew CQDs *in situ* from citric acid and ethylene-diamine on the TiO_2 surface through the pyrolysis method to form a hybridized CQD/TiO_2 photo-anode. This photo-anode was used in the solar cell and an excellent PCE of 0.87% was observed, which was higher than all of the reported PCEs of CQD-based solar cells at that time through the adoption of a simple post-adsorption method. This CQD layer enhanced the absorption and reduced the PL of the CQD/TiO_2 layer, which resulted in more electron–hole pair generation and the transfer of carriers to the TiO_2 layer, respectively. As a result, the overall PCE of the fabricated solar cell was increased.[137]

The band alignments of TiO_2 and CQDs are suitable for causing the injection of photo-generated electrons of CQDs into the conduction band of the adjacent TiO_2 in intimate contact.[138]

In 2019, Bhavita Mistry *et al.* prepared un-doped CQDs (quantum yields 5.2%) and nitrogen-doped CQDs (quantum yield 9.8%) and used them as green sensitizers in the fabrication of TiO_2-based quantum dot solar cells. They observed that the presence of nitrogen in CQDs facilitated photo carrier injection in the TiO_2 layer that improved the photocurrent of the solar cell device and the highest PCE of 0.56% was recorded (for 0.25% nitrogen-doped CQDs), which was almost double that of the PCE of the un-doped CQDs solar cell (0.30% PCE) when measured under 1 sun. They further noted that the PCE (0.25% nitrogen-doped CQDs) was almost doubled (PCE 1.20%) under a low light intensity of 0.1 sun illumination (AM 1.5).[139]

In 2020, Qiming Yang *et al.* synthesized N-CQDs using hydrothermal methods for different durations (0.5, 1, 2, 4, 8, 16 hours) as shown in Fig. 20(a). Each of these N-CQDs possessed different characteristics (Fig. 20(b)) and they were employed as co-sensitizers in DSSCs (N719 dye) fabricated by the group; enhanced performance was observed for all the solar cells. One of the fabricated devices exhibited the highest PCE, up to 9.15% (with N-CQDs synthesized for 2 hours) under irradiation at one standard sun (AM 1.5), which was much higher than the 8.5%

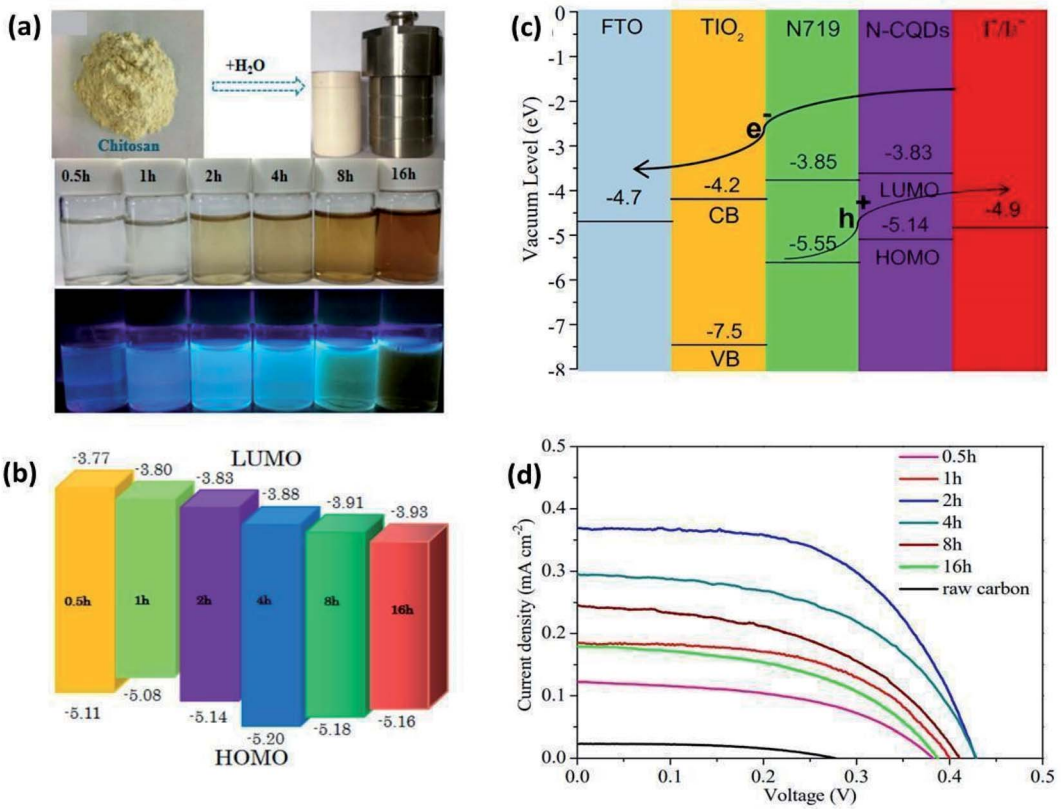

Fig. 20 (a) Conversion processes from chitosan powders to carbon quantum dots (CQDs) by a hydrothermal method and images of nitrogen-doped carbon quantum dot (N-CQD) aqueous solutions synthesized at different heating times under UV light irradiation. (b) The energy level of N-CQDs with different heating times. (c) Energy level distribution and charge transfer processes at the interface. (d) Characteristic photocurrent density–voltage (*J*–*V*) curves for N-CQDs sensitized solar cells under simulated sunlight (AM1.5, 100 mW cm^{-2}) (this figure has been adapted/reproduced from ref. 140 with permission from MDPI, Copyright 2020).

efficiency of the controlled device without N-CQDs as shown in Fig. 20(c) and (d). The enhancement was attributed to the following: (i) the energy levels of N-CQD match well with the energy levels of TiO_2 and the reduction potential of I^-/I^{3-}, therefore, the electrons can inject into the TiO_2 but not into the electrolyte, thus serving as an electron-blocking layer. (ii) The N-CQDs, under photoexcitation can serve as charge transfer antennas to receive and transmit energy to the N719 dye through the Förster resonance energy transfer (FRET) mechanism. Consequently, this mechanism significantly enhanced the light absorption ability of the device. (iii) Optimized N-CQDs exhibited excellent up-convention luminescence, which broadened the absorption spectrum of the device and enhanced the light-harvesting ability in the long-wavelength range.[140]

5.3 CQDs as an electron transport layer (ETL)

The purpose of an ETL between the active layer and the cathode is to extract electrons from the active layer towards the cathode and reduce the recombination of free electrons and holes on defects that exist on the interface (active layer and cathode). TiO_2 and ZnO films are widely used metal oxide ETLs in perovskite solar cells (PSCs). To date, TiO_2 has been used as an ETL in most reported PSCs and is also widely applied as the ETL in DSSCs. TiO_2 has a favourable band edge (HOMO/LUMO) position (−7.63 eV/−4.4 eV) for the extraction and injection of charge carriers, facile fabrication and, most importantly, low cost. However, low electron mobility, a high density of trap states below the conduction band (CB), and relatively high processing temperatures are significant problems. Some of the issues of TiO_2 are addressed by ZnO as it has a conductivity several orders of magnitude that of TiO_2, thus significantly minimizing the recombination losses and it also does not require high-temperature processing. However, ZnO also has degradation problems like TiO_2, which reduces the device stability.[141,142] They came across another ETL material, namely tin oxide (SnO_2), which appears as a possible alternative to both ZnO and TiO_2 in certain aspects. SnO_2 requires low-temperature processing, high electron mobility, adequate HOMO/LUMO position, excellent stability, and high transparency in the visible and near-infrared regions. However, metal oxide ETLs (TiO_2, ZnO, SnO_2) are chemically and physically more stable than organic ETLs but have a relatively higher population of defects and traps on the surface as compared to organic ETLs.[142]

CQDs are emerging among the various organic materials as favourable ETL due to their photo-stability, low toxicity, good electron extraction capability, easy bandgap tunability, *etc.* CQDs as ETLs are employed by researchers in two ways: (i) completely replacing the existing ETL, or (ii) co-mingling with the existing ETL to improve its performance.

In 2016, Lingpeng Yan *et al.* synthesized the CQDs by chemical vapour deposition (CVD) in an Ar atmosphere using C_2H_2 as the carbon source, having an average diameter of 3.5 nm. Their group fabricated the solution-processed organic solar cell (ITO/PEDOT:PSS/donor:acceptor/CQDs/Al) with CQDs as the ETL as shown in Fig. 21. The results indicated that the optimized PCE of P3HT:$PC_{61}BM$, PTB7:$PC_{61}BM$ and PTB7-TH:$PC_{71}BM$ devices using CQD as ETLs reached 3.11%, 6.85% and 8.23%, respectively, which are comparable with the LiF (as ETL)-based devices. CQDs-ETL offered lower resistance and thus a better interfacial connection between the Al electrode and the active layer. This lower interfacial resistance and better electron injection resulted in excellent device performance. The long-term thermal stability of these devices having CQDs-ETLs was also improved significantly due to reduced diffusion of CQDs in the active layer.[143]

In 2017, Hao Li *et al.* synthesized CQDs through a one-step alkali-assisted ultrasonic chemical method from glucose. Their group used the CQDs/TiO_2 composite layer as the ETL in planar n–i–p hetero-junction perovskite solar cells and boosted the PCE to 18.89%.

The presence of CQDs enhanced the electronic coupling between the $CH_3NH_3PbI_{3-x}Cl_x$ and TiO_2 ETL interface, which improved the electron transport property (charge extraction and injection) at TiO_2/perovskite (from perovskite to TiO_2). This resulted in enhanced short-circuit current density (J_{SC}), open-circuit voltages (V_{OC}).[144]

In 2019, Xiaomeng Zhu *et al.* built a planar heterojunction (PHJ) $CH_3NH_3PbI_3$ perovskite solar cell using CQDs-doped PCBM as the electron transport layer having device structure FTO/PEDOT:PSS/$MAPbI_3$/PCBM:CQDs/BCP/Ag. The doping with CQDs led to a PCE of 18.1% in comparison to 13% PCE

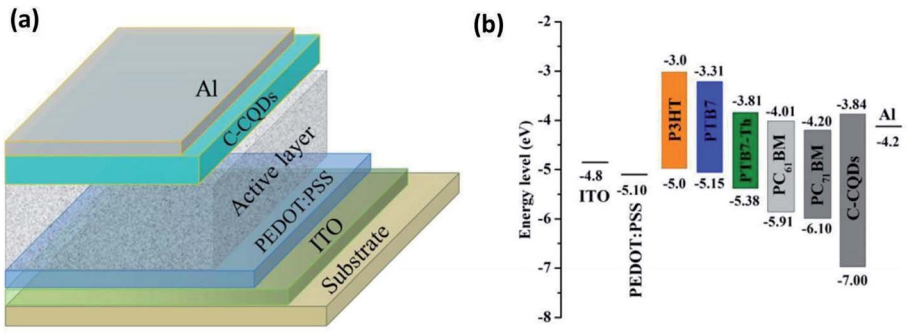

Fig. 21 (a) Organic solar cell device structure with CQDs (C in C-CQDs indicates the carbon vapour deposition method). (b) Energy level diagram of the solar cells with CQDs as ETLs and P3HT:$PC_{61}BM$, PTB7:$PC_{61}BM$ or PTB7-Th:$PC_{71}BM$ as the active layer (This figure has been adapted/reproduced from ref. 143 with permission from Elsevier, Copyright 2016).

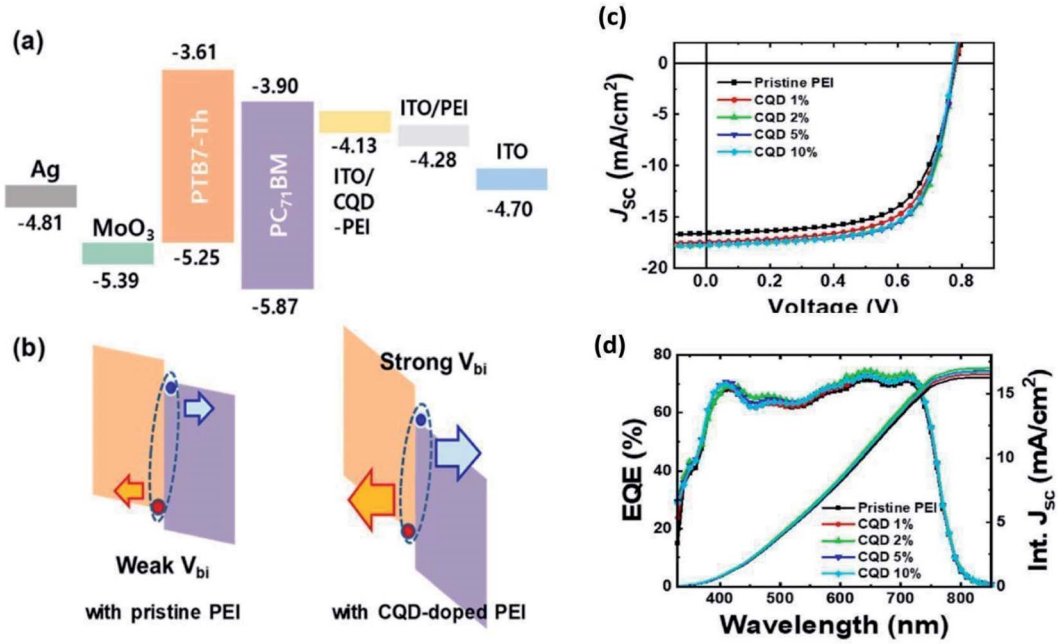

Fig. 22 (a) Energy level diagram of PTB7-Th:PC71BM solar cells. The work-functions of ITO, ITO with PEI, and ITO with CQD-doped PEI were measured by Kelvin probe force microscopy. (b) A diagram of the summarized concept; CQD-doped PEI induced a stronger internal field due to the lower work-function. This strengthened internal field induced better exciton dissociation efficiency. (c) The *J*–*V* characteristics of PTB7-Th:PC71BM solar cells with pristine PEI and CQD-doped PEI with various doping ratios. (d) EQE curves of PTB7-Th:PC71BM solar cells with pristine PEI and CQD-doped PEI with various doping ratios (this figure has been adapted/reproduced from ref. 146 with permission from Elsevier, Copyright 2021).

(39.2% increment) of the pure PCBM-based devices. Also, the CQD doping improved the long-term stability of perovskite solar cells by preventing the diffusion of I^-.[145]

In 2021, S. Park *et al.* synthesized CQDs having NH_2 ligands using neutral red powder and ethylene-diamine from microwave irradiation. They incorporated these CQDs in different ratios in the polyethyleneimine (PEI) layer of fabricated solar cells (ITO/CQD-doped PEI/PTB7-Th:$PC_{71}BM$/MoO_3/Ag). The purpose of the PEI layer in solar cells is to modify (reduce) the work function of ITO, and the presence of CQDs in PEI enhances this effect as shown in Fig. 22(a) and (b). As a result, the incorporation of CQDs in PEI effectively enhanced the performance of all the solar cells (different CQD concentrations). The effects of CQD concentration on J_{SC} and % EQE are shown in Fig. 22(c) and (d). The highest PCE recorded was 9.468% for 2% CQDs in comparison to PCE of 8.549% for pristine PEI layer-based solar cells. Their group concluded that the enhancement of solar cell efficiency could be attributed to (i) the improved electron transport properties as a result of CQD doping and (ii) the increase in the exciton dissociation probability due to the strengthened internal field.[146]

5.4 CQDs as the hole transport layer (HTL)

In order to facilitate more efficient charge separation and prevent interfacial recombination within these devices, HTLs have been employed to obtain high-performing devices. The most widely used HTL is PEDOT:PSS but its strong acidity and hygroscopicity reduce the device stability. In addition, its insulating nature reduces the electrical conductivity and hence reduces the device performance.[147] The inorganic semiconductor materials-based HTLs are known for improved device stability but they suffer from the problem of high manufacturing cost. Therefore, CQDs are the best alternatives that offer a win–win situation over the said materials.[119,147]

In 2016, Sofia Paulo *et al.* synthesized CQDs from citric acid and *p*-phenylenediamine using a hydrothermal approach. The cyclic voltammetry measurements confirmed that the HOMO and LUMO energy levels of CQDs are suitable for hole transfer and electron blocking from the perovskite to CQDs. They used CQDs as the HTM (hole transport material) for perovskite solar cells for the very first time in MAPI (methylammonium lead iodide) solar cells and observed a PCE of 3%. This efficiency was quite low in comparison to the PCE of 8.06% observed with another similar device fabricated using spiro-oMeTAD as the HTL. This poor performance of CQDs as HTL-based devices was due to the poor perovskite coverage over the mp-TiO_2 surface, as revealed by ESEM analysis of the devices.[148]

In 2021, a new approach was proposed by Duong *et al.*, utilizing the potential of both PEDOT:PSS and CQDs. Their group synthesized the N-CQDs (nitrogen-doped) using a solvothermal process and O-CQDs (oxidised) using a chemical oxidation method and studied their impact as HTL on the performance of fabricated solar cells in the presence of PEDOT:PSS. They found that the performance of solar cells improved when CQDs were incorporated and the highest PCE of

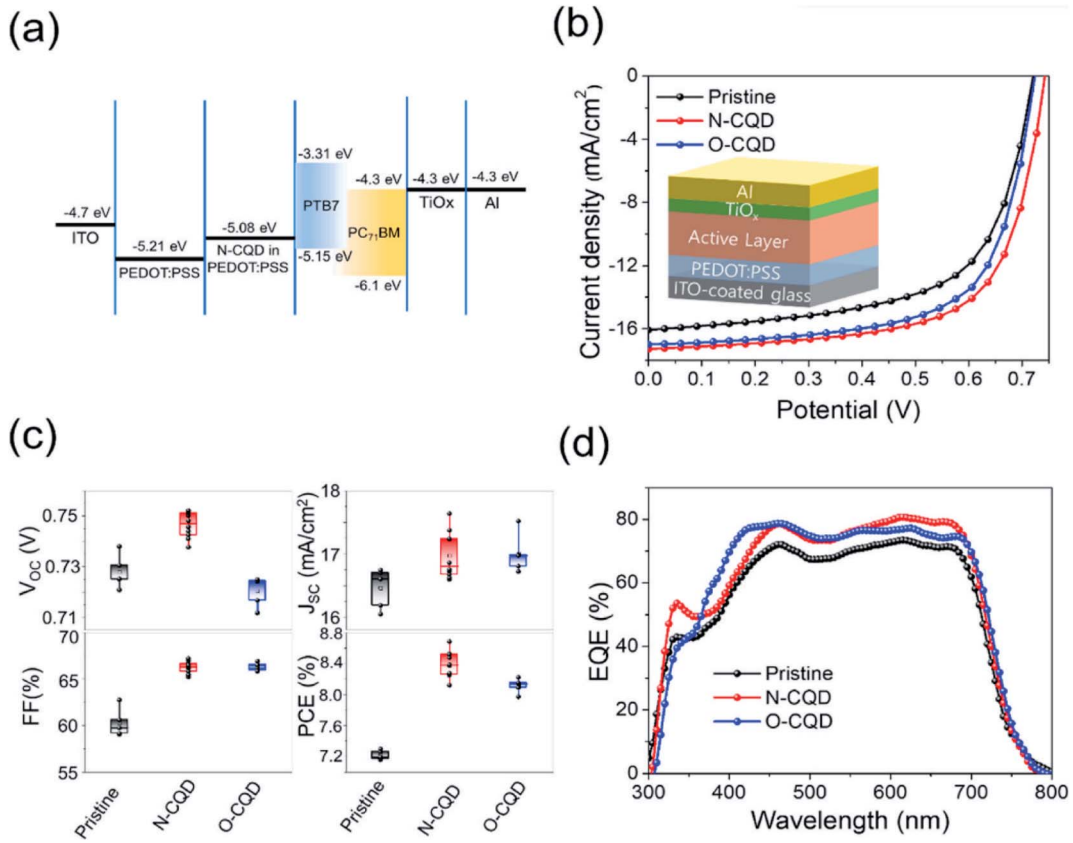

Fig. 23 OPV device performance and characterization. (a) Energy band diagram of the OPV device. (b) Current *vs.* potential (*J*–*V*) curves (inset: OPV device with the structure ITO/PEDOT:PSS/active layer/TiO_x/Al). (c) Photovoltaic response, and (d) EQE spectra of OPV devices (this figure has been adapted/reproduced from ref. 149 with permission from Elsevier, Copyright 2021).

8.57% was recorded with N-CQDs in comparison to 8.17% for O-CQDs and 7.26% in the absence of CQDs, as shown in Fig. 23. The incorporation of N-CQDs in PEDOT:PSS drastically (i) reduced the resistance, (ii) increased the work function, (iii) modified the surface energy, and (iv) smoothed the surface morphology of PEDOT:PSS. Moreover, it weakened the electrostatic interaction between PEDOT and PSS, which resulted in the π–π stacking of PEDOT and the hydrophilic interaction of PSS with N-CQDs as shown in Fig. 24. The interactions in the presence of N-CQDs were quite strong in comparison to oxidized CQDs (O-CQDs). The combination of PEDOT:PSS and

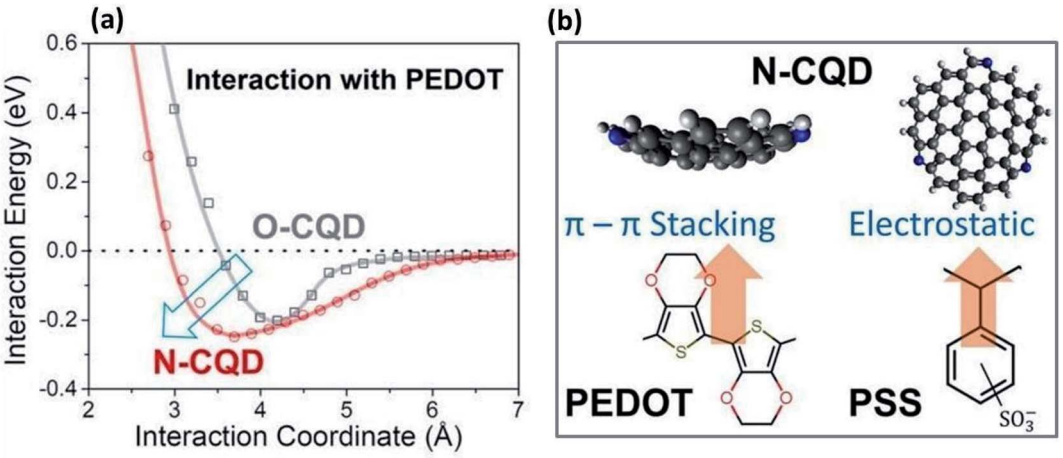

Fig. 24 (a) Potential energy scan for each pair of N-CQD/PEDOT and O-CQD/PEDOT; (b) π–π stacking of PEDOT with N-CQDs and electrostatic interactions of PSS with N-CQDs (this figure has been adapted/reproduced from ref. 149 with permission from Elsevier, Copyright 2021).

Table 3 Performance characteristics of the P3HT:CQDs based bulk heterojunction solar cells (this table has been reproduced from ref. 151 with permission from Elsevier, Copyright 2018)

Device structure	V_{OC} (V)	J_{SC} (mA cm^{-2})	FF	PCE (%)
ITO/ZnO/P3HT/MoO_3/Al	0.55	0.27	0.52	0.08
ITO/ZnO/P3HT:C-CQDs/MoO_3/Al(2.5%)	0.60	0.64	0.57	0.22
ITO/ZnO/P3HT:C-CQDs/MoO_3/Al(5%)	0.62	0.77	0.60	0.29
ITO/ZnO/P3HT:C-CQDs/MoO_3/Al(10%)	0.63	0.62	0.61	0.24
ITO/ZnO/P3HT:H-CQDs/MoO_3/Al(5%)	0.56	0.36	0.50	0.10

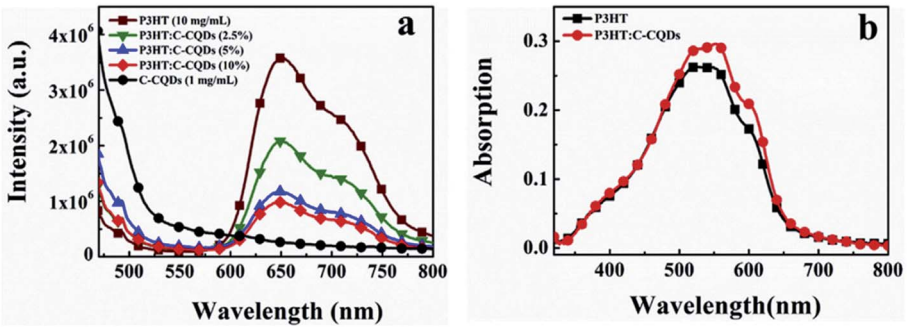

Fig. 25 (a) PL spectra of P3HT (10 mg ml^{-1}), C-CQDs (1 mg ml^{-1}) and P3HT:C-CQDs (P3HT: 10 mg ml^{-1}, C-CQDs content: 0, 2.5, 5, and 10 wt% *vs.* P3HT) composite films at an excitation of 450 nm. (b) UV-Vis absorption spectra of P3HT and P3HT:C-CQDs (1 : 5%) in the solid state (this figure has been adapted/reproduced from ref. 151 with permission from Elsevier, Copyright 2018).

N-CQDs enhanced the charge extraction and charge injection, resulting in the improved performance of the solar cells.[149]

5.5 CQDs as donor/acceptor

Many reports are available where CQDs have completely replaced the fullerene derivatives as acceptor materials in photovoltaic devices.[119] Some research groups have considered the incorporation of CQDs in the active layers as "CQDs as acceptor" material but in this review, we have categorised it as "CQDs as dopant", where CQDs may either accept or donate electrons.

In 2015, Feng *et al.* synthesized CQDs, by a hydrothermal method, having an average diameter of 6.2 nm and a pretty good QY of 12.1%. Their group noticed that the PL of P3HT was quenched drastically upon the incorporation of the synthesized CQDs in P3HT (mass ratio 1 : 1). The quenching was attributed to the transfer of electrons from the P3HT to CQDs; *i.e.*, the CQDs accepted electrons from the photo-excited P3HT. The adequate charge transfer takes place because the bandgap energies of the CQDs align well with those of the P3HT.[150]

In 2018, Bo Cui *et al.* synthesized C-CQDs by chemical vapour deposition (CVD) in an Ar atmosphere using C_2H_2 as a carbon source, having an average diameter of 3.5 nm. Their group fabricated the solution-processed inverted organic solar cell (ITO/ZnO/P3HT: C-CQDs/MoO_3/Al), where P3HT acted as a donor with C-CQDs as an acceptor. The amount of the C-CQDs in the active layer was varied as 0, 2.5, 5.0 and 10 wt% (ratio to P3HT) and the performances of all the solar cells were compared. The photo-induced charge transfer occurred between P3HT and C-CQDs because photoluminescence quenching was seen in the P3HT:C-CQDs composite film. It was recorded that V_{OC} and FF increased with the increase in C-CQDs concentration and reached the maximum value for 10 wt% CQDs. Likewise, J_{SC} also increased with C-CQDs concentration but reached its maximum value for 5 wt% C-CQDs and then decreased, and the highest PCE was exhibited by 5 wt% C-CQDs based solar cells.[151] The effects of C-CQDs concentration on the performance of solar cells is shown in Table 3.

The PCE of this device was 0.29%, which was ~2.5 times higher in comparison to the device without using C-CQD (0.08%).[151] The enhancement in the performance of solar cells in the presence of C-CQDs is attributed to the improved absorption by the C-CQD:P3HT composite film and efficient

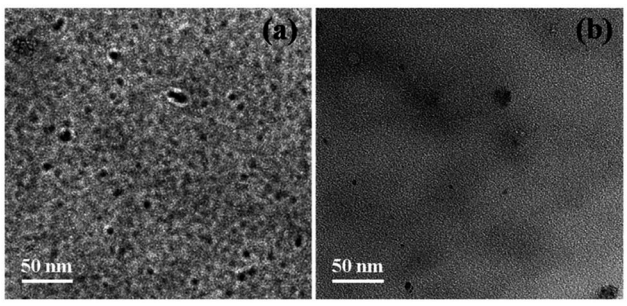

Fig. 26 (a) FETEM image of P3HT:C-CQDs composite films (1 : 5%). (b) FETEM image of P3HT:H-CQDs composite films (1 : 5%) (this figure has been adapted/reproduced from ref. 151 with permission from Elsevier, copyright 2018).

charge transfer from P3HT (donor) to C-CQDs (acceptor) as shown in Fig. 25.

They also compared the performance of the hydrothermally synthesized CQDs (H-CQDs) and found the PCE of only 0.1% for 5 wt% H-CQDs. The inferior performance with H-CQDs was due to the aggregation (poor dispersion) of H-CQDs in the P3HT matrix,[151] which was seen *via* the FETEM image shown in Fig. 26.

In addition to the acceptor, CQDs can function well as electron donors or co-electron acceptors when coupled with the PCBM fullerene derivatives. In 2016, Alberto Privitera *et al.* synthesized N-CQDs functionalized with different thiophene-containing groups. The functionalization was done to (i) enhance the electron-donating ability of the CQDs and (ii) improve their solubility in nonpolar solvents. They demonstrated that the PL of a thin film of the CQD:PCBM blend gets quenched significantly due to the transfer of electrons from CQDs (donor) to the PCBM (acceptor), which was verified by electron paramagnetic resonance (EPR). With the help of time-resolved EPR spectroscopy, they also observed that different functionalization derivatives on CQDs modified the charge transfer efficiency of the CQD:PCBM blend.[155] At present, very few studies exist that focus on the CQDs as electron donors and thus it offers wide room for further investigation to exploit its full potential.

5.6 CQDs as a dopant

Doping is a very frequently used technique to modify the optoelectronic properties of the base material. Reports have revealed that CQDs can be alternative eco-friendly dopant materials for commercial solar cells in the near future. In 2018, Bo Cui *et al.* synthesized CQDs by chemical vapour deposition (CVD) in an Ar atmosphere using C_2H_2 as a carbon source having an average diameter of 3.5 nm. Their group fabricated the solution-processed organic solar cell (ITO/ZnO/P3HT:CQDs:$PC_{61}BM$/MoO_3/Al), with P3HT as the donor, $PC_{61}BM$ as the acceptor and CQDs as the doping material (varying doping concentrations 0, 0.025, 0.05, 0.075 and 0.1 wt%). They observed that the PCE efficiency increased from 3.3% to 3.67% (11% enhancement) as the dopant (CQDs) concentration increased from 0 to 0.075 wt%, but the PCE decreased to 3.55% with a further increase in the doping concentration to 0.1%. The enhancement in PCE is attributed to (i) the absorption and scattering by well-dispersed CQDs in the active layer, which might improve J_{SC}, and (ii) the lower series resistance of the device doped with CQDs that improved J_{SC} and the fill factor (FF).[151]

In 2021 Kiran *et al.* fabricated DSSCs and found that the PCE of the cell was boosted to 8.75% after doping the active layer with synthesized N-CQDs (co-active layer) under single-sun irradiation. The incorporation of the N-CQDs in the photo-active layer synergically enhanced the absorbance and reduced the recombination between the photo-anode and electrolyte. They also employed the N-CQDs as sensitizers and co-sensitizers in DSSCs and consequently, enhanced performance was also observed in both cases. The maximum enhancement was demonstrated when N-CQDs were applied as the co-active layer. A large number of anchoring sites for dyes, highly conducting photo-anode, fast charge carrier transportation, and inherent light-emitting photo-fluorescent properties of N-CQDs in mesoporous titania were considered to be responsible for this enhancement.[156]

A comparative study of the effects of CQDs on the performances of different types of solar cells is summarized below in Table 4.

6. CQD-assisted white LEDs (WLEDs)

The CQDs have broad emission characteristics (full width half maxima > 80 nm) in comparison to the commercial rare-earth phosphors and traditional semiconductor QDs that exhibit narrow emission bandwidth. The broad emission exhibited by CQDs is due to their strong electron-phonon coupling, as well as highly dispersed particle size.[157–159] This makes CQDs suitable materials for application in WLEDs.

The emission spectrum of the WLED spectrum ranges from 400 to 760 nm.[158,160] WLEDs, due to their advantages of high luminous efficacy, high luminance, long lifetime, fast response speed and energy conservation, have become strong contenders as future solid-state lighting sources.[161,162]

There are mainly two approaches through which CQD-based WLEDs are fabricated. In one of the approaches, CQDs are used as light-converting phosphors that are optically pumped by blue or UV LED chips (employed as primary light sources) to generate white light. This type of WLED is sometimes referred to as phosphor-converted WLEDs (pc-WLEDs). In another approach, CQDs are used as an emitting layer and the electroluminescence properties of CQDs are utilized to generate the white light. Here, the electrons and holes are forced to move into the active CQD layer by an external voltage and they recombine radiatively. This type of WLED is sometimes referred to as electroluminescent WLEDs (e-WLEDs).[163] Interestingly, e-WLEDs exhibit higher efficiency in contrast to pc-WLEDs.[164]

Originally, CQD-based WLEDs were prepared by simply coating yellow CQDs on blue GaN chips.[165] Due to the lack of a sufficient red component, these cold WLEDs (correlated color temperature, CCT > 5000 K) exhibit an inferior color rendering index (CRI) and the emitted excessive blue light from the chips is harmful to human retina.[164] Thus, a sufficient red emission component is required to get warm WLEDs (CCT < 4000 K). This necessitates the employment of red emission CQDs in WLED and consequently, red CQDs (R-CQDs) are becoming increasingly important. Efficient R-CQDs are crucial for preparing high-performance warm WLEDs but are rarely reported because the required larger sizes of sp^2 π-conjugation domains make them more susceptible to defect formation and more vulnerable to environmental perturbation.[163]

In 2017, Zifei Wang *et al.* developed R-CQDs (QY up to 53%) and used them in combination with their blue-CQD, green-CQD phosphors and they successfully obtained CQD phosphor-based warm WLEDs exhibiting CIE coordinates (0.3924, 0.3912), CCT (3875 K) and CRI (97) as shown in Fig. 27. The highest luminous efficiency of the optimized warm WLED was 31.3 lm W-1, which

Table 4 Effect of CQDs on the performance of solar cells[b]

Synthesis technique	Type of solar cell	Role of CQDs	Solar cell structure (with CQD)	% PCE[a] (without CQD), *A*	% PCE[a] (with CQD), *B*	% ΔPCE (*B* − *A*)	Ref.
Dehydration [chemical oxidation]	NCTiSC	Sensitizer	FTO/TiO_2/CQD/electrolyte/Pt-FTO	0.03%	0.13%	0.10%	122
Hydrothermal	SiNwSC	EDS layer	Si/SiNWs/CQDs/PVA	10.85%	10.96%	0.11%	130
Microwave irradiation	MSC	Sensitizer	FTO/TiO_2/CQD/electrolyte/counter electrode	—	0.24%	NA	116
CVD	OSC	ETL	ITO/PEDOT:PSS/active layer/ETL (CQDs)/ Al (active layer = P3HT:PC_{61}BM, PTB7:PC_{61}BM, PTB7-TH:PC71BM)	1.75% 6.28% 7.59%	3.11% 6.85% 8.23%	1.36% 0.57% 0.64%	143
Hydrothermal	PSC	HTM	FTO/d-TiO_2/mp-TiO_2/MAPI/HTM/Au	0.71%	3.00%	2.29%	148
Pyrolysis	QDSC	Sensitizer	FTO/TiO_2/N-CQD/gel electrolyte/Pt-FTO	—	0.79%	NA	136
Alkali-assisted ultrasonic chemical method	PSC	ETL	ITO/CQDs/TiO_2/perovskite/spiro-OMeTAD/Au	15.15%	18.90%	3.75%	144
Pyrolysis	NCTiSC	Sensitizer	FTO/TiO_2/CQD/polysulfide/Cu_2S	—	0.87%	NA	137
CVD	OSC	Electron acceptor	ITO/ZnO/P3HT:C-CQDs/MoO_3/Al	0.08%	0.29%	0.21%	151
CVD	OSC	Dopant	ITO/ZnO/P3HT:C-CQDs:PC_{61}BM/MoO_3/Al	3.30%	3.67%	0.37%	151
Hydrothermal	DSSC	EDS layer	FTO/TiO_2/CQDs/electrolyte/Pt-FTO	7.30%	8.20%	0.90%	131
Microwave irradiation	i-PSC	ETL	FTO/PEDOT:PSS/$MAPbI_3$/PCBM:CQDs/BCP/Ag	16.10%	18.10%	2.00%	145
Solvothermal	NCTiSC	Sensitizer	FTO/TiO_2/mp-TiO_2/CQD/electrolyte/Pt-FTO	—	1.20%	NA	139
Hydrothermal	DSSC	Co-sensitizer	FTO/TiO_2/N719 dye/CQDs/electrolyte/Pt–Ni-FTO	8.50%	9.15%	0.65%	140
Hydrothermal	c-SiSC	EDS layer	Not mentioned	17.39%	18.40%	5.80%	133
Microwave irradiation	i-OSC	ETL	ITO/PEI-CQDs/PTB7-Th:PC71BM/MoO_3/Ag	8.549%	9.468%	0.919%	146
Solvothermal	OSC	HTL	ITO/PEDOT:PSS-CQDs/PTB7:PC_{71}BM/TiO_x/Al	7.26%	8.57%	1.31%	149

[a] Under one standard sun (AM 1.5). [b] NCTiSC: nanocrystalline TiO_2 solar cell, SiNwSC: silicon nanowire solar cells, MSC: mesoscopic solar cell, QDSC: quantum dot solar cell, OSC: organic colar cell, PSC: perovskite solar cell, i-PSC: inverted perovskite solar cell, c-SiSC: crystalline silicon solar cell, i-OSC: inverted organic solar cell.

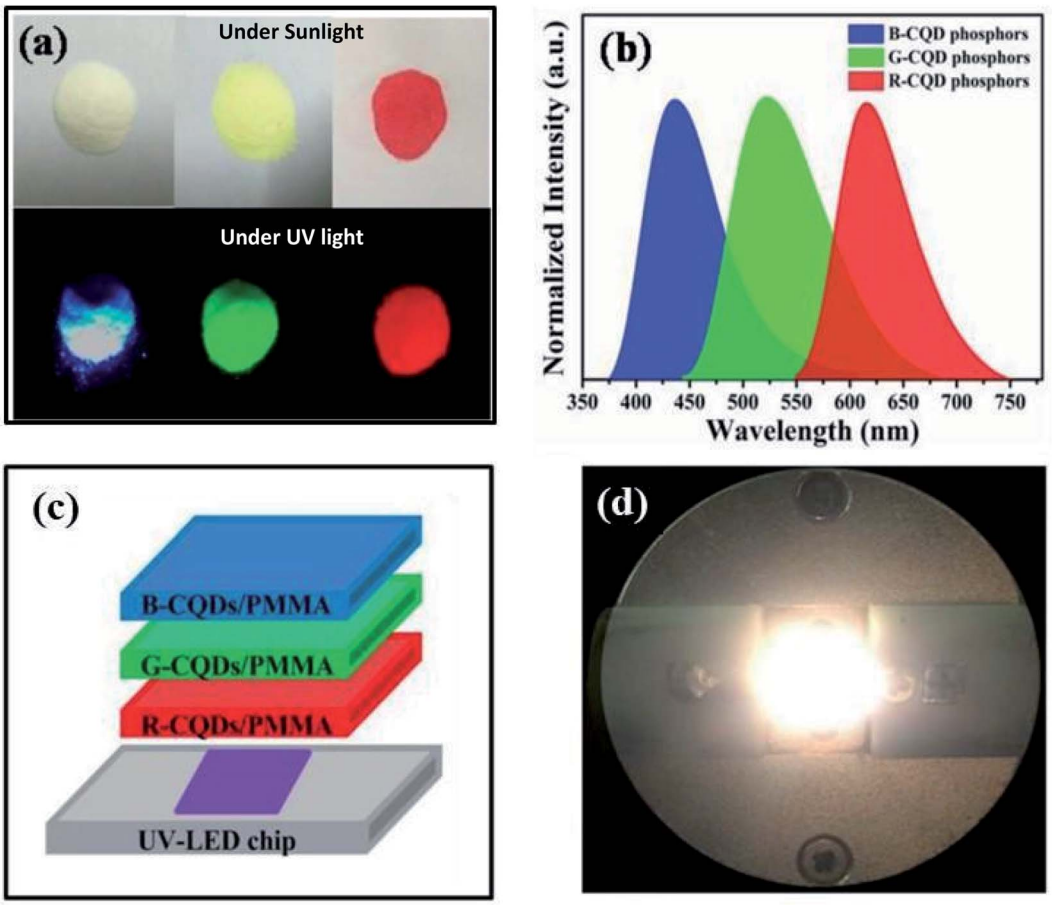

Fig. 27 (a) Images of blue, green, and red CQD phosphors under sunlight and UV light. (b) Emission spectra of the mentioned CQDs. (c) Schematic diagram of warm WLEDs consisting of blue, green and red CQDs films. (d) Photograph of the operating warm WLED with brilliant warm white emission (this figure has been adapted/reproduced from ref. 166 with permission from Wiley-VCH, Copyright 2017).

is comparable to that of semiconductor QD- and rare earth phosphor-based WLEDs.[166] R-CQDs must possess both (i) high QY and (ii) good solubility in organic solvents for preparing CQD-based warm e-WLEDs.[163] Therefore, efficient R-CQDs were widely studied for warm WLEDs (CCT < 4000 K) for both pc-WLEDs and e-WLEDs.

Single-component white emission CQDs (SCWE-CQDs) have also attracted intensive attention from researchers for WLED applications as they can further imitate sunlight to achieve high color quality white emission. SCWE-CQDs offer advantages such as no color fading over time, no phase separation and simple device fabrication procedures.[167] SCWE has been realized by surface defect state emission (multiple energy levels)[168] and π–π stacking effects.[169]

In 2017, Jinyang Zhu *et al.* prepared white emission carbon dots (CDs) by introducing hexadecyltrimethylammonium bromide (CTAB) to modulate the emitting states of CDs (Fig. 27 (a)). The results showed that the QY improved to 12.7% from 5.4% and the long-wavelength intensity of CD-CTAB increased, indicating that CTAB modification resulted in more contributions to the surface-related emissions and thus led to the SCWE properties.[170]

Heteroatom doping groups also contribute to the surface states in CQDs to realize SCWE due to their different electronic structures and electronegativities as compared with carbon. Surface states are also introduced through the doping of heteroatoms. Since different heteroatoms exhibit different electronic structures and electronegativities as compared with carbon, SCWE can also be realized.

In 2016, Sungan Do *et al.* synthesized nitrogen and sulfur-doped carbon nanodots (N-CNDs and S-CNDs, respectively). Upon studying the chemical structure and energy structure of the N-CNDs and S-CNDs, respectively, they believed that the excited electrons were transferred from the LUMO to the O, N, S states, which on de-excitation recombined with the holes in the HOMO, contributing to the SCWE combined with blue (420 nm)/green (514 nm)/yellow (575 nm) emission.[171] However, surface defect states limit the efficient charge injection in the active emissive layer of CQDs, thus limiting the performance of electroluminescent WLEDs applications. Therefore, efficient bandgap SCWE-CQDs are needed for their further application.

The π–π stacking effect commonly leads to red-shifted and wider emission peaks for CQDs, which offer an interesting prospect to realize efficient SCWE with high CRI by simultaneously utilizing the fluorescence of individual CQDs and their aggregations inducing a red-shifting emission band.[169]

However, the larger aggregation size of CQDs makes them prone to self-quenching, which reduces the emission intensity

of red light in the emission spectral region. Therefore, it is highly essential to overcome self-quenching and also to increase the aggregation size of CQDs so that the emission peaks get further broadened and shift the aggregation-induced emission band at long wavelengths to the red spectral region.[172] In 2018, D. H. Kim *et al.* for the first time, realized high-performance warm CQD based e-WLEDs due to their high-efficiency bandgap red emission and good solubility. Parts of the SCWE-CQDs were also used as the active emission layers in the electroluminescent WLEDs. However, owing to the nature of the surface defect-state emission, the lower luminescence, and carrier transfer performance, the efficiency of these kinds of WLEDs were lower.[173]

If the CQDs possess fluorescence and phosphorescence simultaneously, not only can they achieve ultra-broad emission peaks, they could also improve the theoretical maximum efficiency in electroluminescent WLEDs. In order to achieve that, we need to introduce such heteroatoms as N, O, S and P into the luminescent skeletons to facilitate the intersystem crossing, and to modulate the aggregation behaviors to suppress the non-radiative dissipation.[165]

In 2019, Ting Yuan synthesized blue-yellow fluorescence-phosphorescence dual emissive carbon nitride quantum dots (W-CNQDs) that resulted in 25% white emission efficiency, which is the highest value among white-emitting materials to date. Experimental and theoretical investigations revealed that the carbonyl groups at the rim of the W-CNQDs play a key role in promoting intersystem crossing and inducing intermolecular electronic coupling, affording intensive yellow phosphorescence.[174]

7. Conclusion and future prospects

In this feature article, we have portrayed the recent progress in the field of CQDs, focusing on their structures, synthetic methods, surface modification, doping, optical characteristics, luminescence mechanism, and application in the field of photovoltaics.

CQDs have a core–shell structure in which the core can be either graphitic crystalline (sp^2) or amorphous (mixed sp^2/sp^3). Most researchers have reported graphitic crystalline (sp^2) cores. The type of core depends on the synthesis parameters (synthesis method, precursors, solvent, reaction time, temperature, pH, *etc.*). The shells of CQDs are typically amorphous, consisting of functional groups such as oxygen-based or amino-based groups, polymer chains, *etc.*, depending on the starting materials or dopant species. Citric acid is currently the most commonly used precursor and it has produced CQDs with high QYs (refer to Table 1). Among the various synthesis methods, the bottom-up routes are cost-effective and eco-friendly but offer poor control over the size of CQDs. On the other hand, the top-down routes offer some room for size control of CQDs but they are expensive.

The optical properties of CQDs are extremely fascinating and they can be easily altered by various means. As per the above-detailed investigation, the following observations were made. (i) Surface engineering (functionalization or passivation) and doping/co-doping of heteroatoms (N, B, F) have been extensively practised by many researchers and are proven to be effective in enhancing the QY of CQDs to a large extent. (ii) The inclusion of heteroatoms (either in the CQD core or functionalized around the periphery), leads to a bathochromic shift in optical properties (both absorbance and emission). (iii) Synthetic parameters and the type of dopant have a tremendous influence on the ultimate QY of the synthesized CQDs. High QYs, above 90%, have been reported (blue emission) in N-doped CQDs after optimizing various synthetic parameters. However, the explanations for the upgrade in the QY of the doped/co-doped CQDs in contrast to the undoped CQDs have not been completely assessed by many researchers. The QY and PL are extremely important parameters in assessing the utility of CQDs in applications like photovoltaics, bio-sensing, bio-imaging, *etc.*

The photoluminescence mechanisms have been reviewed in detail in this article to clarify the origin of their photoluminescence and excitation-dependent emission. Vast numbers of papers have been published in the past fifteen years on the CQD synthesis by different techniques and different starting materials, and contrary behaviours have been observed. Therefore, the mechanisms reported in the literature cannot be claimed as general, but they can be applied to a specific subset of CQDs. Three mechanisms have been reported: (i) core state (size-dependent emission or quantum confinement (QC) effect), (ii) surface state and (iii) molecular state. The core state model is suitable for describing the emission from crystalline CQDs, where the dimensions of the core or the presence of graphitic nitrogen cause the redshifting of the optical properties. It is difficult to control the size of the conjugated π-domains in CQDs, thus the quantum size effect is not easy to use to modulate the color-emission from CQDs. Though some researchers give strong evidence for QC theory, several published papers do not have the data to support this theory, thus it is not the most common theory. According to the surface states model, emission originates from the surface states. The functional groups and heteroatoms on the CQDs create the surface states within the bandgap. Different functional groups on CQDs have different structural configurations and hence different energy states and consequently, a large number of transition modes. Different states play dominating roles under different excitations and result in excitation-dependent emission. Controlling the surface states is the most primary and easy method to modulate the color emission from CQDs in which N-related functional groups have been very effective. As such, this theory has been proposed very frequently as seen in the above literature review, and has received general acceptance. According to the molecular model, fluorescent molecular fragments formed during CQD synthesis are responsible for the emission. Many research articles give strong evidence in support of this theory but the scope of this explanation is limited to specific organic carbon precursors such as citric acid and also it fails to completely explain the excitation dependent emission. There are few reports on the use of molecular state mechanisms to modulate the color-emission from CQDs because reactions are difficult to control. The contradiction in the literature reflects variations in the CQDs' properties based on the preparation methods.

The enormous surface area, good conductivity, and quick charge transfer of CQDs enrich them with extraordinary potential for photovoltaic application. CQDs have been used as sensitizers/co-sensitizers, energy downshifting layers (EDSL), electron transporting layers (ETL), hole transport materials (HTM) in different solar cells, and their presence has improved the overall performance of solar cells (as shown in Table 4). CQDs in the solar panel encapsulation layer has shown enhancements in the performance of solar panels.

R-CQDs are necessary for the fabrication of warm WLEDs whose emission is closer to pure white light. Bandgap SCWE-CQDs with high QYs and solubility are urgently required for improved luminescence and carrier transfer performance of SCWECQD-based electroluminescent WLEDs. Room temperature phosphorescence and thermally-activated delayed fluorescence are required to successfully realize highly efficient e-WLEDs.

Although intense research has been conducted in the last fifteen years on CQDs, many challenges need to be resolved for the widespread adoption of CQDs. (1) It is critical to synthesize CQDs of desired structure and size because precise control over various synthesis parameters is required, which is hardly available to date with a few exceptions. As such, there is a need to develop the manufacturing processes to efficiently control the core structure or the chemical composition of the emitting surface centres. This will allow (i) the precise tuning of color emission and QY on a large scale, (ii) large-scale production of CQDs that will lead to the rapid growth of CQDs-based commercial applications, and (iii) a better comprehension of the emission mechanism. (2) The large degree of inconsistency within the literature, related to the material's classification, synthesis approach, purification, and subsequent characterizations of the CQDs properties hinders the progress of the CQDs field. Consistency in the said areas is a must for precise comparative study and appropriate conclusions. (3) The CQDs have low values of QY except for some limited cases and the QY are even lower or compromised when measured at longer wavelengths. Efforts must be made to extend the spectrum of CQDs, especially in the near-IR region, which will create opportunities for CQDs to find widespread applications including organic bioelectronics. (4) Though the incorporation of CQDs has improved the performance of solar cells, their true potential has not been realized yet due to insufficient knowledge of the charge transfer mechanism associated with CQDs. Thus, profound knowledge of charge transfer dynamics is needed for fabricating high-performance CQDs-based solar cells. (6) Though R-CQDs have been reported by many researchers, long-wavelength emission and high QYs of these CQDs are difficult to realize, which are necessary for achieving warm WLEDs of high color quality. Despite these challenges, CQDs hold a bright future as an alternative to conventional fluorescent materials and seem to be the leading material in the near future for commercial solar panels.

Author contributions

Pawan Kumar: conceptualization, literature survey, writing – review & editing, revision, and Shweta Dua: literature survey, writing, editing and Ravinder Kaur: subject guidance, Mahesh Kumar: review and Geeta Bhatt: conceptualization, structurization, editing, review, polishing, supervision and resources.

Conflicts of interest

We declare that we have no conflicts of interest to this review article. We declare that we do not have any commercial or associative interest that represents a conflict of interest in connection with the review article.

Acknowledgements

Authors are thankful to the University of Delhi and Vice Chancellor, Prof. Yogesh Singh for encouraging and facilitating the faculty in pursuing research. Authors also submit their appreciation to Bhaskaracharya College of Applied Sciences, University of Delhi in providing the conducive environment for research activities.

References

1 K. D. Patel, R. K. Singh and H. W. Kim, Carbon-based nanomaterials as an emerging platform for theranostics, *Mater. Horiz.*, 2019, **6**, 434–469.
2 X. Wang, Y. Feng, P. Dong and J. Huang, A Mini Review on Carbon Quantum Dots: Preparation, Properties, and Electrocatalytic Application, *Front. Chem.*, 2019, **7**, 671.
3 J. Zuo, T. Jiang, X. Zhao, X. Xiong, S. Xiao and Z. Zhu, Preparation and Application of Fluorescent Carbon Dots, *J. Nanomater.*, 2015, **2015**, 787862.
4 X. Xu, R. Ray, Y. Gu, H. J. Ploehn, L. Gearheart, K. Raker and W. A. Scrivens, Electrophoretic Analysis and Purification of Fluorescent Single–Walled Carbon Nanotube Fragments, *J. Am. Chem. Soc.*, 2004, **126**, 12736–12737.
5 Y. P. Sun, B. Zhou, Y. Lin, W. Wang, K. A. S. Fernando, P. Pathak, M. J. Meziani, B. A. Harruff, X. Wang, H. Wang, P. G. Lu, H. Yang, M. E. Kose, B. Chen, L. M. Veca and S. Y. Xie, Quantum-Sized Carbon Dots for Bright and Colorful Photoluminescence, *J. Am. Chem. Soc.*, 2006, **128**, 7756–7757.
6 F. Ahmad and A. M. Khan, Carbon Quantum Dots: Nanolights, *Int. J. Petrochem. Sci. Eng.*, 2017, **2**, 247–250.
7 Y. Wang and A. Hu, Carbon quantum dots: synthesis, properties and applications, *J. Mater. Chem. C*, 2014, **2**, 6921–6939.
8 L. Tang, R. Ji, X. Cao, J. Lin, H. Jiang, X. Li, K. S. Teng, C. M. Luk, S. Zeng, J. Hao and S. P. Lau, Deep ultraviolet photoluminescence of water-soluble self-passivated graphene quantum dots, *ACS Nano*, 2012, **6**, 5102–5110.
9 K. Hola, A. B. Bourlinos, O. Kozak, K. Berka, K. M. Siskova, M. Havrdova, J. Tucek, K. Safarova, M. Otyepka, E. P. Giannelis and R. Zboril, Photoluminescence effects of graphitic core size and surface functional groups in carbon dots: COO- induced red-shift emission, *Carbon*, 2014, **70**, 279–286.

10 A. Sciortino, E. Marino, B. Dam, P. Schall, M. Cannas and F. Messina, Solvatochromism Unravels the Emission Mechanism of Carbon Nanodots, *J. Phys. Chem. Lett.*, 2016, **7**, 3419–3423.
11 A. Dager, T. Uchida, T. Maekawa and M. Tachibana, Synthesis and characterization of Mono-disperse Carbon Quantum Dots from Fennel Seeds: Photoluminescence analysis using Machine Learning, *Sci. Rep.*, 2019, **9**, 14004.
12 W. Zhang, S. F. Yu, L. F. Fei, L. Jin, S. Pan and P. Lin, Large-area color controllable remote carbon white-light light-emitting diodes, *Carbon*, 2015, **85**, 344–350.
13 C. M. Martindale, G. A. M. Hutton, C. A. Caputo, S. Prantl, R. Godin, J. R. Durrant and E. Reisner, Enhancing Light Absorption and Charge Transfer Efficiency in Carbon Dots through Graphitization and Core Nitrogen Doping, *Angew. Chem., Int. Ed.*, 2017, **56**, 1–6.
14 T. Yu, H. Wang, C. Guo, Y. Zhai, J. Yang and J. Yuan, A rapid microwave synthesis of green-emissive carbon dots with solid-state fluorescence and pH-sensitive properties, *R. Soc. Open Sci.*, 2018, **5**, 1–15.
15 H. Li, Z. Kang, Y. Liu and S. T. Lee, Carbon nanodots: synthesis, properties and applications, *J. Mater. Chem.*, 2012, **22**, 24230–24253.
16 Y. Zheng, D. Yang, X. Wu, H. Yan, Y. Zhao, B. Feng, K. Duan, J. Weng and J. Wang, A facile approach for the synthesis of highly luminescent carbon dots using vitamin-based small organic molecules with benzene ring structure as precursors, *RSC Adv.*, 2015, **5**, 90245–90254.
17 H. Hou, C. E. Banks, M. Jing, Y. Zhang and X. Ji, Carbon Quantum Dots and Their Derivative 3D Porous Carbon Frameworks for Sodium-Ion Batteries with Ultralong Cycle Life, *Adv. Mater.*, 2015, **27**, 7861–7866.
18 A. C. Ferrari, Raman spectroscopy of graphene and graphite: Disorder, electron–phonon coupling, doping and nonadiabatic effects, *Solid State Commun.*, 2007, **143**, 47–57.
19 X. Zhang, J. Wang, J. Liu, J. Wu, H. Chen and H. Bi, Design and preparation of a ternary composite of graphene oxide/carbon dots/polypyrrole for supercapacitor application: Importance and unique role of carbon dots, *Carbon*, 2017, **115**, 134–146.
20 M. Semeniuk, Z. Yi, V. Poursorkhabi, J. Tjong, S. Jaffer, Z. H. Lu and M. Sain, Future Perspectives and Review on Organic Carbon Dots in Electronic Applications, *ACS Nano*, 2019, **13**, 6224–6255.
21 K. D. Bomben, J. F. Moulder, W. F. Stickle and P. E. Sobol, *Handbook of X-Ray Photoelectron Spectroscopy: A Reference Book of Standard Spectra for Identification and Interpretation of XPS*, Physical Electronics, Eden Prairie, 1995.
22 Y. Zhou, S. K. Sharma, Z. Peng and R. M. Leblanc, Polymers in Carbon Dots: A Review, *Polymers*, 2017, **9**, 1–20.
23 B. Gayen, S. Palchoudhury and J. Chowdhury, Carbon Dots: A Mystic Star in the World of Nanoscience, *J. Nanomater.*, 2019, 3451307.
24 I. Singh, R. Arora, H. Dhiman and R. Pawha, Carbon Quantum Dots: Synthesis, Characterization and Biomedical Applications, *Turk. J. Pharm. Sci.*, 2018, **15**, 219–230.
25 J. M. Keenan, Y. Zhou and R. M. Leblanc, Recent Development of Carbon Quantum Dots Regarding their Optical Properties, Photoluminescence Mechanism, and Core Structure, *Nanoscale*, 2019, **11**, 4634–4652.
26 H. Ding, S. B. Yu, J. S. Wei and H. M. Xiong, Full-Color Light-Emitting Carbon Dots with a Surface-State-Controlled Luminescence Mechanism, *ACS Nano*, 2015, **10**, 484–491.
27 S. Paulo, E. Palomares and E. M. Ferrero, Graphene and Carbon Quantum Dot-Based Materials in Photovoltaic Devices: From Synthesis to Applications, *Nanomaterials*, 2016, **6**, 1–20.
28 Y. Liu, H. Huang, W. Cao, B. Mao, Y. Liu and Z. Kang, Advance in carbon dots: a perspective from traditional quantum dots, *Mater. Chem. Front.*, 2020, **4**, 1586–1613.
29 H. Zhu, X. Wang, Y. Li, Z. Wang, F. Yang and X. Yang, Microwave synthesis of fluorescent carbon nanoparticles with electrochemiluminescence properties, *Chem. Commun.*, 2009, 5118–5120.
30 A. Chae, Y. Choi, S. Jo, Nur'aeni, P. Paoprasert, S. Y. Park and I. In, Microwave-assisted synthesis of fluorescent carbon quantum dots from an A2/B3 monomer set, *RSC Adv.*, 2017, **7**, 12663–12669.
31 C. Fan, K. Ao, P. Lv, J. Dong, D. Wang, Y. Cai and Q. We, Fluorescent nitrogen-doped carbon dots *via* single-step synthesis applied as fluorescent probe for the detection of Fe^{3+} ions and anti-counterfeiting inks, *Nano*, 2018, **13**, 1850097.
32 A. Zhang, C. Y. Liu and Y. Liu, A Novel One-Step Approach to Synthesize Fluorescent Carbon Nanoparticles, *Eur. J. Inorg. Chem.*, 2010, **2010**, 4411–4414.
33 T. Ogi, K. Aishima, F. A. Permatasari, F. Iskandar, E. Tanabe and K. Okuyama, Kinetics of nitrogen-doped carbon dot formation *via* hydrothermal synthesis, *New J. Chem.*, 2016, **40**, 5555–5561.
34 Y. Zhao, S. Jing, X. Peng, Z. Chen, Y. Hu, H. Zhuo, R. Sun and L. Zhong, Synthesizing green carbon dots with exceptionally high yield from biomass hydrothermal carbon, *Cellulose*, 2019, **27**, 415–428.
35 H. Yang, B. Zhou, Y. Zhang, H. Liu, Y. Liu, Y. He and S. Xia, Valorization of Expired Passion Fruit Shell by Hydrothermal Conversion into Carbon Quantum Dot: Physical and Optical Properties, *Waste Biomass Valorization*, 2020, **12**, 2109–2117.
36 P. Kumar, G. Bhatt, R. Kaur, S. Dua and A. Kapoor, Synthesis and modulation of the optical properties of carbon quantum dots using microwave radiation, *Fullerenes, Nanotubes, Carbon Nanostruct.*, 2020, **28**, 724–731.
37 Q. Wang, X. Liu, L. Zhang and Y. Lv, Microwave-assisted synthesis of carbon nanodots through an eggshell membrane and their fluorescent application, *Analyst*, 2012, **137**, 5392–5397.
38 M. P. Mingos and D. R. Baghurst, Applications of Microwave Dielectric Heating Effects to Synthetic Problems in Chemistry, *Chem. Soc. Rev.*, 1991, **20**, 1–47.

39 S. S. M. Filho, S. I. E. Andrade, M. B. Lima and M. C. U. Araujo, Synthesis of highly fluorescent carbon dots from lemon and onion juices for determination of riboflavin in multivitamin/mineral supplements, *J. Pharm. Anal.*, 2019, **9**, 209–216.

40 V. Roshni and O. Divya, One-step microwave-assisted green synthesis of luminescent N-doped carbon dots from sesame seeds for selective sensing of Fe(III), *Curr. Sci.*, 2017, **112**, 385–390.

41 H. Vanessaa, W. Wenshuo, D. Cornelia, W. Simona, T. Martina and P. Wolfgang, Microwave-assisted one-step synthesis of white light-emitting carbon dot suspensions, *Opt. Mater.*, 2018, **80**, 110–1119.

42 A. Başoğlu, Ü. Ocak and A. Gümrükçüoğlu, Synthesis of Microwave-Assisted Fluorescence Carbon Quantum Dots Using Roasted–Chickpeas and its Applications for Sensitive and Selective Detection of Fe^{3+} Ions, *J. Fluoresc.*, 2020, **30**, 515–526.

43 R. Liu, D. Wu, S. Liu, K. Koynov, W. Knoll and Q. Li, An Aqueous Route to Multicolor Photoluminescent Carbon Dots Using Silica Spheres as Carriers, *Angew. Chem., Int. Ed.*, 2009, **48**, 4598–4601.

44 H. Liu, T. Ye and C. Mao, Fluorescent carbon nanoparticles derived from candle soot, *Angew. Chem., Int. Ed.*, 2007, **46**, 6473–6475.

45 D. Pan, J. Zhang, Z. Li, C. Wu, X. Yan and M. Wu, Observation of pH-, solvent-, spin-, and excitation-dependent blue photoluminescence from carbon nanoparticles, *Chem. Commun.*, 2010, **46**, 3681–3683.

46 B. C. M. Martindale, G. A. M. Hutton, C. A. Caputo and E. Reisner, Solar Hydrogen Production Using Carbon Quantum Dots and a Molecular Nickel Catalyst, *J. Am. Chem. Soc.*, 2015, **137**, 6018–6025.

47 H. Wang, P. Sun, S. Cong, J. Wu, L. Gao, Y. Wang, X. Dai, Q. Yi and G. Zou, Nitrogen-Doped Carbon Dots for "green" Quantum Dot Solar Cells, *Nanoscale Res. Lett.*, 2016, **11**, 1–6.

48 M. Rong, Y. Feng, Y. Wang and X. Chen, One-pot solid phase pyrolysis synthesis of nitrogen-doped carbon dots for Fe^{3+} sensing and bioimaging, *Sens. Actuators, B*, 2017, **245**, 868–874.

49 J. Yu, C. Liu, K. Yuan, Z. Lu, Y. Cheng, L. Li, X. Zhang, P. Jin, F. Meng and H. Liu, Luminescence Mechanism of Carbon Dots by Tailoring Functional Groups for Sensing Fe^{3+} Ions, *Nanomaterials*, 2018, **8**, 233.

50 H. Peng and J. T. Sejdic, Chemistry of Materials. Simple Aqueous Solution Route to Luminescent Carbogenic Dots from Carbohydrates, *Chem. Mater.*, 2009, **21**, 5563–5565.

51 M. Wu, Y. Wang, W. Wu, C. Hu, X. Wang, J. Zheng, Z. Li, B. Jiang and J. Qiu, Preparation of functionalized water-soluble photoluminescent carbon quantum dots from petroleum coke, *Carbon*, 2014, **78**, 480–489.

52 C. Tan, S. Zuo, Y. Zhao and B. Shen, Preparation of multicolored carbon quantum dots using $HNO_3/HClO_4$ oxidation of graphitized carbon, *J. Mater. Res.*, 2019, **34**, 3428–3438.

53 J. Deng, Q. Lu, N. Mi, H. Li, M. Liu, M. Xu, L. Tan, Q. Xie, Y. Zhang and S. Yao, Electrochemical Synthesis of Carbon Nanodots Directly from Alcohols, *Chem.–Eur. J.*, 2014, **20**, 4993–4999.

54 R. Gao, Z. Wu, L. Wang, J. Liu, Y. Deng, Z. Xiao, J. Fang and Y. Liang, Green Preparation of Fluorescent Nitrogen-Doped Carbon Quantum Dots for Sensitive Detection of Oxytetracycline in Environmental Samples, *Nanomaterials*, 2020, **10**, 1561.

55 J. Zhou, C. Booker, R. Li, X. Zhou, T. K. Sham, X. Sun and Z. Ding, An Electrochemical Avenue to Blue Luminescent Nanocrystals from Multiwalled Carbon Nanotubes (MWCNTs), *J. Am. Chem. Soc.*, 2007, **129**, 744–745.

56 L. Zheng, Y. Chi, Y. Dong, J. Lin and B. Wang, Electrochemiluminescence of Water-Soluble Carbon Nanocrystals Released Electrochemically from Graphite, *J. Am. Chem. Soc.*, 2009, **131**, 4564–4565.

57 P. R. Ipte, S. Kumar and A. K. Satpati, Electrochemical synthesis of carbon nano spheres and its application for detection of ciprofloxacin, *J. Environ. Sci. Health*, 2019, **55**, 142–150.

58 H. Xiao, J. Zhanga, M. Zhao, J. Ma, Y. Li, T. Hu, Z. Zheng, J. Jia and H. Wu, Electric field-assisted synthesis of Pt, carbon quantum dots-coloaded graphene hybrid for hydrogen evolution reaction, *J. Power Sources*, 2020, **451**, 227770.

59 C. D. Buendia, R. T. Mendieta, A. Pyatenko, E. Falomir, M. F. Alonso and G. M. Vega, Fabrication by Laser Irradiation in a Continuous Flow Jet of Carbon Quantum Dots for Fluorescence Imaging, *ACS Omega*, 2018, **3**, 2735–2742.

60 D. Carolan, C. Rocks, D. B. Padmanaban, P. Maguire, V. Svrcek and D. Mariotti, Environmentally friendly nitrogen-doped carbon quantum dots for next generation solar cells, *Sustainable Energy Fuels*, 2017, **1**, 1611–1619.

61 S. L. Hu, K. Y. Niu, J. Sun, J. Yang, N. Q. Zhao and X. W. Du, One-step synthesis of fluorescent carbon nanoparticles by laser irradiation, *J. Mater. Chem.*, 2009, **19**, 484–488.

62 S. Hu, J. Liu, J. Yang, Y. Wang and S. Cao, Laser synthesis and size tailor of carbon quantum dots, *J. Nanopart. Res.*, 2011, **13**, 7247–7252.

63 K. Dimos, Carbon Quantum Dots: Surface Passivation and Functionalization, *Curr. Org. Chem.*, 2016, **20**, 682–695.

64 M. Bottini, C. Balasubramanian, M. I. Dawson, A. Bergamaschi, S. Bellucci and T. Mustelin, Isolation and Characterization of Fluorescent Nanoparticles from Pristine and Oxidized Electric Arc-Produced Single-Walled Carbon Nanotubes, *J. Phys. Chem. B*, 2006, **110**, 831–836.

65 C. M. Carbonaro, R. Corpino, M. Salis, F. Mocci, S. V. Thakkar, C. Olla and P. C. Ricci, On the Emission Properties of Carbon Dots: Reviewing Data and Discussing Models, *Journal of Carbon Research*, 2019, **5**, 2–15.

66 A. Sharma, T. Gadly, S. Neogy, S. K. Ghosh and M. Kumbhakar, Molecular Origin and Self-Assembly of Fluorescent Carbon Nanodots in Polar Solvents, *J. Phys. Chem. Lett.*, 2017, **8**, 1044–1052.

67 M. A. Jhonsi, *State of the Art in Nano-bioimaging*, Intech, 2018.
68 L. Li and T. Dong, Photoluminescence Tuning in Carbon Dots: Surface Passivation or/and Functionalization, Heteroatom Doping, *J. Mater. Chem. C*, 2018, **6**, 7944–7970.
69 H. Peng and T. Sejdic, Simple aqueous solution route to luminescent carbogenic dots from carbohydrates, *Chem. Mater.*, 2009, **21**, 5563–5565.
70 S. Cong and Z. Zhao, *Visible-Light Photocatalysis of Carbon-Based Materials*, Intech, 2017.
71 Y. Dong, R. Wang, H. Li, J. Shao, Y. Chi, X. Lin and G. Chen, Polyamine-functionalized carbon quantum dots for chemical sensing, *Carbon*, 2012, **50**, 2810–2815.
72 G. Kandasamy, Recent Advancements in Doped/Co-Doped Carbon Quantum Dots for Multi-Potential Applications, *Journal of Carbon Research*, 2019, **5**, 1–42.
73 J. Zhou, X. Shan, J. Ma, Y. Gu, Z. Qian, J. Chena and H. Feng, Facile synthesis of P-doped carbon quantum dots with highly efficient photoluminescence, *RSC Adv.*, 2014, **4**, 5465–5468.
74 A. B. Bourlinos, G. Trivizas, M. A. Karakassides, M. Baikousi, A. Kouloumpis, D. Gournis, A. Bakandritsos, K. Hola, O. Kozak, R. Zboril, *et al.*, Green and simple route toward boron doped carbon dots with significantly enhanced non-linear optical properties, *Carbon*, 2015, **83**, 173–179.
75 G. Zuo, A. Xie, J. Li, T. Su, X. Pan and W. Dong, Large Emission Red-Shift of Carbon Dots by Fluorine Doping and Their Applications for Red Cell Imaging and Sensitive Intracellular Ag^{+} Detection, *J. Phys. Chem. C*, 2017, **121**, 26558–26565.
76 W. Wu, L. Zhan, W. Fan, J. Song, X. Li, Z. Li, R. Wang, J. Zhang, J. Zheng, M. Wu and H. Zeng, Cu–N Dopants Boost Electron Transfer and Photooxidation Reactions of Carbon Dots, *Angew. Chem., Int. Ed.*, 2015, **54**, 6540–6544.
77 T. T. Meiling, R. Schürmann, S. Vogel, K. Ebel, C. Nicolas, A. R. Milosavljevic and I. Bald, Photophysics and Chemistry of Nitrogen-Doped Carbon Nanodots with High Photoluminescence Quantum Yield, *J. Phys. Chem. C*, 2018, **122**, 10217–10230.
78 D. Qu, M. Zheng, L. Zhang, H. Zhao, Z. Xie, X. Jing, R. E. Haddad, H. Fan and Z. Sun, Formation mechanism and optimization of highly luminescent N-doped graphene quantum dots, *Sci. Rep.*, 2014, **4**, 1–9.
79 Y. Liu, C. Y. Liu and Z. Y. Zhang, Graphitized carbon dots emitting strong green photoluminescence, *J. Mater. Chem. C*, 2013, **1**, 4902–4907.
80 Z. C. Yang, M. Wang, A. M. Yong, S. Y. Wong, X. H. Zhang, H. Tan, A. Y. Chang, X. Li and J. Wang, Intrinsically fluorescent carbon dots with tunable emission derived from hydrothermal treatment of glucose in the presence of monopotassium phosphate, *Chem. Commun.*, 2011, **47**, 11615–11617.
81 L. Wang, S. J. Zhu, H. Y. Wang, Y. F. Wang, Y. W. Hao, J. H. Zhang, Q. D. Chen, Y. L. Zhang, W. Han, B. Yang and H. B. Sun, Unraveling Bright Molecule-Like State and Dark Intrinsic State in Green-Fluorescence Graphene Quantum Dots *via* Ultrafast Spectroscopy, *Adv. Opt. Mater.*, 2013, **1**, 264–271.
82 Z. Sun, X. Li, Y. Wu, C. Wei and H. Zeng, Origin of green luminescence in carbon quantum dots: specific emission bands originate from oxidized carbon groups, *New J. Chem.*, 2018, **42**, 4603–4611.
83 B. Zhi, X. X. Yao, Y. Cui, G. Orr and C. L. Haynes, Synthesis, applications and potential photoluminescence mechanism of spectrally tunable carbon dots, *Nanoscale*, 2019, **11**, 20411–20428.
84 H. Ding, X. H. Li, X. B. Chen, J. S. Wei, X. B. Li and H. M. Xiong, Surface states of carbon dots and their influences on luminescence, *J. Appl. Phys.*, 2020, **127**, 231101–231121.
85 S. H. Jin, D. H. Kim, G. H. Jun, S. H. Hong and S. Jeon, Tuning the photoluminescence of graphene quantum dots through the charge transfer effect of functional groups, *ACS Nano*, 2013, **7**, 1239–1245.
86 F. Liu, M. H. Jang, H. D. Ha, J. H. Kim, Y. H. Cho and T. S. Seo, Facile Synthetic Method for Pristine Graphene Quantum Dots and Graphene Oxide Quantum Dots: Origin of Blue and Green Luminescence, *Adv. Mater.*, 2013, **25**, 3657–3662.
87 B. Zhi, Y. Cui, S. Wang, B. Frank, D. N. Williams, R. P. Brown, E. S. Melby, R. J. Hamers, Z. Rosenzweig, D. H. Fairbrother, G. Orr and C. L. Haynes, Malic Acid Carbon Dots: from Super-Resolution Live-Cell Imaging to Highly Efficient Separation, *ACS Nano*, 2018, **12**, 5741–5752.
88 F. Yuan, T. Yuan, L. Sui, Z. Wang, Z. Xi, Y. Li, X. Li, L. Fan, Z. Tan, A. Chen, M. Jin and S. Yang., Engineering triangular carbon quantum dots with unprecedented narrow bandwidth emission for multicolored LEDs, *Nat. Commun.*, 2018, **9**, 2249.
89 H. Li, X. He, Z. Kang, Y. Liu, J. Liu, S. Lian, C. H. A. Tsang, X. B. Yang, S. T. Lee and H. Huang, Water-soluble fluorescent carbon quantum dots and photocatalyst design, *Angew. Chem., Int. Ed.*, 2010, **49**, 4430–4434.
90 F. Yuan, Z. Wang, X. Li, Y. Li, Z. Tan, L. Fan and S. Yang, Bright Multicolor Bandgap Fluorescent Carbon Quantum Dots for Electroluminescent Light-Emitting Diodes, *Adv. Mater.*, 2017, **29**, 1–6.
91 J. L. Moll, *Physics of semiconductors*, McGraw-Hill, New York, 1964.
92 R. L. Calabro, D. S. Yang and D. Y. Kim, Liquid-phase laser ablation synthesis of graphene quantum dots from carbon nano-onions: Comparison with chemical oxidation, *J. Colloid Interface Sci.*, 2018, **527**, 132–140.
93 K. Chan, S. H. K. Yap and K. T. Yong, Biogreen Synthesis of Carbon Dots for Biotechnology and Nanomedicine Applications, *Nano-Micro Lett.*, 2018, **10**, 72.
94 S. J. Phanga and L. L. Tan, Recent advances in carbon quantum dot (CQD) - based two dimensional materials for photocatalytic applications, *Catal. Sci. Technol.*, 2019, **9**, 5882–5905.
95 W. Kwon, J. Lim, J. Lee, T. Park and S. W. Rhee, Sulfur-incorporated carbon quantum dots with a strong long-

wavelength absorption band, *J. Mater. Chem. C*, 2013, **1**, 2002–2008.

96 L. Cao, X. Wang, M. J. Meziani, F. Lu, H. Wang, P. G. Luo, Y. Lin, B. A. Harruff, L. M. Veca, D. Murray, S. Y. Xie and Y. P. Sun, Carbon Dots for Multiphoton Bioimaging, *J. Am. Chem. Soc.*, 2007, **129**, 11318–11319.

97 X. Wang, L. Cao, F. Lu, M. J. Meziani, H. Li, G. Qi, B. Zhou, B. A. Harruff, F. Kermarrec and Y. P. Sun, Photoinduced electron transfers with carbon dots, *Chem. Commun.*, 2009, 3774–3776.

98 Y. Zheng, H. Liu, J. Li, J. Xiang, M. Panmai, Q. Dai, Y. Xu, S. Tie and S. Lan, Controllable Formation of Luminescent Carbon Quantum Dots Mediated by the Fano Resonances Formed in Oligomers of Gold Nanoparticles, *Adv. Mater.*, 2019, **31**, 1901371.

99 Y. Zhang, Y. Hu, J. Lin, Y. Fan, Y. Li, Y. Lv and X. Liu, Excitation Wavelength Independence: Toward Low-Threshold Amplified Spontaneous Emission from Carbon Nanodots, *ACS Appl. Mater. Interfaces*, 2016, **8**, 25454–25460.

100 K. Yuan, X. Zhang, R. Qin, X. Ji, Y. Cheng, L. Li, X. Yang, Z. Lu and H. Liu, Surface state modulation of red emitting carbon dots for white light-emitting diodes, *J. Mater. Chem. C*, 2018, **6**, 12631–12637.

101 J. Yu, C. Liu, K. Yuan, Z. Lu, Y. Cheng, L. Li, X. Zhang, P. Jin, F. Meng and H. Liu, Luminescence Mechanism of Carbon Dots by Tailoring Functional Groups for Sensing Fe^{3+} Ions, *Nanomaterials*, 2018, **8**, 233.

102 X. Li, H. Wang, Y. Shimizu, A. Pyatenko, K. Kawaguchi and N. Koshizaki, Preparation of carbon quantum dots with tunable photoluminescence by rapid laser passivation in ordinary organic solvents, *Chem. Commun.*, 2011, **47**, 932–934.

103 Y. Xiong, J. Schneider, E. V. Ushakova and A. L. Rogach, Influence of molecular fluorophores on the research field of chemically synthesized carbon dots, *Nano Today*, 2018, **23**, 124–139.

104 J. Schneider, C. J. Reckmeier, Y. Xiong, M. V. Seckendorff, A. S. Susha, P. Kasak and A. L. Rogach, Molecular Fluorescence in Citric Acid Based Carbon Dots, *J. Phys. Chem. C*, 2016, **121**, 2014–2022.

105 Y. Song, S. Zhu, S. Zhang, Y. Fu, L. Wang, X. Zhao and B. Yang, Investigation from chemical structure to photoluminescent mechanism: a type of carbon dots from the pyrolysis of citric acid and an amine, *J. Mater. Chem. C*, 2015, **3**, 5976–5984.

106 M. Righetto, A. Privitera, I. Fortunati, D. Mosconi, M. Zerbetto, M. L. Curri, M. Corricelli, A. Moretto, S. Agnoli, L. Franco, R. Bozio and C. Ferrante, Spectroscopic Insights into Carbon Dot Systems, *J. Phys. Chem. Lett.*, 2017, **8**, 2236–2242.

107 C. J. Reckmeier, J. Schneider, Y. Xiong, J. Häusler, P. Kasák, W. Schnick and A. L. Rogach, Aggregated Molecular Fluorophores in the Ammonothermal Synthesis of Carbon Dots, *Chem. Mater.*, 2017, **29**, 10352–10361.

108 Y. Song, S. Zhu, S. Zhang, Y. Fu, L. Wang, X. Zhao and B. Yang, Investigation from chemical structure to photoluminescent mechanism: a type of carbon dots from the pyrolysis of citric acid and an amine, *J. Mater. Chem. C*, 2015, **3**, 5976–5984.

109 Z. Liu, H. Zou, N. Wang, T. Yang, Z. Peng, J. Wang, N. Li and C. Huang, Photoluminescence of carbon quantum dots: coarsely adjusted by quantum confinement effects and finely by surface trap states, *Sci. China: Chem.*, 2018, **61**, 490–496.

110 Y. Deng, D. Zhao, X. Chen, F. Wang, H. Song and D. Shen, Long lifetime pure organic phosphorescence based on water soluble carbon dots, *Chem. Commun.*, 2013, **49**, 5751–5753.

111 C. Lu, Q. Su and X. Yang, Ultra-long room-temperature phosphorescent carbon dots: pH sensing and dual-channel detection of tetracyclines, *Nanoscale*, 2019, **11**, 16036–16042.

112 A. Tadesse, M. Hagos, D. R. Devi, K. Basavaiah and N. Belachew, Fluorescent-Nitrogen-Doped Carbon Quantum Dots Derived from Citrus Lemon Juice: Green Synthesis, Mercury(II) Ion Sensing, and Live Cell Imaging, *ACS Omega*, 2020, **5**, 3889–3898.

113 H. Eskalena, S. Uruș, S. Cömertpaye, A. H. Kurtf and Ş. Özgan, Microwave-assisted ultra-fast synthesis of carbon quantum dots from linter: Fluorescence cancer imaging and human cell growth inhibition properties, *Ind. Crops Prod.*, 2020, **147**(1–9), 112209.

114 A. H. S. Júniora, D. L. P. Macuvele, H. G. Riella, C. Soares and N. Padoin, Novel carbon dots for zinc sensing from Campomanesia phaea, *Mater. Lett.*, 2021, **283**, 128813.

115 Md. R. Hasan, N. Saha, T. Quaid and M. T. Reza, Formation of Carbon Quantum Dots *via* Hydrothermal Carbonization: Investigate the Effect of Precursors, *Energies*, 2021, **14**, 986.

116 J. T. Margraf, F. Lodermeyer, V. Strauss, P. Haines, J. Walter, W. Peukert, R. D. Costa, T. Clark and D. M. Guldi, Using Carbon Nanodots as Inexpensive and Environmentally Friendly Sensitizers in Mesoscopic Solar Cells, *Nanoscale Horiz.*, 2016, **1**, 220–226.

117 G. Jeong, *et al.*, Microwave-Assisted Synthesis of Multifunctional Fluorescent Carbon Quantum Dots from A4/B2 Polyamidation Monomer Sets, *Appl. Surf. Sci.*, 2021, **542**(1–10), 148471.

118 P. Romero, F. Alves, M. D. Stringasci, H. H. Buzzá, H. Ciol, N. M. Inada and V. S. Bagnato, One-Pot Microwave-Assisted Synthesis of Carbon Dots and *in vivo* and *in vitro* Antimicrobial Photodynamic Applications, *Front. Microbiol.*, 2021, **12**, 662149.

119 B. Vercelli, The Role of Carbon Quantum Dots in Organic Photovoltaics: A Short Overview, *Coatings*, 2021, **11**, 232.

120 M. C. Barr, J. A. Rowehl, R. R. Lunt, J. Xu, A. Wang, C. M. Boyce, S. G. Im, V. Bulović and K. K. Gleason, Direct Monolithic Integration of Organic Photovoltaic Circuits on Unmodified Paper, *Adv. Mater.*, 2011, **23**, 3500–3505.

121 R. M. Izatt, S. R. Izatt, R. L. Bruening, N. E. Izatt and B. A. Moye, Challenges to achievement of metal sustainability in our high-tech society, *Chem. Soc. Rev.*, 2014, **43**, 2451–2475.

122 P. Mirtchev, E. J. Henderson, N. Soheilnia, C. M. Yip and G. A. Ozin, Solution phase synthesis of carbon quantum dots as sensitizers for nanocrystalline TiO_2 solar cells, *J. Mater. Chem.*, 2012, **22**, 1265–1269.

123 S. N. Baker and G. A. Baker, Luminescent carbon nanodots: emergent nanolights, *Angew. Chem., Int. Ed.*, 2010, **49**, 6726–6744.

124 M. J. Molaei, The optical properties and solar energy conversion applications of carbon quantum dots: A review, *Sol. Energy*, 2020, **196**, 549–566.

125 S. Xie, H. Su, W. Wei, M. Li, Y. Tong and Z. Mao, Remarkable photoelectrochemical performance of carbon dots sensitized TiO_2 under visible light irradiation, *J. Mater. Chem. A*, 2014, **2**, 16365–16368.

126 X. Dou, Z. Lin, H. Chen, Y. Zheng, C. Lu and J. M. Lin, Production of superoxide anion radicals as evidence for carbon nanodots acting as electron donors by the chemiluminescence method, *Chem. Commun.*, 2013, **49**, 5871–5873.

127 T. Ghosh, S. Chatterjee and E. Prasad, Photoinduced Electron Transfer from Various Aniline Derivatives to Graphene Quantum Dots, *J. Phys. Chem. A*, 2015, **119**, 11783–11790.

128 E. A. Stepanidenko, E. V. Ushakova, A. V. Fedorov and A. L. Rogach, Applications of Carbon Dots in Optoelectronics, *Nanomaterials*, 2021, **11**, 364.

129 K. Sharma, V. Sharma and S. S. Sharma, Dye-Sensitized Solar Cells: Fundamentals and Current Status, *Nanoscale Res. Lett.*, 2018, **13**, 381.

130 X. Han, S. Zhong, W. Pan and W. Shen, A simple strategy for synthesizing highly luminescent carbon nanodots and application as effective down-shifting layers, *Nanotechnology*, 2015, **26**, 65402–65412.

131 R. Riaz, M. Ali, T. Maiyalagan, A. S. Anjum, S. Y. Lee, M. J. Ko and S. H. Jeong, Dye-Sensitized Solar Cell (DSSC) coated with Energy Down Shift layer of Nitrogen-doped Carbon Quantum Dots (N-CQDs) for Enhanced Current Density and Stability, *Appl. Surf. Sci.*, 2019, **483**, 425–431.

132 J. E. P. Ceja, A. Z. Raynaud, R. L. Delgado, M. E. A. Ramos, E. S. Flores, R. R. Lepe, F. O. Magallanes, R. G. Gonzalez and A. Ayom, Anomalous Stokes shift of colloidal quantum dots and their influence on solar cell performance, *Microsyst. Technol.*, 2019, 1–9.

133 M. Ali, R. Riaz, S. Bae, H. S. Lee, S. H. Jeong and M. J. Ko, Layer by Layer Self-Assembly of Hollow Nitrogen-Doped Carbon Quantum Dots on Cationized Textured Crystalline Silicon Solar Cells for Efficient Energy Down-Shift, *ACS Appl. Mater. Interfaces*, 2020, **12**, 10369–10381.

134 T. Lv, Y. Tang, H. Fan, S. Liu, S. Zeng and W. Liu, Carbon quantum dots anchored on the anti-reflection silica layer as solid luminescence down-shifting materials in solar panel encapsulation, *Sol. Energy Mater. Sol. Cells*, 2022, **235**, 111450.

135 N. Gao, L. Huang, T. Li, J. Song, H. Hu, Y. Liu and S. Ramakrishna, Application of carbon dots in dye-sensitized solar cells: A review, *J. Appl. Polym. Sci.*, 2019, **137**(1–11), 48443.

136 H. Wang, P. Sun, S. Cong, J. Wu, L. Gao, Y. Wang, X. Dai, Q. Yi and G. Zou, Nitrogen-Doped Carbon Dots for "green" Quantum Dot Solar Cells, *Nanoscale Res. Lett.*, 2016, **11**, 1–6.

137 Q. Zhang, G. Zhang, X. Sun, K. Yin and H. Li, Improving the Power Conversion Efficiency of Carbon Quantum Dot-Sensitized Solar Cells by Growing the Dots on a TiO_2 Photoanode In Situ, *Nanomaterials*, 2017, **7**, 1–9.

138 Z. Zhang, T. Zheng, X. Li, J. Xu and H. Zeng, Progress of Carbon Quantum Dots in Photocatalysis Applications, *Part. Part. Syst. Charact.*, 2016, **33**, 457–472.

139 B. Mistry, H. K. Machhi, R. S. Vithalani, D. S. Patel, C. K. Modia, M. Prajapati, K. R. Surati, S. S. Soni, P. K. Jha and S. R. Kane, Harnessing the N-Dopant Ratio to Carbon Quantum Dots for Enhancing the Power Conversion Efficiency of Solar Cell, *Sustainable Energy Fuels*, 2019, **3**, 3182–3190.

140 Q. Yang, W. Yang, Y. Zhang, W. Ge, X. Yang and P. Yang, Precise Surface State Control of Carbon Quantum Dots to Enhance Charge Extraction for Solar Cells, *Nanomaterials*, 2020, **10**, 460–471.

141 J. B. Essner and G. A. Baker, The emerging roles of carbon dots in solar photovoltaics: a critical review, *Environ. Sci.: Nano*, 2017, **4**, 1216–1263.

142 T. Singh, J. Singh and T. Miyasaka, Role of Metal Oxide Electron-Transport Layer Modification on the Stability of High Performing Perovskite Solar Cells, *ChemSusChem*, 2016, **9**, 2559–2566.

143 L. Yan, Y. Yang, C. Q. Ma, X. Liu, H. Wang and B. Xu, Synthesis of carbon quantum dots by chemical vapor deposition approach for use in polymer solar cell as the electrode buffer layer, *Carbon*, 2016, **109**, 598–607.

144 H. Li, W. Shi, W. Huang, E. P. Yao, J. Han, Z. Chen, S. Liu, Y. Shen, M. Wang and Y. Yang, Carbon quantum dots/TiOx electron transport layer boosts efficiency of planar heterojunction perovskite solar cells to 19%, *Nano Lett.*, 2017, **17**, 2328–2335.

145 X. Zhu, J. Sun, S. Yuan, N. Li, Z. Qiu, J. Jia, Y. Liu, J. Dong, P. Lv and B. Cao, Efficient and stable planar perovskite solar cells with carbon quantum dots-doped PCBM electron transport layer, *New J. Chem.*, 2019, **43**, 7130–7135.

146 S. Park, H. Lee, S. W. Park, T. E. Kim, S. H. Park, Y. K. Jung and S. Cho, Improved exciton dissociation efficiency by a carbon-quantum-dot doped workfunction modifying layer in polymer solar cells, *Curr. Appl. Phys.*, 2021, **21**, 140–146.

147 J. B. Essnera and G. A. Baker, The emerging roles of carbon dots in solar photovoltaics: a critical review, *Environ. Sci.: Nano*, 2017, **4**, 1216–1263.

148 S. Paulo, G. Stoica, W. Cambaraua, E. M. Ferrero and E. Palomares, Carbon quantum dots as new hole transport material for perovskite solar cells, *Synth. Met.*, 2016, **222**, 17–22.

149 D. N. Nguyen, S. H. Roh, D.-H. Kim, J. Y. Lee, D. H. Wang and J. K. Kim, Molecular manipulation of PEDOT: PSS for efficient hole transport by incorporation of N-doped carbon quantum dots, *Dyes Pigm.*, 2021, **194**, 109610.

150 X. Feng, Y. Zhao, L. Yan, Y. Zhang, Y. He, Y. Yang and X. Liu, Low-Temperature Hydrothermal Synthesis of Green Luminescent Carbon Quantum Dots (CQD), and Optical Properties of Blends of the CQD with Poly(3-hexylthiophene), *J. Electron. Mater.*, 2015, **44**, 3436–3443.

151 B. Cui, L. Yan, H. Gu, Y. Yang, X. Liu, C. Q. Ma, Y. Chen and H. Jia., Fluorescent carbon quantum dots synthesized by chemical vapor deposition: An alternative candidate for electron acceptor in polymer solar cells, *Opt. Mater.*, 2017, **75**, 166–173.

152 L. Tong, X. Wang, Z. Chen, Y. Liang, Y. Yang, W. Gao, Z. Liu and B. Tan, One-Step Fabrication of Functional Carbon Dots with 90% Fluorescence Quantum Yield for Long-Term Lysosome Imaging, *Anal. Chem.*, 2020, **92**, 6430–6436.

153 H. Lin, J. Huang and L. Ding, Preparation of Carbon Dots with High-Fluorescence Quantum Yield and Their Application in Dopamine Fluorescence Probe and Cellular Imaging, *J. Nanomater.*, 2019, **2019**(1–9), 5037243.

154 L. Tian, D. Ghosh, W. Chen, S. Pradhan, X. Chang and S. Chen, Nanosized Carbon Particles from Natural Gas Soot, *Chem. Mater.*, 2009, **21**, 2803–2809.

155 A. Privitera, M. Righetto, D. Mosconi, F. Lorandi, A. A. Isse, A. Moretto, R. Bozio, C. Ferrante and L. Franco., Boosting carbon quantum dots/fullerene electron transfer *via* surface group engineering, *Phys. Chem. Chem. Phys.*, 2016, **18**, 31286–31295.

156 K. P. Shejale, A. Jaiswal, A. Kumar, S. Saxena and S. Shukla, Nitrogen doped carbon quantum dots as Co-active materials for highly efficient dye sensitized solar cells, *Carbon*, 2021, **183**, 169–175.

157 F. Yuan, P. H. He, Z. Xi, X. Li, Y. Li, H. Zhong, L. Fan and S. Yang, Highly efficient and stable white LEDs based on pure red narrow bandwidth emission triangular carbon quantum dots for wide-color gamut backlight displays, *Nano Res.*, 2019, **12**, 1669–1674.

158 F. Yuan, *et al.*, Bright high-colour-purity deep-blue carbon dot light-emitting diodes *via* efficient edge amination, *Nat. Photonics*, 2020, **14**, 171–176.

159 S. Y. Lim, W. Shen and Z. Gao, Carbon quantum dots and their applications, *Chem. Soc. Rev.*, 2015, **44**, 362–381.

160 Q. Wang, S. Zhang, B. Wang, X. Yang, B. Zou, B. Yang and S. Lu, Pressure-triggered aggregation-induced emission enhancement in red emissive amorphous carbon dots, *Nanoscale Horiz.*, 2019, **41**, 227–1231.

161 F. Yaun, T. yuan, L. Sui, Z. Wang, Z. Xi, Y. Li, X. Li, L. Fan, Z. Tan, A. Chen, M. Jin and S. Yang, Engineering triangular carbon quantum dots with unprecedented narrow bandwidth emission for multicolored LEDs, *Nat. Commun.*, 2018, **9**, 2249.

162 L. Wang, W. Li, L. Yin, Y. Liu, H. Guo, J. Lai, Y. Han, G. Li, M. Li, J. Zhang, R. Vajtai, P. M. Ajayan and M. Wu, Full color fluorescent carbon quantum dots, *Sci. Adv.*, 2020, **6**, 1–8.

163 P. He, Y. Shi, T. Meng, T. Yuan, Y. Li, X. Li, Y. Zhang, L. Fan and S. Yang, Recent advances in white light-emitting diodes of carbon quantum dots, *Nanoscale*, 2020, **12**, 4826–4832.

164 M. Du, Y. Feng, D. Zhu, T. Peng, Y. Liu, Y. Wang and M. R. Bryce, Novel Emitting System Based on a Multifunctional Bipolar Phosphor: An Effective Approach for Highly Efficient Warm-White Light-Emitting Devices with High Color-Rendering Index at High Luminance, *Adv. Mater.*, 2016, **28**, 5963–5968.

165 T. Yuan, T. Meng, P. He, Y. X. Shi, Y. Li, X. Li, L. Fan and S. Yang, Carbon quantum dots: an emerging material for optoelectronic applications, *J. Mater. Chem. C*, 2019, **7**, 6820–6835.

166 Z. Wang, F. Yuan, X. Li, Y. Li, H. Zhong, L. Fan and S. Yang, 53% Efficient Red Emissive Carbon Quantum Dots for High Color Rendering and Stable Warm White-Light-Emitting Diodes, *Adv. Mater.*, 2017, **29**, 1702910.

167 T. Meng, T. Yuan, X. Li, Y. Li, L. Fan and S. Yang, Ultrabroad-band, red sufficient, solid white emission from carbon quantum dot aggregation for single component warm white light emitting diodes with a 91 high color rendering index, *Chem. Commun.*, 2019, **55**, 6531–6534.

168 S. Lu, R. Cong, S. Zhu, X. Zhao, J. Liu, J. S. Tse, S. Meng and B. Yang, pH-Dependent Synthesis of Novel Structure-Controllable Polymer-Carbon NanoDots with High Acidophilic Luminescence and Super Carbon Dots Assembly for White Light-Emitting Diodes, *ACS Appl. Mater. Interfaces*, 2016, **8**, 4062–4068.

169 Y. Wu, H. Zhang, A. Pan, Q. Wang, Y. Zhang, G. Zhou and L. He, White-Light-Emitting Melamine-Formaldehyde Microspheres through Polymer-Mediated Aggregation and Encapsulation of Graphene Quantum Dots, *Adv. Sci.*, 2018, **6**, 1801432.

170 J. Zhu, X. Bai, Y. Zhai, X. Chen, Y. Zhu, G. Pan, H. Zhang, B. Dong and H. Song, Carbon dots with efficient solid-state photoluminescence towards white light-emitting diodes, *J. Mater. Chem. C*, 2017, **5**, 11416–11420.

171 S. Do, W. Kwon, Y. H. Kim, S. R. Kang, T. Lee, T. W. Lee and S. W. Rhee, N,S-Induced Electronic States of Carbon Nanodots Toward White Electroluminescence, *Adv. Opt. Mater.*, 2015, **4**, 276–284.

172 G. Q. Yin, H. Wang, X. Q. Wang, B. Song, L. J. Chen, L. Wang, X. Q. Hao, H. B. Yang and X. Li, Self-assembly of emissive supramolecular rosettes with increasing complexity using multi topic terpyridine ligands, *Nat. Commun.*, 2018, **9**, 567.

173 D. H. Kim and T. W. Kim, Ultrahigh-luminosity white-light-emitting devices based on edge functionalized graphene quantum dots, *Nano Energy*, 2018, **51**, 199–205.

174 T. Yuan, F. Yuan, X. Li, Y. Li, L. Fan and S. Yang, Fluorescence–phosphorescence dual emissive carbon nitride quantum dots show 25% white emission efficiency enabling single-component WLEDs, *Chem. Sci.*, 2019, **10**, 9801–9806.